International Scientific-Technical and Production Journal

The Paton WELDING JOURNAL

August 2003 # 8

English translation of the monthly «Avtomaticheskaya Svarka» (Automatic Welding) journal published in Russian since 1948

Founders: *The E.O. Paton Electric Welding Institute of the NAS of Ukraine International Association «Welding»* **Publisher:** *International Association «Welding»*

Address:
E.O. Paton Electric Welding Institute,
International Association «Welding»,
11, Bozhenko str., 03680, Kyiv, Ukraine
Tel.: (38044) 227 67 57
Fax: (38044) 268 04 86
E-mail: journal@paton.kiev.ua
http://www.nas.gov.ua/pwj

State Registration Certificate
KV 4790 of 09.01.2001

Subscriptions:
$460, 12 issues per year,
postage and packaging included.
Back issues available.

CONTENTS

STABILIZATION OF THE PROCESS OF CONSUMABLE ELECTRODE PULSE-ARC WELDING

B.E. PATON, P.P. SHEJKO, A.M. ZHERNOSEKOV and **Yu.O. SHIMANOVSKY**
E.O. Paton Electric Welding Institute, NASU, Kyiv, Ukraine

Developed systems of automatic stabilization of the process of consumable electrode pulse-arc welding (CEPAW) are described, allowing stabilization of mean values of arc voltage and welding current, under the impact of disturbances. This leads to lowering of the probability of porosity and lack-of-fusion in Al–Mg alloys, decrease in spattering and sputtering, as well as stabilization of the width of welds in CEPAW of carbon steels.

Keywords: consumable electrode pulse-arc welding, automation, process stabilization, disturbing factors, feedback, weld appearance, pores

Gas-shielded consumable-electrode arc welding is still leading against the other arc welding process in the overall scope of welded structure fabrication. Consumable electrode pulse-arc welding (CEPAW) has a special place here. After its development in 1963–1965, this process has been further enhanced and is widely accepted in many industrial sectors. It provides effective solutions for many technological tasks. The main advantages of the process include effective control of metal transfer, which permits welding to be performed in different positions in space; reducing critical welding current, which provides an expansion of the technological range of working currents, reduces spatter, loss of alloying elements in the electrode and base metal, improves the performance of welded structures; ability to weld various steels (all types of carbon structural, alloyed steels), many non-ferrous metals (Al-, Cu-, Ti-based alloys). CEPAW is widely used now in aerospace engineering, shipbuilding, chemical and oil and gas engineering, pipeline transportation instead of a low-efficient and expensive non-consumable electrode welding. Welding stresses and strains are greatly reduced, thus increasing the accuracy of item fabrication.

Under production conditions the CEPAW process is subject to various disturbances, which violate its steady progress (systematic nature of metal transfer, stability of arc length, welding voltage and current), which leads to deviations of the indices of the welded joint quality from the necessary values, i.e. non-uniformity of the geometrical dimensions of welds, appearance of defects in them, and, consequently, deterioration of the mechanical properties of welded joints as a whole. The sources of power and kinematic disturbances are voltage ripple in the industrial mains, unstable feed of welding wire and speed of welding, variation of electrode extension. Technological disturbances are due to disturbances in the technology of preparation and assembly, or running against tacks. Edges misalignment may lead to appearance of rolls or lack of root penetration, and a greater gap in butt welded joints often is the cause for weld metal sagging and burn-through. In addition, in semi-automatic CEPAW it is also necessary to take into account the subjective influence of the welder, his skill and fatigue during the working day.

The power sources for CEPAW are the sources with many control parameters, namely pulse frequency, pulse current duration and amplitudes, base current, etc. Therefore, the task of automatic stabilization of CEPAW process with inevitable appearance of various disturbance factors (single and concurrent) is urgent and quite complicated. It is necessary to perform a thorough analysis of the most significant disturbing factors, evaluate their influence on the welding process, determine the controlled parameters, which are the most responsible for the CEPAW quality, select the most effective regulation impacts and construct automatic regulation systems, which allow compensating the disturbance impact on the quality of joints, made by CEPAW.

Work on automation of the CEPAW process is conducted in several areas. The first is related primarily to development of the programmable, so-called synergetic power sources, when the current pulse parameters are first set in the processor program and during welding are rigidly coupled to the wire feed rate. Presetting the current pulse parameters and their variation are performed at the change of the type of material being welded, diameter and composition of electrode wire, and shielding gas composition [1–3]. Other more complex adaptive systems are available, which allow for the geometry of material preparation for welding and its thickness, based on mathematical relationships, established using a bank of experimentally derived data [4, 5].

The second direction consists in development of systems with arc voltage feedback for automatic stabilization of arc length by making an impact on the power source. The latter approach has been actively developed by specialists of the Canadian Institute of Welding, who are using the «patented function of closed-loop control with arc following to compensate for variation of arc length» and are applying such a process for pipeline welding [6, 7].

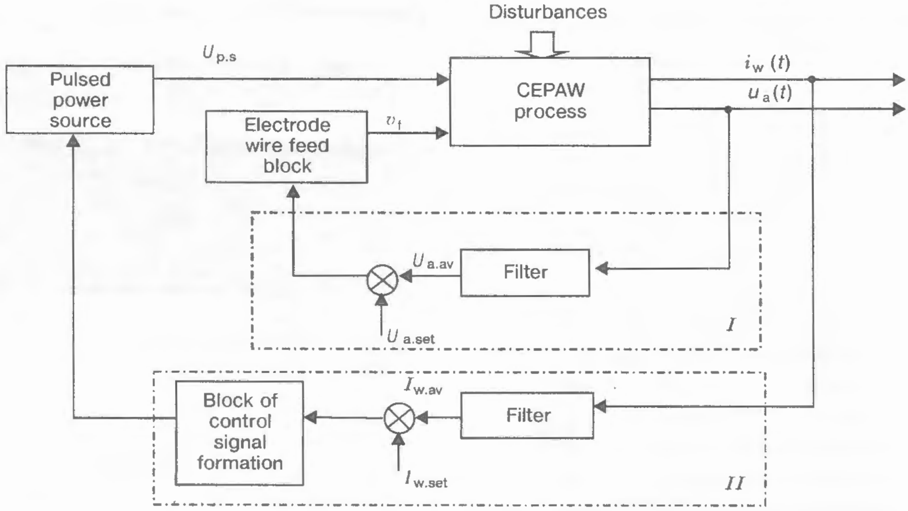

Figure 1. Block-diagram of the system of stabilization of $U_{a.av}$ (*I*) and $I_{w.av}$ (*II*)

The above methods of development of CEPAW automation are not optimal, as they do not allow for the entire diverse spectrum of disturbing factors and require numerous experiments (data bank).

This paper describes approaches to CEPAW automation, based on theoretical work of the staff of the E.O. Paton Electric Welding Institute [8–10]. The impact of any disturbing factors during welding leads to changes of both metal transfer and average values of arc voltage and welding current. It is known that average values of arc voltage and welding current in CEPAW determine the main parameters of the weld, namely the width and depth of penetration [11–15]. Variations of average arc voltage, alongside the deviations of weld width from the set technological values, may also cause (due to the arising variations of arc length) appearance of defects of the type of pores, undercuts, lacks-of-fusion, rolls in the welds and deterioration of their appearance. Deviation of the average value of welding current from the preset value may lead to lacks-of-penetration or burns-through, which is inadmissible. An integrated impact of the above defects and deviations impairs the mechanical properties of weld metal and performance of the welded joint as a whole.

A fundamental difference of the developed method of automatic stabilization of the CEPAW process from the synergetic and other known methods is use of both voltage feedback and current feedback with applying impact on various links, involved in the above process. Current feedback is applied to the power source and voltage feedback — to the drive of welding wire feed. The rationality of such an approach is substantiated by several reasons. First, the probability of appearance of defects in welds at variations of wire feed rate is reduced. Secondly, unlike the synergetic method, which essentially consists in maintenance of equal amounts of the melted and fed wires, when a constant value of welding current is not provided, in this case a rigid stabilization of welding current and soft stabilization of the arc length (arc voltage) is performed. This process may be regarded as an analog of self-regulation of the arc parameters, where one of the parameters remains practically unchanged. Thirdly, use of just the current feedback with applying impact to the pulsed power source leads to instability of arc length, namely increasing elongations and shortening [16], which was also established in our experiments on CEPAW of aluminium alloys.

The block-diagram of one of the variants of construction of the systems of automatic stabilization of $U_{a.av}$ and $I_{w.av}$, developed at the E.O. Paton Electric Welding Institute, is given in Figure 1. The systems of $U_{a.av}$ and $I_{w.av}$ stabilization are designed as an attachment-block to the pulsed power source of the arc. A possibility of operation of the system of $U_{a.av}$ stabilization and joint operation of the systems of $U_{a.av}$ and $I_{w.av}$ stabilization are provided. Automatic stabilization of $U_{a.av}$ is performed using feedback signals by the current values of $u_a(t)$ by automatic correction of welding wire feed rate, and that of $I_{w.av}$ by the impact on the welding current parameters, generated by the pulsed power source of the arc, respectively.

Table 1. Modes of bead deposition on a plate of steel St.3 under the impact of a linear disturbance

Mode No.	I_w, *A*	U_a, *V*	*Conditions*
1	140–110	23–25.5	Without stabilization systems
2	140–130	23 + 0.8	$U_{a.av}$ stabilization

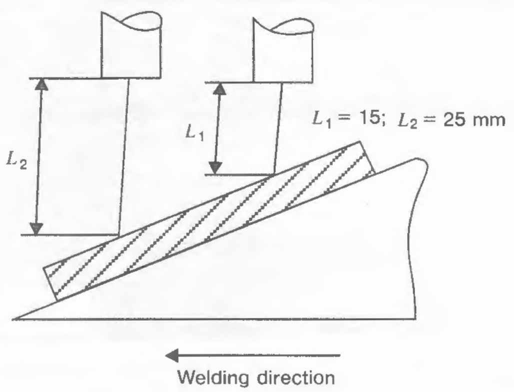

Figure 2. Schematic of bead deposition under the impact of linear disturbance along electrode wire extension

Table 2. Modes of bead deposition on a plate of alloy AMg6 under the action of linear disturbances

Mode No.	I_w, *A*	U_a, *V*	*Conditions*
3	130–110	22–24.5	Without stabilization systems
4	130–120	22 + 0.5	$U_{a.av}$ stabilization
5	130	22–23	$U_{a.av}$ and $I_{w.av}$ stabilization

Power source I-169, developed at the E.O. Paton Electric Welding Institute was selected as the pulsed power source of the arc for CEPAW. It has passed multiple pilot-production verification in many plants, which are manufacturing advanced critical pieces of equipment of various aluminum and steel alloys.

The influence of the process of bead deposition at linear disturbances by the length of the electrode wire by a schematic, given in Figure 2, was studied. Deposits were made of steel St.3 in shielding gases Ar + 20 % CO_2 with Sv-08G2S wire of 1.2 mm diameter at welding speed of 23 m/h. Modes of deposition in the downward direction at linear change of electrode extension are given in Table 1.

Electric parameters of the process were recorded with light-beam oscillograph N-117. Figure 3 gives oscillograms of average values of arc voltage in surfacing steel St.3 by a schematic, given in Figure 2. As is seen, in CEPAW with a system of automatic stabilization of the process with arc voltage feedback variations of $U_{a.av}$ during the action of the disturbing factor are reduced (Figure 3), and random short-circuits are also eliminated, i.e. the length of the welding arc and arc voltage are stabilized. This leads to reduction of spattering by 50 % and production of sound, fine-rippled weld of a stable width. Figure 4 shows the appearance of welds, made under the impact of disturbances by a schematic, given in Figure 2.

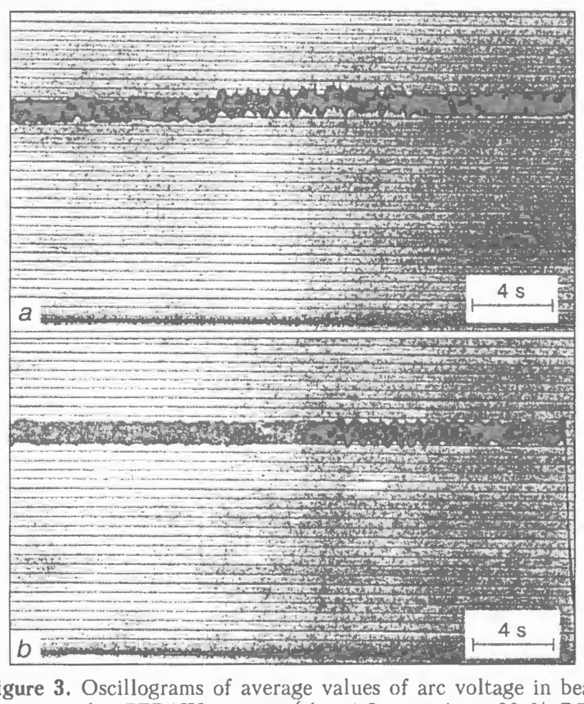

Figure 3. Oscillograms of average values of arc voltage in bead deposition by CEPAW process (d = 1.2 mm; Ar + 20 % CO_2; Sv-08G2S wire) without the stabilization systems (*a*) and with voltage stabilization (*b*)

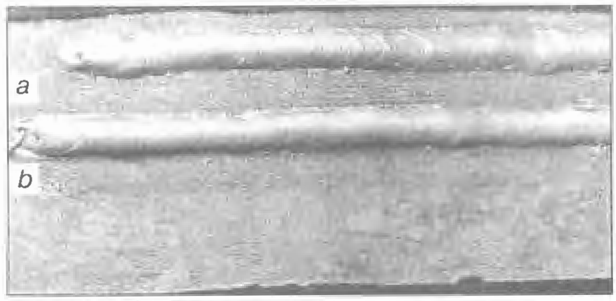

Figure 4. Appearance of welds in bead deposition by CEPAW process (d = 1.2 mm; Ar + 20 % CO_2; Sv-08G2S wire) without the stabilization systems (a) and with voltage stabilization (*b*)

Operation of the systems of $U_{a.av}$ and $I_{w.av}$ stabilization was also experimentally studied in CEPAW of Al–Mg alloys of AMg6 type. Figure 5 gives the appearance of welds, made in argon with Sv-AMg6 wire of 1.6 mm diameter on a plate of alloy AMg6 10 mm thick, under the impact of a linear disturbance on the process by the schematic, shown in Figure 2. The welding speed was 20 m/h. Bead deposition modes are given in Table 2. Figure 6 gives the transverse macrosections of welds, deposited in modes No.3–5 in Table 2.

Mode No.5, when the systems of stabilization of both the current and voltage are operating, deviations of arc voltage turn out to be higher than in operation of just the system of stabilization by voltage. This is accounted for by differences in the operating principles of both the systems and in the parameters of equipment, generating the regulating impact. The ac-

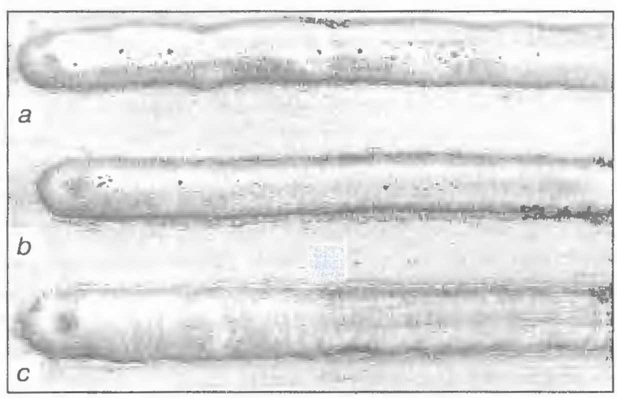

Figure 5. Appearance of welds in bead deposition by CEPAW process on plates of alloy AMg6 in argon with Sv-AMg6 wire under the action of linear disturbance by the schematic in Figure 2: *a* — without stabilization systems; *b* — with voltage stabilization; *c* — with current and voltage stabilization

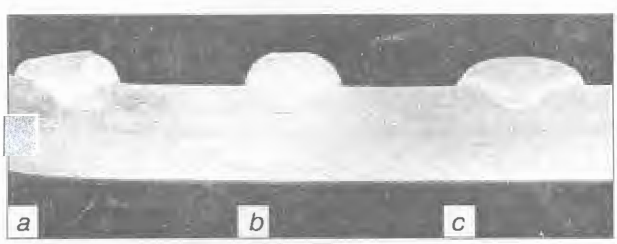

Figure 6. Longitudinal macrosections of welds (closer to weld end) without stabilization systems (*a*), with voltage stabilization (*b*) and with current and voltage stabilization (*c*)

tuator link of the system of current stabilization is the electronic circuit of power source I-169, which is a sufficiently quick-acting and stable link. The actuator link of the system of voltage stabilization is the mechanism of welding wire feed, which is exposed to the impact of many additional disturbing factors (rubbing in or end play of bearings, reduction gear, slipping or clamping of rollers, causing an unstable or non-uniform rate of the electrode wire feed, reel, overlapping or non-uniform winding of the wire on the reel, etc.), which significantly lowers its response and accuracy.

Thus, at joint operation of both the systems, the system of current stabilization prevails over the voltage stabilization system in terms of its response, which is exactly indicated by the welding parameters for sample No.5.

As is seen from Figures 5 and 6, application of systems of $U_{a.av}$ and $I_{w.av}$ stabilization significantly reduces porosity under the impact of linear disturbances by electrode extension on the CEPAW process, which is confirmed by the data of X-ray examination. In addition, application of the systems results in stabilization of weld width, better fusion of weld metal with base metal along the entire length, and improvement of penetration shape.

CONCLUSIONS

1. A variant of CEPAW process automation is proposed by stabilization of average values of welding current and arc voltage.

2. Application of systems of automatic stabilization of voltage and current significantly lowers the porosity of weld metals in CEPAW of Al–Mg alloys with linear disturbances along the electrode wire extension, stabilizes weld width, improves the penetration shape and provides a guaranteed fusion of weld metal with base metal.

3. Application of the systems of automatic stabilization of average values of arc voltage in deposition of welds on carbon steels reduces the number of short-circuits during the action of linear disturbances, which allows improving weld appearance and reducing the spatter.

1. Amin, M. (1981) Synergic pulse MIG welding. *Metal Construction*, **6**, 349–353.
2. Amin, M. (1983) Pulse current parameters for arc stability and controlled metal transfer in arc welding. *Ibid.*, **5**, 272–278.
3. Smati, Z. (1986) Automatic pulsed MIG welding. *Ibid.*, **1**, 38–44.
4. Breat, J.-L. (1989) MIG pulse et robotique. *Souder*, **2**, 25–43.
5. Breat, J.-L. (1989) MIG pulse et robotique. *Ibid.*, **3**, 19–24.
6. Ditschun, A., Dorling, D., Clover, A. et al. (1985) The development and application of pulsed FM-GMA welding. In: *Proc. of 1st Int. Conf. on Adv. Weld. Syst.*, London, Nov. 19–21, 1985.
7. Dorling, D. (1992) Applying pulsed GMA welding to pipeline construction. *Welding J.*, **10**, 39–44.
8. Paton, B.E., Lebedev, V.K. (1966) *Electric equipment for arc and slag welding*. Moscow: Mashinostroenie.
9. Paton, B.E., Shejko, P.P. (1967) Automatic control of pulsed arc welding process. *Avtomatich. Svarka*, **1**, 3–8.
10. Paton, B.E., Shejko, P.P., Pashulya, M.P. (1971) Automatic control of metal transfer in pulsed arc welding. *Ibid.*, **9**, 3–5.
11. Lapchinsky, V.F., Potapievsky, A.G., Steblovsky, B.A. et al. (1966) Pulsed argon-arc welding of aluminium alloys. *Ibid.*, **7**, 50–53.
12. Allum, C.J., Quintino, L. (1985) Control of fusion characteristics in pulsed current MIG welding. Part 1. Dependence of fusion characteristics on process parameters. *Metal Construction*, **4**, 242–245.
13. Allum, C.J. (1985) Welding technology data: pulsed MIG welding. *Weld. and Metal Fabr.*, **1**, 24–26, 28–30.
14. Grubic, K., Andric, S. (1996) Factors of pulse MIG welding, their relationships and effects. *Joining of Materials*, **2**, 63–66.
15. Mandal, A., Parmar, R.S. (1996) Effects of pulse parameters on weld bead geometry, *Ibid.*, **2**, 69–75.
16. Matthes, K.-J., Kusch, M. (2000) Einfluss der Modulationsart der Stromquelle auf das Schweißergebnis. *Praktiker*, **10**, 386–391.

ESTIMATION OF PERMISSIBLE SIZES OF WELDS FOR MOUNTING T-JOINTS AND SLEEVES ON ACTIVE MAIN PIPELINES

V.I. MAKHNENKO, V.S. BUT, E.A. VELIKOIVANENKO, G.F. ROZYNKA and **N.I. PIVTORAK**
E.O. Paton Electric Welding Institute, NASU, Kyiv, Ukraine

Considered is the effect of geometric sizes of pipelines, T-joints and sleeves on permissible sizes of the welds, allowing for variations in the working pressure in a pipeline, as well as variants of a technology for mounting of sleeves (T-joints) without interruption of operation of the pipeline.

Keywords: *mathematical modelling, ultimate load, tough fracture, two-parameter criterion, sharp cavity, main pipelines, T-joints, sleeve, circumferential welds, weld sizes, working pressure*

The use of special design solutions for making full-strength branch pipes in the form of T-joints (Figure 1) or mounting of circular safety sleeves in a zone of detected defects in the wall of a pipeline without interruption of operation of the latter [1, 2 etc.] is a generally accepted practice.

Circumferential connection welds are made by using different variants of the solutions, among which the most common ones are joints with fillet welds (Figure 2, *a*) and lap-butt joints connecting three elements, i.e. pipeline wall and two elements of a sleeve or T-joint (Figure 2, *b*).

The issue of determination of sufficient sizes of a load-bearing portion of the weld in both variants, depending upon different input parameters and conditions, has received almost no discussion in the literature, which makes a substantiated approach to its handling more difficult. In this study the authors made an attempt to address this issue on the basis of their experience gained from strength design of welded joints with adjoining sharp cavities [3–5 etc.], which is characteristic of the joints shown in Figure 2.

Main principles of the suggested calculation procedure. Static (quasi-static) loading of welded joints (Figure 2) with an adjoining sharp cavity is considered. A critical condition of metal at the apex of the above sharp cavity is determined by the two-parameter criterion of the following type:

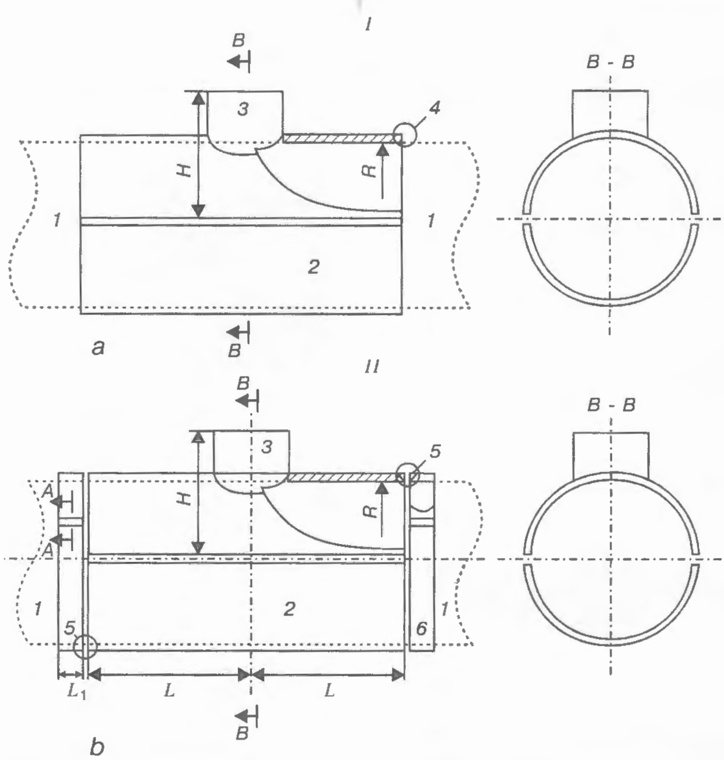

Figure 1. Split T-joint of type *I* (*a*) and *II* with technological rings (*b*): *1* — pipeline; *2* — sleeve (T-joint); *3* — branch pipe; *4* — fillet weld; *5* — lap-butt joint; *6* — additional part of the split sleeve

$$f\left(\frac{K_\omega}{K_{Ic}\eta}\,\frac{P}{P_p}\right) = 0, \tag{1}$$

where K_ω is the stress intensity coefficient at the apex of the sharp cavity under load P considered within the framework of the maximum normal tear hypothesis [6]; K_{I_c} is the fracture toughness of a material at the sharp cavity apex (Figure 2), i.e. in the weld material; η is the coefficient allowing for the fact that the adjoining sharp cavity apex has a root face that is approximately equal to gap width 2ρ, and that the conditions of deformation of the weld metal differ from those of plane deformation [3–5]; and P_p is the ultimate load on a weld section based on the conditions of tough behaviour of the material.

The type of function in (1) is set from the data of studies [3, 7 etc.]. The most popular dependence now is that taken from study [7]:

$$K_r = (1 - 0.14L_r^2)\,[0.3 + 0.7\exp(-0.05L_r^6)] \tag{2}$$

at $L_r \le L_{r\,\max}$;

$$K_r = 0 \text{ at } L_r > L_{r\,\max},$$

where $K_r = K_\omega / K_{I_c}\eta$; $L_r = P/P_p$.

As shown in study [7], function (2) provides a sufficiently good approximation of experimental data (Figure 3) for many structural steels.

For the diagrams of loading of welded joints shown in Figure 2 using [3–5], the following can be written down for a fillet weld:

$$K_\omega(\varphi) = K_I(\varphi)\,\frac{1 - 3x\xi}{(1 + x^2)^{3/2}}, \tag{3}$$

where $x = \dfrac{2\xi}{1 + \sqrt{1 + 8\xi^2}}$; $\xi = \dfrac{K_{II}(\varphi)}{K_I(\varphi)}$ is the ratio of the stress intensity factor of transverse shear K_{II} to that of normal tear K_I for loads acting on the weld section of φ = const (Figure 2, *a*).

Loads in this section can be expressed in terms of moment $M = M_2 - M_1$ induced by axial stresses σ_{zz} in their non-uniform distribution through thickness of the walls, δ_1 and δ_2, respectively, in the vicinity of the weld, i.e.

$$\begin{aligned} M_2 &= \int_{-\delta_2/2}^{\delta_2/2} \sigma_{zz}\left(1 + \frac{\zeta_2}{R}\right)\zeta_2 d\zeta_2; \\ M_1 &= \int_{-\delta_1/2}^{\delta_1/2} \sigma_{zz}\left(1 + \frac{\zeta_1}{R}\right)\zeta_1 d\zeta_1, \end{aligned} \tag{4}$$

and in terms of a shearing force:

$$Q_r = \int_{z_0}^{h(\varphi = 0) = a} \sigma_{rr} dz, \tag{5}$$

where σ_{rr} are the radial stresses on surface $\varphi = 0$ (Figure 2).

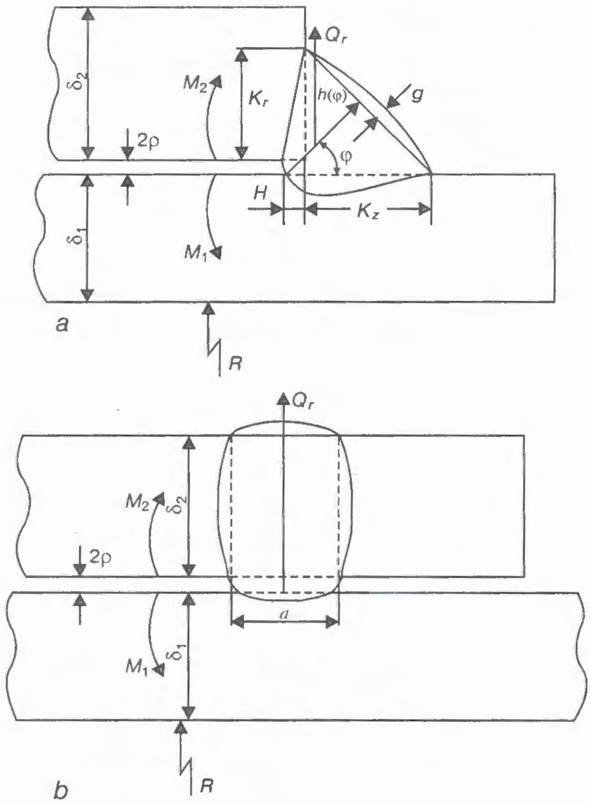

Figure 2. Schematics of loading of the joints: *a* — joints with fillet welds; *b* — lap-butt joints

$M = M_2 - M_1$ and Q_r being known, determine $K_I(\varphi)$ and $K_{II}(\varphi)$ for a fillet weld (Figure 2, *a*) from dependencies [3–5]:

$$\begin{aligned} K_I(\varphi) &= 0.5369\left[\frac{Q_r\cos\varphi}{\sqrt{h(\varphi)}} + 8\,\frac{M}{(h(\varphi))^{3/2}}\right]; \\ K_{II}(\varphi) &= \frac{2}{\sqrt{\pi h(\varphi)}}\,Q_r\sin\varphi. \end{aligned} \tag{6}$$

Those for a butt-lap joint (Figure 2, *b*) are determined as follows:

$$K_I = \frac{Q_r}{\sqrt{\pi a}} + \frac{2M}{\sqrt{\pi}a^{3/2}}; \quad K_{II} = 0. \tag{7}$$

In estimation of an ultimate tough fracture load for the weld sections, it is necessary to add to moment

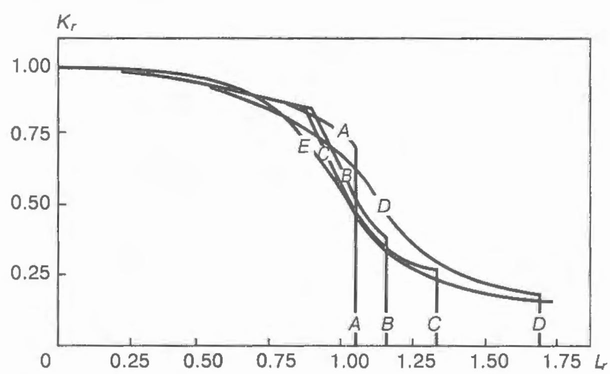

Figure 3. Limiting state diagrams $K_r = f(L_r)$ for different types of structural steels: *A* — high-strength steel EN408; *B* — pressure vessel steel A533B; *C* — low-carbon steel containing manganese; *D* — austenitic steel; *E* — corresponding to formula (2)

M and force Q_r circumferential stresses $\sigma_{\beta\beta}$ which, like M and Q_r, are also a function of geometry of the joint and applied pressure.

Accordingly, P/P_p can be represented in the following form:

$$\frac{P}{P_p} = \frac{\sigma_i(P)}{\sigma_{i\,p}}, \tag{8}$$

where $\sigma_i(P) = \sqrt{\sigma_{\varphi\varphi}^2 + \sigma_{\beta\beta}^2 - \sigma_{\beta\beta}\sigma_{\varphi\varphi} + 3\sigma_{\varphi\eta}^2}$ is the intensity of stresses in a weld section of φ = const;

$$\sigma_{\varphi\varphi} = \frac{4M}{h^2(\varphi)} + \frac{Q_r \cos\varphi}{h(\varphi)}; \quad \sigma_{\varphi\eta} = \frac{Q_r \sin\varphi}{h(\varphi)};$$

$$\sigma_{i\,p} = \frac{\sigma_y + \sigma_t}{2}, \tag{9}$$

where σ_y is the yield stress of a material and σ_t is its tensile strength.

For a variant of a butt-lap joint relationships (8) and (9) are valid at $\varphi = 0$ and $h = a$.

Results of numerical studies. It follows from the above-said that the limiting state can be estimated provided that the tool is available for determination of load functions M, Q_r and $\sigma_{\beta\beta}$ at preset geometric sizes and a scenario of mounting a T-joint or sleeve, as well as conditions of filling the sharp cavity adjoining the weld with gas. Consider three main loading scenarios.

Scenario I. Mounting and welding of a structure are done at a zero excessive pressure in a pipeline, and then the pipeline and the sharp cavity are loaded with a working pressure of $P_1 = 5.5$ MPa and $P_2 = 7.5$ MPa.

Scenario II. Mounting and welding of a structure are done at loading a pipeline with a working pressure of $P_1 = 5.5$ MPa or $P_2 = 7.5$ MPa, and then the same pressure is generated in the sharp cavity.

Scenario III. Mounting and welding of a sleeve are done at a loaded pipeline ($P_1 = 5.5$ MPa or $P_2 = 7.5$ MPa), and then the pipeline is unloaded to a zero excessive pressure.

An additional scenario was also considered, where mounting and welding of a structure were done under a pressure of $P_0 = \kappa P_1$ ($0 \le \kappa \le 1$), and then the pressure in the pipe and sharp cavity was raised to $P_1 = 5.5$ MPa.

Results of each specific calculation is an estimate of the required values of legs $K_n = K_z = K_r$ or a_n, at which the non-fracture condition is met according to criterion (1).

Generation of the required data on values M, Q_r and $\sigma_{\beta\beta}$ for the above loading scenarios involved solution of a respective elasto-plastic problem under the following assumptions: the axisymmetric case was considered, which was sufficiently close to the variant of a circular sleeve located outside the defect, and determined the state outside the hole for the case of

Variations in minimum values of a_n and K_n depending upon the geometric sizes of a pipeline, pressure and material mechanical properties

Variant No.	P, MPa	δ_2, mm	δ_1, mm	σ_y, MPa	K_{I_c}, MPa·mm$^{1/2}$	Scenario I		Scenario II		Scenario III	
						a_n	K_n	a_n	K_n	a_n	K_n
1	5.5	12	7–14	360	1000	6	4	7	7	5	5
2					1500	6	4	7	7	5	5
3				440	1000	5	6	8	6	5	5
4					1500	5	6	5	6	5	5
5	7.5	14	7–14	360	1000	7	5	9	10	6	6
6					1500	7	5	9	9	6	6
7				440	1000	7	4	8	14	6	6
8					1500	7	4	7	8	6	6
9	5.5	28	11–26	360	1000	17	18	28	–	17	26
10					1500	13	9	18	–	13	16
11			9–26	440	1000	17	20	26	–	17	23
12					1500	12	9	20	–	12	16
13	7.5	47	15–26	360	1000	22	30	38	–	23	39
14					1500	18	4	29	–	15	27
15			12–26	440	1000	22	30	36	–	23	39
16					1500	18	4	28	–	16	31

Note. In variants Nos.1–8 $2R$ = 520 mm; Nos.9–16 – $2R$ = 1420 mm.

a T-joint; the effect of plastic strains at the sharp cavity apex on the required values of M, Q_r and $\sigma_{\beta\beta}$ was ignored; and stresses associated with the thermal cycle of welding of elements considered in Figure 1 were also neglected. It was also assumed in this case that welding under loading led partially to decrease in a longitudinal shrinkage and, accordingly, residual welding stresses, the effect of which shows up primarily in variations in values of $\sigma_{\beta\beta}$. Contribution of these stresses to the mechanism of a possible brittle fracture of the welds under consideration is insignificant (they were ignored in calculations of K_ω), and the more so to the tough fracture under static loading.

The problem was solved by the finite elements method using software developed by the E.O. Paton Electric Welding Institute [8 etc.].

The following input data were used for the calculations the results of which are given below: pipeline material — pipe steel; elasticity modulus — $2\cdot10^6$ MPa; Poisson's ratio $\nu = 0.3$. Three variants of strength characteristics were considered: 1st — $\sigma_y = 270$ MPa and $\sigma_t = 412$ MPa; 2nd — $\sigma_y = 360$ MPa and $\sigma_t = 550$ MPa; 3rd — $\sigma_y = 440$ MPa and $\sigma_t = 588$ MPa. Material of welded joints was close in its properties to the base metal, except for the K_{I_c} values. For deriving conservative estimates of permissible sizes of the weld and allowing for a very wide scatter of experimental data obtained for the weld metal with respect to K_{I_c}, based on the experience [3–5] the K_{I_c} value for the weld was assumed to be equal to 1500–1000 MPa·mm$^{1/2}$. The value of coefficient η in (1) and (2) was calculated in accordance with [3–5] in the following form:

$$\eta = \eta_1(\rho)\eta_2(h), \qquad (10)$$

где $\eta_1(\rho) = 1$, if $\rho < \rho_0 = 0.1$ mm;
$\eta_1(\rho) = \sqrt{\rho/\rho_0}$, if $\rho \geq \rho_0$;
$\eta_2(h) = 1$, if $h(\varphi) > h_m \approx 1.75\left(\dfrac{\sigma_y}{K_{I_c}}\right)^2$;
$\eta_2(h) = \sqrt{h_m/h}$, if $h(\varphi) < h_m$.

Here $h = h(\varphi)$ is used for the fillet weld and the a value is used for the butt-lap joint.

Results of the calculations made to determine a_n or K_n for specific geometric sizes of a pipeline, such as $2R$, δ_1 and δ_2 at $\rho < 0.1$ mm, and length of the sleeve (T-joint) along axis z equal to $2L \geq 2R$, are given in the Table. In a case of small diameters of a pipeline, i.e. $2R \leq 426$ mm, variations in values of

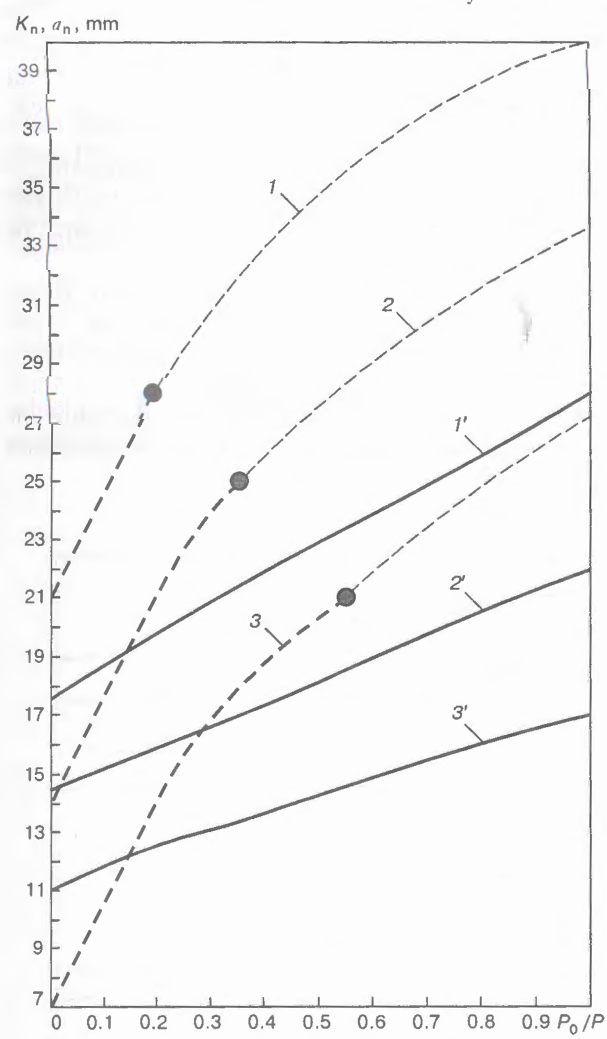

Figure 4. Effect of excessive pressure in a pipeline, P_0, in mounting of a sleeve (T-joint) on minimum sizes of the weld at $P = 5.5$ MPa: dashed lines — K_n, solid lines — a_n (scenario *II*); *1, 1'* — $2R = 1420$ mm ($\delta_1 = 26$ mm, $\delta_2 = 28$ mm); *2, 2'* — $2R = 1220$ mm ($\delta_1 = 21$ mm, $\delta_2 = 25$ mm); *3, 3'* — $2R = 1020$ mm ($\delta_1 = 16$ mm, $\delta_2 = 21$ mm)

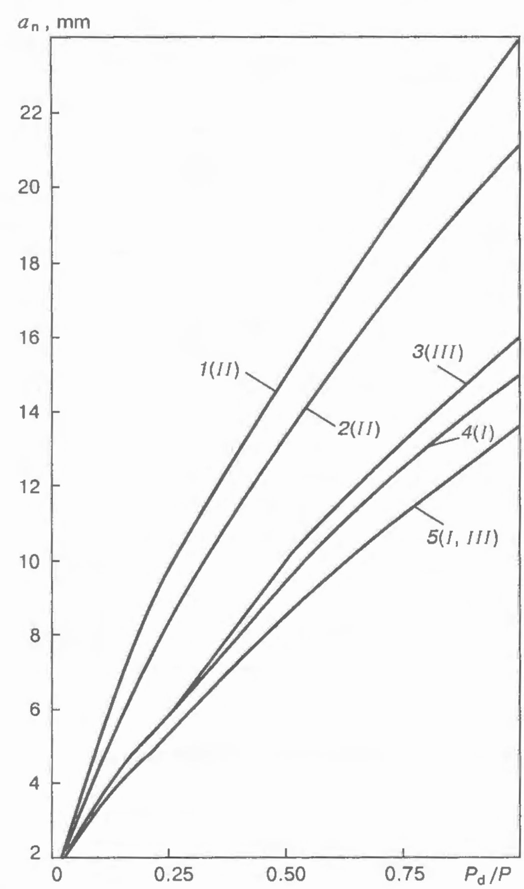

Figure 5. Effect of the ratio of pressures P_d/P on sizes a_n for scenarios *I*–*III* at $P = 5.5$ MPa, $\sigma_y = 440$ MPa, $\delta_1 = 18$ mm, $\delta_2 = 25$ mm, $K_{I_c} = 1000$ MPa·mm$^{1/2}$: *1, 3, 4* — $2R = 1420$; *2, 5* — 1220 mm

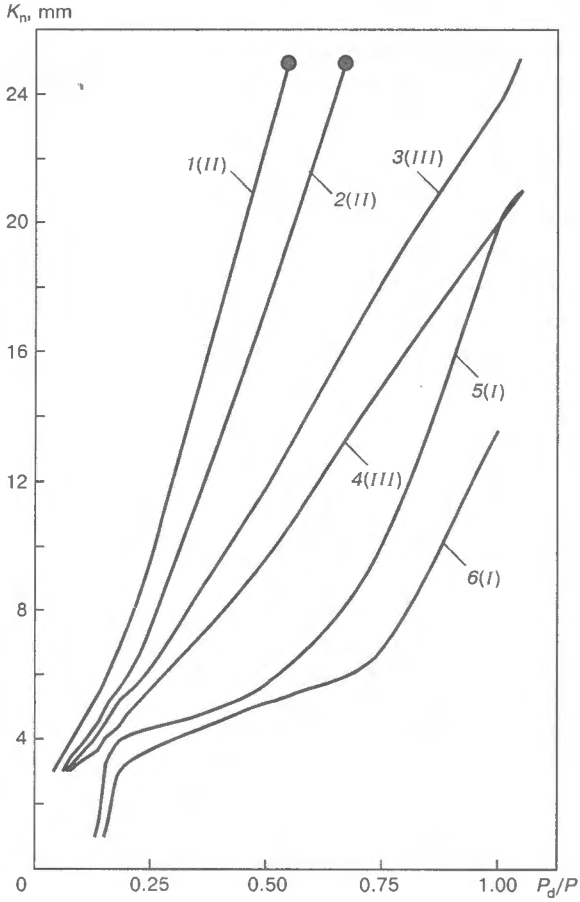

Figure 6. Effect of the ratio of pressures P_d/P on sizes K_n for scenarios *I–III* (see input data in Figure 5): *1, 3, 5* — $2R = 1420$; *2, 4, 6* — 1220 mm

$\delta_1 > 7$ mm and K_{I_c} in a range of $1000 < K_{I_c} < 1500$ MPa·mm$^{1/2}$ have no effect on a_n and K_n with all the scenarios considered, which is attributable to relatively small radial displacements the values of which are proportional to R^2.

With a diameter of the pipeline equal to $2R \geq 720$ mm, there are cases where the size of the leg of a fillet weld, K (without reinforcement) does not fit thickness δ_2 of the sleeve. Increase in strength of a material (variant with $\sigma_y = 440$ MPa) does not always lead to decrease in the required sizes of the weld, which is especially noticeable in the case of fillet welds. This is associated with increase in the role of the brittle fracture mechanism with increase in the h values at $h < h_m$.

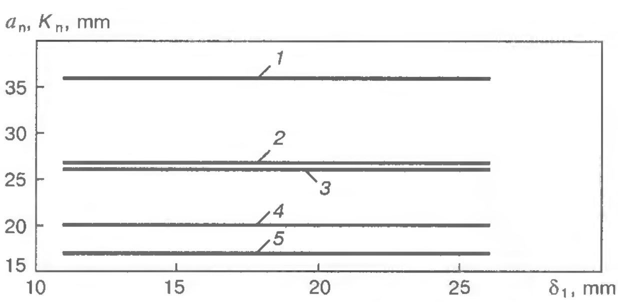

Figure 7. Effect of thickness δ_1 of the pipeline with a diameter of $2R = 1420$ mm on a_n (*2, 5*) and K_n (*1–3*) at $P = 5.5$ MPa, $\delta_2 = 28$ mm, $\sigma_y = 440$ MPa and $K_{I_c} = 1000$ MPa·mm$^{1/2}$: *1, 2* — scenario *II*; *3* — *III*; *4* — *I*; *5* — *I* and *III*

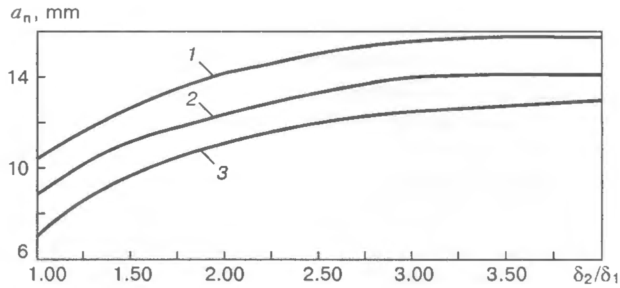

Figure 8. Effect of sleeve thickness δ_2 at a fixed value of δ_1 of the pipeline with a diameter of $2R = 1020$ mm on a_n at $P = 5.5$ MPa, $\sigma_y = 440$ MPa and $K_{I_c} = 1000$ MPa·mm$^{1/2}$ (scenario *III*): *1* — $\delta_1 = 18$; *2* — 14; *3* — 11 mm

Scenarios *I* and *III* (see the Table) require smaller sizes of the welds. Thus, scenario *II*, where a structure (see Figure 1) is mounted and welded under a working pressure that fills the sharp cavity, is most dangerous, especially for larger-diameter pipelines.

Therefore, a special study was completed to investigate a quantitative effect of pressure P_0 in welding a structure on the required sizes of the weld in pipelines of large diameters $2R = 1020–1420$ mm. Such results for scenario *II* are shown in Figure 4. The Figure also shows ranges of applicability of P_0/P that ensure meeting of the $\delta_2 \geq K$ condition for the cases of using a fillet equal-leg weld without reinforcement (curves *1–3*).

Considered also were the variants of mounting of a sleeve (T-joint) under a decreased pressure P_d and subsequent operation of this region of the pipeline under this pressure.

Examples of calculation of sizes a_n (Figure 5) and K_n (Figure 6) are given for specific pipelines. It follows from the Figures that decrease in the working pressure leads to a substantial decrease in the required sizes of the welds, whereas this is undesirable for operation of the pipeline, although may be permitted under certain conditions.

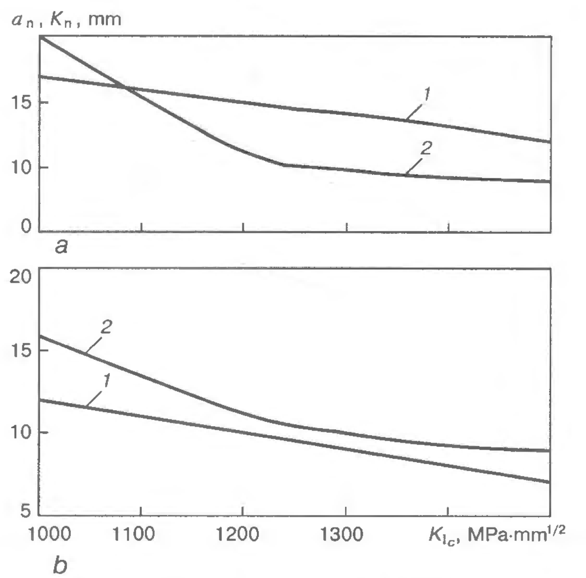

Figure 9. Effect of K_{I_c} on sizes of the weld, a_n (*1*) and K_n (*2*) at $P = 5.5$ MPa, $\sigma_y = 440$ MPa and $K_{I_c} = 1000$ MPa·mm$^{1/2}$: *a* — $2R = 1420$ mm; $\delta_2 = 28$ mm (scenario *I*); *b* — $2R = 720$ mm, $\delta_2 = 16$ mm (scenario *II*)

The Table gives limits of thickness δ_1 for the main pipe. However, the effect of the δ_1 values on the final result is not shown. At fixed values of δ_2 given in the Table and ranges of variations in values of δ_1 (ibid.) the effect of the latter on a_n and K_n is very insignificant, which is demonstrated in Figure 7. It can be well seen here that at $\delta_2 = 28$ mm, $2R = 1420$ mm and $P = 5.5$ MPa the δ_1 values ranging from $11 < \delta_1 < 26$ mm have an insignificant effect on a_n and K_n.

Considered also was the effect of δ_2 at a fixed value of δ_1 on the required sizes of the weld. Figure 8 shows this for a pipeline with $2R = 1020$ mm at $P = 5.5$ MPa and $\delta_1 = 11-18$ mm (scenario *III*). It can be seen from the Figure that increase in the ratio of $\delta_2/\delta_1 \geq 1$ is accompanied by increase in the a_n parameter. In this case the growth of a_n occurs more intensively at $\delta_2/\delta_1 = 1$ and slows down at $\delta_2/\delta_1 > 2$.

The effect of variations in the K_{I_c} values in a range of $1000 \leq K_{I_c} \leq 1500$ MPa·mm$^{1/2}$ on K_n and a_n shown in Figure 9 is indicative of the fact that the a_n values are more sensitive to this variations. It should be noted in conclusion that the calculated values of a_n and K_n are conservative enough both with a tough and brittle mechanism of the limiting state, and that the P_p values corresponding to a tough fracture at maximum stresses of about $1/2(\sigma_y + \sigma_t)$, as follows from [3–5 etc.], are underrated. Actual stresses are within a range of $\sigma_t \leq \sigma_{max} \leq S_k$ (here S_k is the stress in a rupture test), i.e. the safety factor for tough fracture is not less than 1.3–1.5.

As far as the brittle fracture is concerned, the selected values of K_{I_c} at a level of 1000–1500 MPa·mm$^{1/2}$ = (31.6–47.4) MPa·mm$^{1/2}$ provide the safety factor for the brittle fracture mechanism which is not less than the 2–2.5 times as high, the weld metal being sufficiently sound.

The above conservative character of the calculations is justifiable for such critical structures as main pipelines, and agrees with a standard design practice accepted in many countries.

CONCLUSIONS

1. The joints under consideration experience the highest loads with scenario *II*, where welding is performed at a working pressure and then the same pressure is formed in the adjoining sharp cavity.

2. Decrease in pressure in mounting of a sleeve (T-joint) to $P_0 < P$ leads to decrease in loading of the welds.

3. Decrease in pressure used for mounting of a sleeve (T-joint) and a working pressure to $P_d < P$ is a cardinal method providing decrease in loading of the welded joints.

1. *API Standard 1104*. Welding of pipelines and related facilities. Appendix B-serves welding. Publ. Sept. 1999.
2. Makhnenko, V.I., But, V.S., Velikoivanenko, E.A. (2001) Mathematical modelling of pitting defects in active oil and gas pipelines and development of a numerical methods for estimation of permissible parameters of arc welding repair of defects. *The Paton Welding J.*, **11**, 3–10.
3. Makhnenko, V.I., Ryabchuk, T.G. (1991) Computerisation of fillet welded joint design. *Avtomatich. Svarka*, **11**, 1–6.
4. Makhnenko, V.I., Ryabchuk, T.G., Pochinok, V.E. et al. (1995) Prediction of load-carrying capacity of parts of round shaft type in welding with maximum deformations. *Ibid.*, **5**, 12–16.
5. Makhnenko, V.I., Ryabchuk, T.G., Pochinok, V.E. (1996) Calculation of resistance of fillet overlap welded joint of cylindrical shells (tubes). *Ibid.*, **3**, 3–6.
6. Andrejkiv, A.E. (1982) *3D problems of theory of cracks*. Kyiv: Naukova Dumka.
7. Milne, J. (1983) Failure assessment diagrams and estimates: a comparison for ferritic and austenitic steels. *Int. J. Pressure Vessels and Piping*, **13**, 107–125.
8. Makhnenko, V.I., Velikoivanenko, E.A., Makhnenko, O.V. et al. (2000) Investigation of effect of phase transformations on residual stresses in circumferential welding of pipes. *The Paton Welding J.*, **5**, 3–8.

STRUCTURE AND TRIBOTECHNICAL CHARACTERISTICS OF COATINGS PRODUCED BY ELECTRIC ARC METALLIZING USING FLUX-CORED WIRES

V.I. POKHMURSKY[1], M.M. STUDENT[1], V.M. DOVGUNYK[1], I.I. SIDORAK[1], Yu.M. KUSKOV[2] and I.I. RYABTSEV[2]
[1]G.V. Karpenko Physical-Mechanical Institute, NASU, Lviv, Ukraine
[2]E.O. Paton Electric Welding Institute, NASU, Kyiv, Ukraine

Effectiveness of application of electric arc metallizing for restoration of worn-out parts of the machines is outlined. Adding of different components, ferrophosphorus in particular, into the charge of flux-cored wires, can decrease significantly the coefficient of friction and wear of coatings in metallizing and increase the service life of the as-restored parts.

Keywords: *electric arc metallizing, flux-cored wire, thermal coating, wear, wear resistance, coefficient of friction, phase transformations, lubricant, graphite, ferrophosphorus, calcium fluoride*

To restore and strengthen the parts of different machines, in particular shafts and axles, operating under the conditions of sliding friction, the electric arc metallizing using flux-cored wires as spraying materials is widely used [1]. The important characteristics of the coatings operating under these conditions are the coefficient of friction, and also wear of parts of a friction pair and its nature.

The aim of this work is to investigate the feasibility of development of flux-cored wires providing coatings which are characterized by high values of tribotechnical characteristics. To decrease the coefficient of friction and wear of parts being restored, the components were added to the flux-cored wire charge, which can affect actively the mentioned characteristics of the coatings produced by the method of electric arc metallizing. Graphite, ferrophosphorus Fe_3P and fluorspar CaF_2 were used as such components.

Procedure of experiments. Experimental flux-cored wires of 1.8 mm diameter were manufactured for electric arc metallizing. Powders of ferrochromeboron FKhB-2, ferrochrome FKh800, iron powder PShO, aluminium PA4, crucible graphite GT-1, fluorspar CaF_2 and ferrophosphorus Fe_3P were used as charge materials. For a sheath, a cold-rolled 0.4×10.0 mm strip of steel 08kp (rimmed) was used. Coefficient of filling of flux-cored wires was 22–23 %. Metallizer ME-2, developed by enterprise «Gazotermik» at G.V. Karpenko PMI of NASU, was used for electric arc metallizing. The conditions of arc metallizing were as follows: arc current 150 A; voltage 32–33 V; spraying with compressed air at 0.6 MPa pressure, distance from metallizer to sample — 100 mm.

Tribotechnical properties of coatings were studied in unit SMTs-2 by disc–block scheme at boundary sliding friction using procedure, described in [2], at contact pressure 5 MPa. Oil M14V2 was used as lubricant. Temperature in the friction zone was measured by a C-A thermocouple, whose junction was located at 0.5 mm distance from the working surface of a mating body. Coatings were deposited on a cylindrical surface of samples in the form of a 40 mm diameter 10 mm thick disc, made from steel 45 of hardness HRC_e 30–32. Coatings were ground to 1 mm thickness and roughness $R_a = 0.63$. Mating bodies in the form of blocks were made from bronze Br.S-30. During investigations the coefficient of friction, wear of sample and mating body, temperature of heating in the friction zone were determined.

Phase composition of coatings in initial state, its changes in near-surface layers after grinding and tests in sliding friction were examined in diffractometer «Dron-3» (radiation CuK_α, U = 32 kV, I = 13 mA) with 0.05° scanning pitch and subsequent computer processing. Rate of scanning was 1°/min, angle of sample inclination to radiation was 1°.

Metallographic examinations of coatings were realized in microscope «Neophot-2». In examination of microstructure of coatings the colour etching was used. Mixture of nitric and picric acids was used as an etching agent [3].

Experimental data and their discussion. Tribotechnical characteristics of coatings deposited by flux-cored wires, whose charge components and estimated chemical composition of coatings are given in Table 1, were investigated. Flux-cored wire FMI-2 [1], which is used for restoration of crankshafts of internal combustion engines by the method of electric arc metallizing, was selected as basic (Table 1, wire No.1). Charge of flux-cored wire FMI-2 consists of a mixture of master alloy of ferrochromeboron (FKhB-2) and aluminium. Ferrophosphorus was added, except aluminium and ferrochromeboron, to the composition of charge of flux-cored wire No.2. Unlike two first flux-cored wires, ferrochrome FKh800 was selected as a base of charge of wires Nos.3–5. As a reference, samples of steel 45 of hardness HRC_e 51–53 were tested.

Table 1. Composition of charge of experimental flux-cored wires and chemical composition of coatings

No. of flux-cored wire and coating	*Composition of charge of flux-cored wire*	*Elements in coating (estimated), wt.%*							
		Cr	*B*	*Al*	*C*	*P*	*Si*	*Ca*	*Fe*
1	FKhB-2 (base) + Al	5.6	3.0	8.80	–	–	0.36	–	Residue
2	FKhB-2 (base) + Fe_3P + Al	4.7	2.5	5.50	–	1.1	0.30	–	Same
3	FKh800 (base) + C + Al + Fe	8.5	–	0.45	2.15	–	0.25	–	»
4	FKh800 (base) + Fe_3P + Al	7.2	–	5.50	0.90	1.1	0.20	–	»
5	FKh800 (base) + CaF_2 + Al	7.2	–	5.50	0.90	–	0.20	2.9	»

It was established as a result of investigations, that coefficient of friction μ is negligibly increased with time for reference friction pair: steel 45–bronze Br.S-30 and stabilized at the 0.09 level (Figure 1, *a*). Similar relationship is observed also for the temperature in the friction zone (set temperature is equal to 45 °C) (Figure 1, *b*).

Coefficient of friction is somewhat lower, 0.07, for the pair of friction: coating No.1–bronze Br.S-30, and the temperature is stabilized at the 60 °C level. Adding of master alloy FKhB-2 and ferrophosphorus to the charge of flux-cored wire No.2 leads to a little increase in coefficient of friction and temperature of friction pair.

The most interesting results were obtained for coatings sprayed by flux-cored wires, whose charge was based on ferrochrome FKh800. Flux-cored wires with additions of graphite and ferrophosphorus (Nos.3 and 4) produce coatings with coefficients of friction equal to 0.018–0.023 that is 4–5 times lower than in pair: steel 45–bronze Br.S-30, and 3–4 times lower than in pair: coating No.1–bronze Br.S-30 (Figure 1, *a*). Here, the set temperature in the zone of friction of coating No.4–bronze Br.S-30 is 25 °C, and the similar characteristic for pair of friction: coating No.3–bronze Br.S-30 somewhat exceeds 40 °C (Figure 1, *b*).

In coating, produced in spraying of flux-cored wire No.5, whose charge contains calcium fluoride CaF_2, firstly the abrupt increase in coefficient of friction up to 0.12, and then its decrease to 0.025 is observed. The same nature is typical of curve of changing the temperature of samples. With increase in friction coefficient to maximum value the temperature is increased up to 90 °C, and then it is decreased to about 45 °C and stabilized.

According to test results (friction path is 10000 m) the lowest wear was observed in coatings Nos.1, 3 and 4, and the highest – in coating No.5 (Figure 2, *a*). Test sample of bronze is subjected to wear to a less extent in the pair with coating from flux-cored wire No.4, containing ferrophosphorus (Figure 2, *b*). The lowest total wear in pair with bronze was observed for coatings Nos.3 and 4.

Structure and phase composition of coatings. Formation of primary structure in the coating depends mainly on composition of components of charge of the flux-cored wires. The presence of carbon in the flux-cored wire both in the form of graphite and bound in carbides in ferrochrome leads to the appearance of residual austenite in the coating. It is shown in [4] that increase in a mass share of carbon in the coating from 0.3 to 1.3 % leads to the increase in amount of residual austenite from 10 to 80 %.

Graphite contained in charge of wires is dissolved partially in drops in wire melting, blown away partially by a compressed air or burnt out [5]. In coating formation the remained graphite is available in a free state in lamellas in the form of inclusions of a spherical shape (Figure 3, *c*).

Ferrophosphorus, reacting actively with a melt of flux-cored wire sheath, forms eutectics, distributed uniformly in lamellas which compose coating. In addition, ferrophosphorus stabilizes α-Fe and with increase in its content in the flux-cored wire charge, the amount of ferritic component in the coating is increased. Combined action of phosphorus and aluminium (also ferrite stabilizer) leads to the fact that the alloyed ferrite becomes a matrix phase of the coating (Table 2).

In melting with flux-cored wire No.5, CaF_2 is not dissolved in a metal matrix of the coating, but it is arranged along the boundaries of crystallized drops (Figure 3, *e*), thus deteriorating drastically the strength of coating (90 MPa). Calcium fluoride does

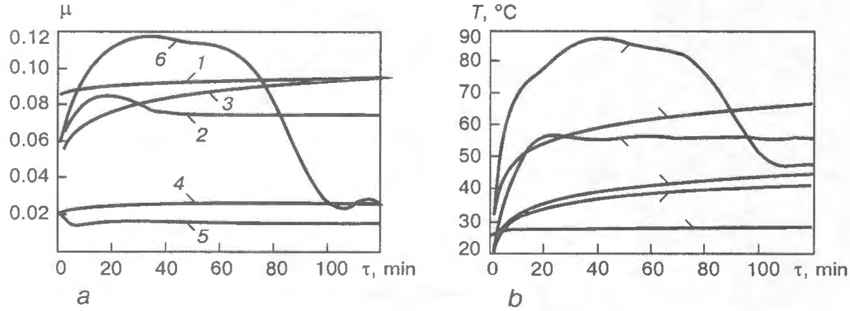

Figure 1. Change in coefficient of friction (*a*) and temperature in friction zone (*b*) of coatings Nos.*1*–*5*; *6* – reference sample of steel 45

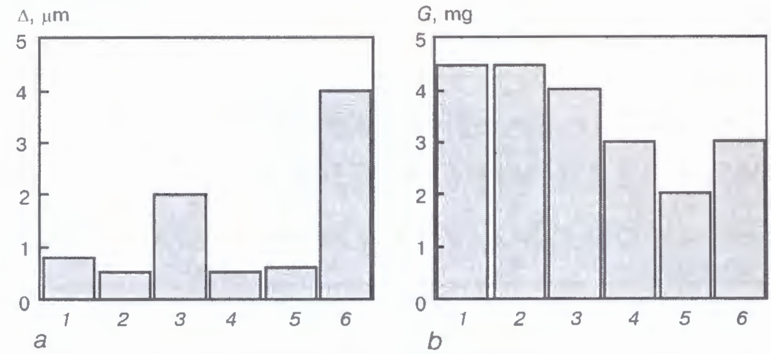

Figure 2. Wear of samples Δ (*a*) and mating bodies *G* (*b*) in pairs of friction: coatings Nos. *1*–*5*–bronze Br.S-30; *6* — steel 45–bronze Br.S-30

not interact with a metal matrix of the coating and does not change its phase composition.

As is known [6, 7], in materials, the structure of which is far from equilibrium, a part of energy released in friction is dissipated in the form of heat into environment, and another part is used for the formation of new structures in a near-surface layer, i.e. a self-organizing of the near-surface layer is occurred. In other words, the phenomenon of structure adaptation of surface layer in the process of friction is realized.

In electric arc metallizing the temperature of molten drops reaches 2200–2500 °C, and their crystallization is occurred during a short period of time ($1\cdot10^{-3}$ s). This results in the formation of a heterogeneous coating at the surface, consisting of an oversaturated solid solution and metastable phases, being far from structural and phase equilibrium. In our opinion, the structural and phase self-organizing of electric arc coatings at the boundary friction occurs as follows.

According to results of phase X-ray diffraction analysis (Table 2), the matrix phase in coating sprayed with flux-cored wire No.1 consists of alloyed solid solution on α-Fe base, there is a negligible amount of borides Fe_2B and FeB, and also nitrides and oxides (Figure 3, *a*).

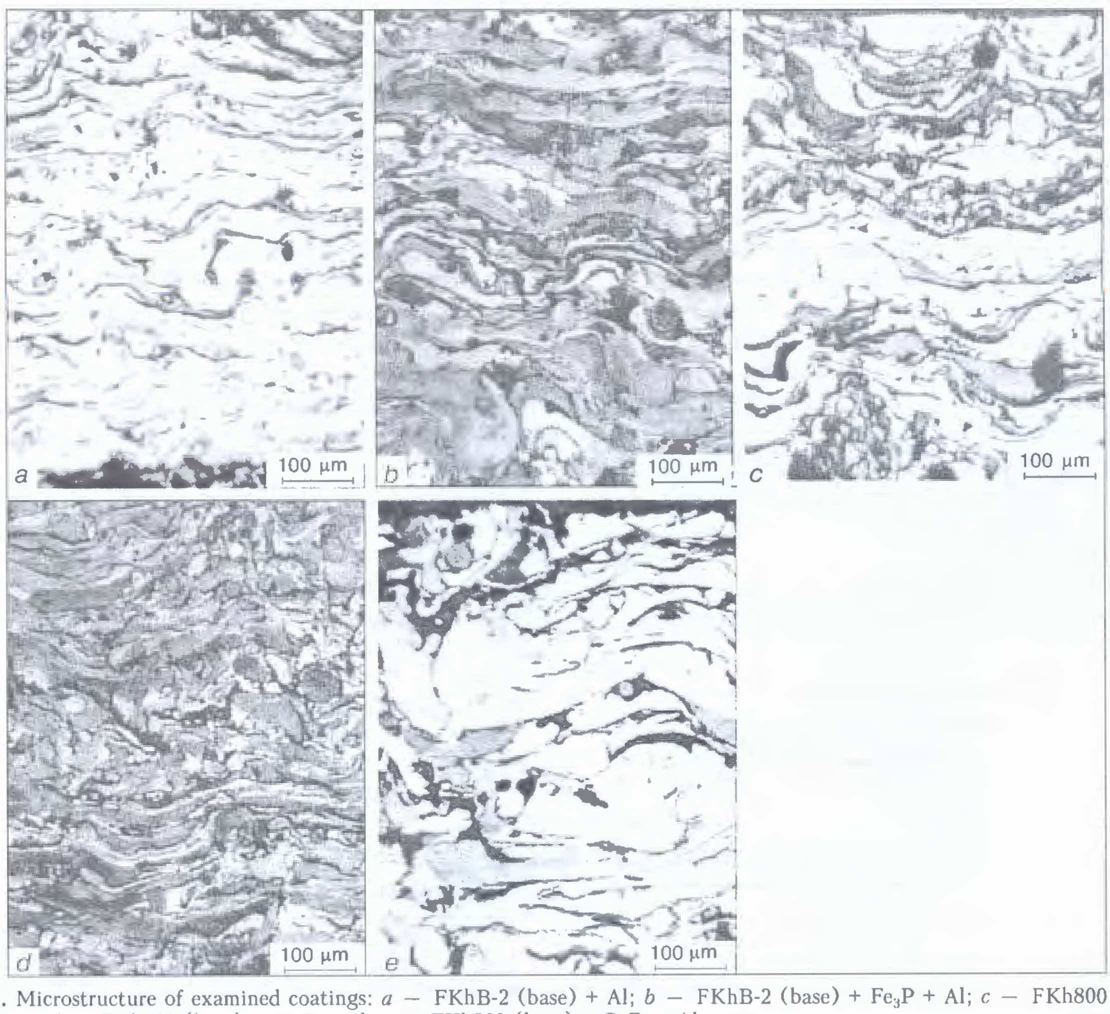

Figure 3. Microstructure of examined coatings: *a* — FKhB-2 (base) + Al; *b* — FKhB-2 (base) + Fe_3P + Al; *c* — FKh800 (base) + C + Al + Fe; *d* — FKh800 (base) + Fe_3P + Al; *e* — FKh800 (base) + CaF_2 + Al

Table 2. Phase composition of coatings

No. of coating	*Composition of charge of flux-cored wire*	*Initial state*		*After friction*	
1	FKhB-2 (base) + Al	α-Fe	Main phase	α-Fe	Main phase
		Fe_2B, FeB	Negligible amount	FeB	Large amount
		CrB	Traces	CrB	Traces
		CrN		CrN	
		FeO		FeO	
		Fe_2O_3		Fe_2O_3	
2	FKhB-2 (base) + Fe_3P + Al	α-Fe	Main phase	α-Fe	Main phase
		FeB	Traces	Fe_3Al	Large amount
		Fe_2P		Al_2O_3	Traces
		FeP		Fe_2P	
		Al_2O_3		FeB	
		Fe_2O_3			
3	FKh800 (base) + C + Al + Fe	γ-Fe	Main phases	γ-Fe	Main phases
		α-Fe	α-Fe/γ-Fe = 3/2	α-Fe	α-Fe/γ-Fe = 1/1
		$Me_{23}C_6$	Traces	$Me_{23}C_6$	Large amount
		CrN		CrN	Traces
		Fe_2O_3		Fe_2O_3	
		Cr_2O_3		Cr_2O_3	
		C		C	
4	FKh800 (base) + Fe_3P + Al	α-Fe	Main phase	α-Fe	Main phases
		Fe_2P	Traces	C	
		CrN		FeAl	Large amount
		Al_2O_3		Me_7C_3	Traces
		Fe_2O_3		Al_2O_3	
		Cr_2O_3		Fe_2O_3	
				Cr_2O_3	
				Me_2O_3	
5	FKh800 (base) + CaF_2 + Al	α-Fe	Main phases	α-Fe	Main phases
		γ-Fe	α-Fe/γ-Fe = 3/2	C	
		Me_3C	Traces	γ-Fe	Large amount
		CaF_2		FeAl	
		CrN		CaF_2	Traces
		Al_2O_3		CrN	
		Cr_2O_3		Al_2O_3	

Proceeding of diffusion process becomes possible in the process of friction in a surface layer of up to 20 μm thickness due to a local temperature burst. A large amount of the new phase, FeB, is formed, leading to the increase in wear-resistance of the coating. Thus, the part of heat energy is used for self-organizing of the surface layer in a friction interaction. Coefficient of friction is high enough (0.075).

Coating No.3 contains graphite, which can be used as a lubricant. Matrix of this coating consists of a solid solution on γ- and α-Fe base at ratio of γ-Fe/α-Fe = 3/2, the traces of carbides, nitrides, graphite and oxides are observed (Table 2, Figure 3, *c*). At friction interaction, the processes are proceeding in a surface layer of up to 10 μm thickness which are similar to those occurring in tempering of alloy steels, in particular carbides $Me_{23}C_6$ are precipitated from a solid solution on γ-Fe base, austenite is depleted with alloying elements and transformed into a temper martensite. More hard phases with a higher wear resistance than in initial state are formed in the surface layer due to a phenomenon of structural adaptation during friction. The presence of graphite in this composition leads to the reduction in coefficient of friction to 0.018–0.020.

A significant difference in tribotechnical characteristics of coatings produced in spraying wires Nos.2 and 4, whose charge contains ferrophosphorus, can be explained as follows. There are elements in both types of coatings, which stabilize ferrite, in particular phosphorus and aluminium. Due to this, the matrix phase of coatings consists of an alloyed solid solution on α-Fe base. However, there is a difference in composition and amount of a strengthening phase of the coating. The strengthening phase in the coating No.2 consists of FeB and Fe_2P (Figure 3, *b*), while in coating No.4 it consists mainly of Fe_2P (Figure 3, *d*).

In the presence of a limited amount of isolated strengthening phosphide inclusions in coating No.4, having higher hardness than that of a ductile matrix, the coefficient of friction and wear have the lower values. At a contact loading in this case the load is distributed on hard inclusions, providing a low coefficient of friction and high resistance of adhesion. Relatively ductile base allows system to take the geometry of contact in the shortest period that decreases the feasibility of appearance of local sources of high pressure, leading to the occurrence of a spalling or adhesion [8]. A certain effect on decrease in friction coefficient can be exerted by the fact the large amount of graphite is formed in coating No.4 after friction that can be used as a lubricant. Probably, this coating by these reasons has the best tribotechnical characteristics.

In coating No.2, whose composition of strengthening phase includes FeB and Fe_2P, the increase in amount of a hard strengthening phase reduces abruptly the ductility of the working layer that leads to the formation of spallings in wear, playing the role of an abrasive, and increasing also the coefficient of friction, wear of sample and mating body.

Coating, containing CaF_2, was produced using flux-cored wire No.5. Phase composition of this coating is a solid solution on α- and γ-Fe base, inclusions of carbides Me_3C, calcium fluoride CaF_2 and oxides (Table 2). As the coating contains a large amount of aluminium (ferritizer), then the structure of coating consists of an alloyed ferrite. Calcium fluoride in the coating structure is presented in the form of black inclusions located at the boundaries of lamellas (Figure 3, *e*).

Process of self-organizing of the coating surface layer in friction is realized as follows. At the initial moment of friction a thin film CaF_2 is formed at the surface. Here, at the first 40 min of friction the coefficient of friction and temperature are increased, respectively from 0.06 to 0.12, and from room temperature to 90 °C. At next testing the decrease in coefficient of friction to 0.02, and the temperature to 45 °C and their stabilizing at this level are observed. Phase analysis of surface layer after tests shows that it contains a large amount of a free graphite and FeAl. It is evident that firstly a free graphite is precipitated from alloyed ferrite in heating during the process of friction, then aluminium is precipitated, forming FeAl in interaction with iron.

Thus, the use of CaF_2 in electric arc coatings is not effective as the thin film of CaF_2, formed at the surface at the initial moment of friction, leads to the increase in coefficient of friction and temperature, and only after some time, when a sufficient amount of free graphite is appeared in the surface layer, the coefficient of friction and temperature are decreased. Besides, such coating is produced more coarse-dispersed (Figure 3, *e*) and has a low strength.

As is seen from experimental data, the high wear resistance and low coefficient of friction are stipulated by the phenomenon of structural adaptation of surface layers of the coatings.

CONCLUSIONS

1. In electric arc metallizing the coatings are formed with a non-equilibrium structure. As a result, a part of heat, generated in the process of friction, is used for the formation of new structures in the near-surface layer, i.e. self-organizing of the surface layer is occurred, in other words the phenomenon of structural adaptation of surface layer in the process of friction is realized.

2. It was established in investigation of tribotechnical coatings that wear resistance and coefficient of friction of the latter depend on phenomenon of structural adaptation of their surfaces. In case, when the self-organizing of surface layer leads only to the formation of strengthening and more wear-resistant phases, the wear resistance is increased, but the coefficient of friction remains high enough. In case of simultaneous precipitation of strengthening phases and lubricant, for example graphite, the high wear resistance is combined with a low coefficient of friction.

3. The investigations showed the challenging use of ferrophosphorus in charge of flux-cored wires for electric arc metallizing to increase the tribotechnical characteristics of the sprayed coatings.

1. Pokhmursky, V.I., Student, M.M., Dovgunyk, V.M. et al. (2002) Flux-cored wires of FeCrB + Al and FeCr + Al + C systems for electric arc metallizing. *The Paton Welding J.*, **3**, 28–31.
2. Pokhmurskii, V., Student, M., Dovhunyk, V. et al. (2002) Wear resistance arc-sprayed coatings from powder wires. In: *Proc. of Int. Thermal Spray Conf. ITSC-2002*, Essen, March 4–6, 2002.
3. (1972) *Metallography of iron*. Vol. 1. Fundamental metallography. Ed. by F.N. Tavadze. Moscow: Metallurgiya.
4. Dovgunyk, V.M., Student, M.M., Sidorak, I.J. et al. (2000) Influence of friction on structure-phase transformations in near-surface layer of FeCr + Al + C thermal coating. *Fiz.-Khim. Mekhanika Materialiv*, **5**, 113–116.
5. Student, M.M. (1998) Burning-out of flux-cored wire charge components in deposition of coatings by electric arc metallisation. In: *Proc. of 4th Int. Conf.-Exhibition on Problems of Corrosion and Anticorrosive Protection of Materials «Corrosion-98»*. Lviv: G.V. Karpenko FMI.
6. Kostetsky, B.I., Nosovsky, I.G., Karaulov, A.K. et al. (1976) *Surface resistance of materials in friction*. Kyiv: Tekhnika.
7. Tushinsky, L.I., Plokhov, A.V. (1986) *Investigation of structure and physical-mechanical properties of coatings*. Novosibirsk: Nauka.
8. Ryabtsev, I.I., Kuskov, Yu.M., Grabin, V.F. et al. (2003) Tribological properties of the Fe–Cr–Mn–P system deposited metal. *The Paton Welding J.*, **6**, 16–20.

ANALYSIS OF STRUCTURAL STATE OF WELD METAL PRODUCED BY USING WELDING WIRES OF THE FERRITIC-PEARLITIC GRADE

V.F. GRABIN, V.V. GOLOVKO, T.G. SOLOMIJCHUK, E.I. GONCHARENKO and **V.A. KOSTIN**
E.O. Paton Electric Welding Institute, Kyiv, Ukraine

It is shown that alloying of low-carbon weld metal with manganese leads to formation of a small amount of pearlite and up to 40–50 vol.% of acicular ferrite in it. Owing to a high acicular ferrite content, weld metal of the Fe–Mn–Mo–Ni alloying system is characterised by a higher level of mechanical properties than weld metal of the Fe–C–Mn alloying system.

Keywords: *low-alloy steels, alloying elements, structural components, non-metallic inclusions, carbon equivalent*

Low-alloy steels are among the most extensively used structural materials. The problem of welding this grade of steels is remaining topical starting from the middle of the 1950s. As shown by results of numerous studies completed in this field, acicular ferrite (AF) is the main structural component that ensures an optimal combination of strength and ductility of weld metal of the ferritic-pearlitic grade. The weld metal with a content of manganese equal to 1.7 wt.% is reported to contain 55–60 vol. % of AF [1]. To increase the share of AF (to more than 60 vol. %), it is necessary to alloy the weld metal with nickel and molybdenum [2]. A technology developed in the middle of the 1960s on the basis of the studies provided for the use of filler metal in the form of welding wires alloyed with manganese, molybdenum and nickel. This technology resulted in the weld metal with high mechanical properties. At the same time, it had a substantial drawback consisting in the fact that it could not ensure a sufficient brittle fracture resistance of welded joints. To eliminate this drawback, welding of high-strength steels is performed using pre- and concurrent heating or wires of the austenitic grade.

The advancement of industry and the associated increase of requirements to the base metal of welded structures led to emergence early in the 1970s of low-alloy steels with a low carbon content. Decrease in the carbon content to 0.080–0.150 wt.% made it possible to substantially raise toughness and brittle fracture resistance of low-alloy steels.

Modern low-alloy steels are sophisticated high-technology products. As such, during the manufacturing process they are subjected to integrated metallurgical and thermal effects. Figure 1 [3] gives the list of the strengthening mechanisms used currently to produce high-strength low-alloy steels of the ferritic-pearlitic grade. As seen from the Figure, it is enough to provide strengthening of solid solution with manganese and silicon to produce steels with a yield stress of up to 275 MPa. At the same time, to produce metal with a higher level of strength properties, it is necessary to subject rolled products to thermomechanical treatment and harden a structure by microalloying; and to provide $\sigma_{0.2}$ > 400 MPa it is necessary to use dispersion strengthening or even dislocation hardening. These are the processes that occur at a sub-microscopic level, and the common practice to control them consists in using inclusions 10–100 nm in size. It should be noted that results of the studies and practice proved the expediency of adding small inclusions also to the weld metal [4]. At present, there are the cases where it is difficult to discriminate dislocation hardening caused by inclusions of about 10 nm in size from strengthening of solid solution due to deformation of ferrite lattice by interstitial atoms.

Welding steels with such a complicated system of alloying, modifying and refining requires a corresponding increase in mechanical properties of the weld metal. Therefore, to provide toughness and ductility of the weld metal at a level of high-strength low-alloy steels, it is necessary to know whether it is possible to use simultaneous alloying with manganese, molybdenum and nickel. As the main factor determining mechanical properties of the weld metal is structure, to solve this problem it is reasonable to focus on the composition of structural components of the weld alloyed with manganese, molybdenum and nickel.

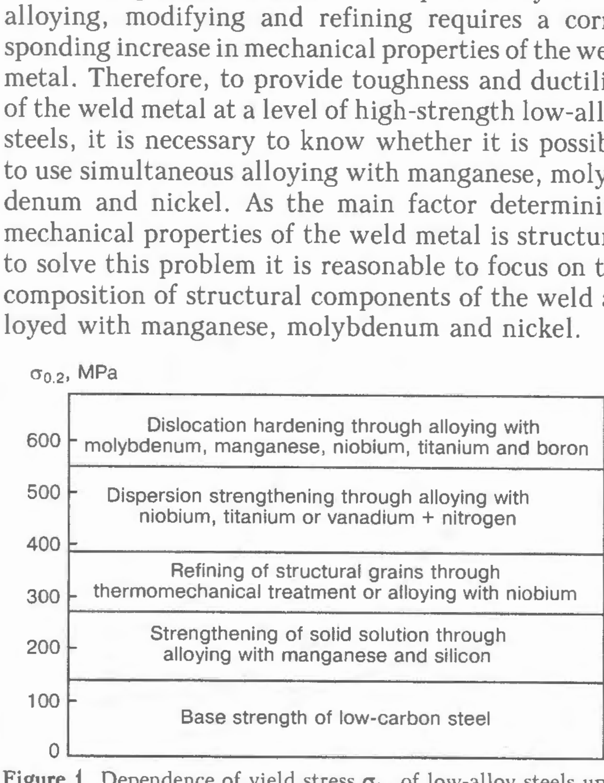

Figure 1. Dependence of yield stress $\sigma_{0.2}$ of low-alloy steels upon the method of their technological metallurgical treatment

Table 1. Chemical composition of weld metal

Weld No.	Content of elements, wt.%				
	C	Si	Mn	Mo	Ni
1	0.090	0.38	0.50	–	–
2	0.087	0.39	0.75	–	–
3	0.090	0.41	0.97	–	–
4	0.076	0.49	1.00	–	–
5	0.082	0.33	1.47	–	–
6	0.079	0.32	1.75	–	–
7	0.092	0.33	1.95	–	–
8	0.084	0.37	2.23	–	–
9	0.080	0.45	1.68	0.31	0.05
10	0.076	0.28	1.02	0.23	0.09
11	0.099	0.39	1.53	0.29	0.38
12	0.068	0.48	1.28	0.22	0.67
13	0.068	0.47	1.42	0.24	0.75
14	0.100	0.37	1.21	0.20	0.75

The purpose of this study was to investigate the possibility of increasing the content of tough structural components in metal of the low-alloy steel welds. Investigated were specimens of metal of multipass welds (deposited metal) made by automatic submerged-arc welding using low-alloy welding wires with a diameter of 4 and 5 mm at a heat input of 37–43 kJ/cm. The investigations were conducted by the IIW procedure [5], which included comparative evaluation of phase and structural composition, measurement of hardness and evaluation of mechanical properties of the weld metal. The content of such structural components as pearlite, bainite and different morphological forms of ferrite, the presence of which in the weld metal exerts a marked effect on its performance, was estimated. Welded joints were made by using wires containing carbon, manganese, molybdenum and nickel (Sv-08GA, Sv-10G2, Sv-08GM, Sv-10GNM), combined with alloying agglomerated fluxes of an increased basicity (BI = 1.2–2.3). Welds with metal containing carbon in a range of 0.076–0.100 wt.% were selected for the investigations. Two series of experimental welds were made. Weld metal of the first series of experiments (No.1–8) differed only in a level of alloying with manganese (0.50–2.23 wt.%). Weld metal of the second series of experiments (No.9–14) contained also nickel and molybdenum, in addition to manganese (Table 1).

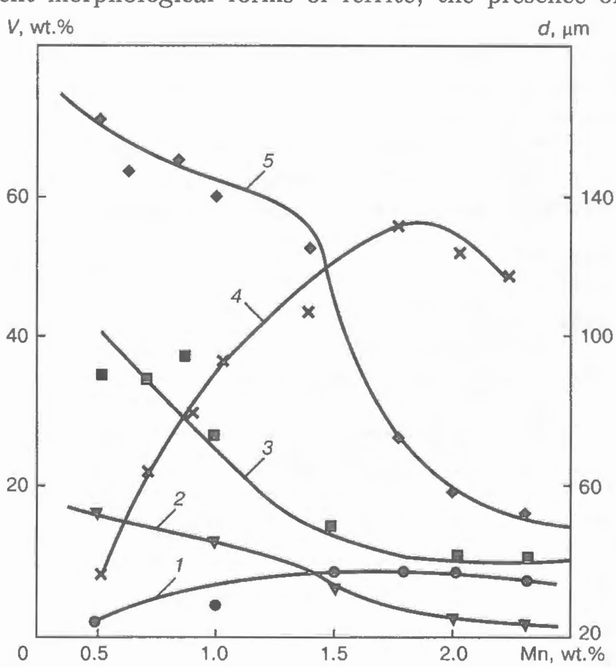

Figure 2. Effect of weight fraction of manganese in weld metal on austenite grain size d (*5*) and content of structural components: *1* — MAC-phase; *2* — P; *3* — PF; *4* — AF

As shown by the metallography results, structure of the weld metal of the above two series consisted of polygonal ferrite (PF), Widmanstaetten ferrite (WF), AF, pearlite (P) and the so-called laminated forms of ferrite (LF). According to the IIW classification, the latter included ferrite with an ordered and unordered secondary phase and a martensite-austenite-carbide phase (MAC-phase).

Quantitative analysis of structural composition of the first series of the welds, the results of which are shown in Figure 2, allows a conclusion that alloying of the weld metal with manganese causes decomposition of the major part of austenite during the cooling process to occur in high-temperature and intermediate ranges, this leading to formation of a considerable amount of P, PF and AF. Depending upon the level of alloying with manganese, the WF content of the weld metal may amount to 5 vol.%. The volume fraction of AF is maximal in the welds alloyed with 1.75 wt.% Mn. Increase in the manganese alloying level is accompanied by increase in the bainite (B) content and hardening of ferrite, whereas in the case of decrease in the manganese content the volume fraction of AF decreases as a result of an increased content of PF and WF. The latter structural component is usually formed in the regions that adjoin boundaries of initial austenite grains, while polygonal ferrite precipitating along the boundaries serves as a sort of a substrate on which the WF component forms and grows. Alloying the weld metal with manganese is accompanied by refining of austenite grain and some change of proportion of the secondary structure components.

It is reported [6] that manganese has a non-uniform distribution in structure of the weld metal. As a rule, part of it is in a fixed form (carbides and sulphides) and part is in iron solid solution, this leading to its hardening. Manganese is distributed between carbides and solid solution in a ratio of about 1 to 4, i.e. its content in solid solution is approximately 4 times as high as in carbides. In Fe–Mn alloys with a low carbon content, manganese often forms not pure carbides but complex compounds of the $(FeMn)_3C$ type, where iron and manganese atoms partially replace each other. Mechanical properties of such a metal are determined not only by the structural factors, but also

Table 2. Structural composition of metal of the second series of experimental welds

Weld No.	Content of structural components, vol.%						
	PF	WF	P	LF	AF	B	MAC-phase
9	20	8	2	22	32	3	13
10	19	6	–	19	41	2	13
11	10	2	–	12	60	–	18
12	6	1	–	10	68	–	15
13	13	1	–	10	62	2	12
14	16	–	–	8	64	–	12

by the degree of hardening of solid solution with manganese. Increase in the manganese content of solid solution leads to decrease in toughness of the weld metal. In the course of our investigations this conclusion was confirmed by the hardness measurement results shown in Figure 3. It can be seen from the Figure that hardness of the weld metal steadily grows with increase in the mass fraction of manganese. In addition, this also causes increase in the content of stronger structural components and refining of grains in structure of the weld metal (see Figure 2).

As follows from [7], a substantial improvement of toughness of the weld metal can be achieved through alloying it with elements that affect kinetics of decomposition of austenite during the process of continuous cooling of a welded joint. These elements include manganese, chromium, molybdenum and nickel. Moreover, combinations of welding consumables and parameters should be selected so that the weld metal has a minimum content and a high degree of dispersion of non-metallic inclusions (NMI).

Like manganese, molybdenum also favours refining of austenite grains and shift of the temperature range of austenite decomposition to an intermediate region. This is accompanied by decrease in the volume fraction of PF interlayers and their thickness along the crystalline grain boundaries. An insignificant addition of molybdenum leads to decrease in the cold shortness threshold of iron and causes almost no decrease in toughness of ferrite. Chromium has a similar effect. Nickel leads to formation of AF in the weld metal. Unlike the majority of alloying elements, it increases a cleavage fracture resistance of metal [8]. However, it should be noted that at a high nickel content the martensite component of the MAC-phase may be partially replaced by austenite, this resulting

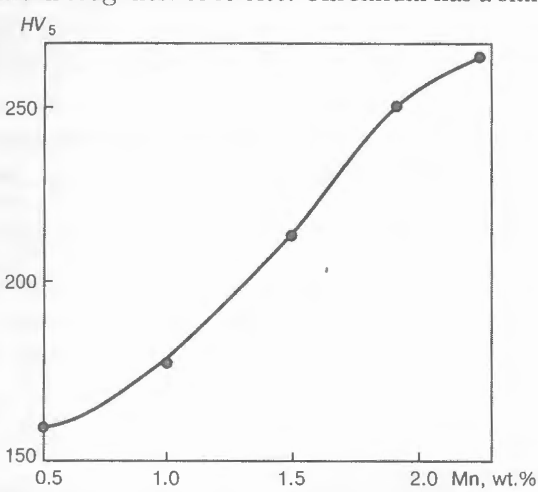

Figure 3. Effect of manganese content on weld metal hardness

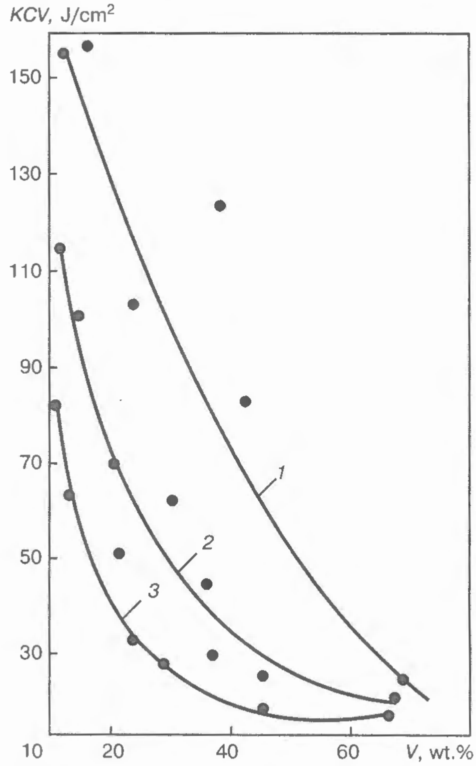

Figure 4. Effect of total content of PF and WF in structure of the weld metal on the level of its impact toughness KCV at different test temperatures: *1* — T_{test} = +20; *2* — –20; *3* — –40 °C

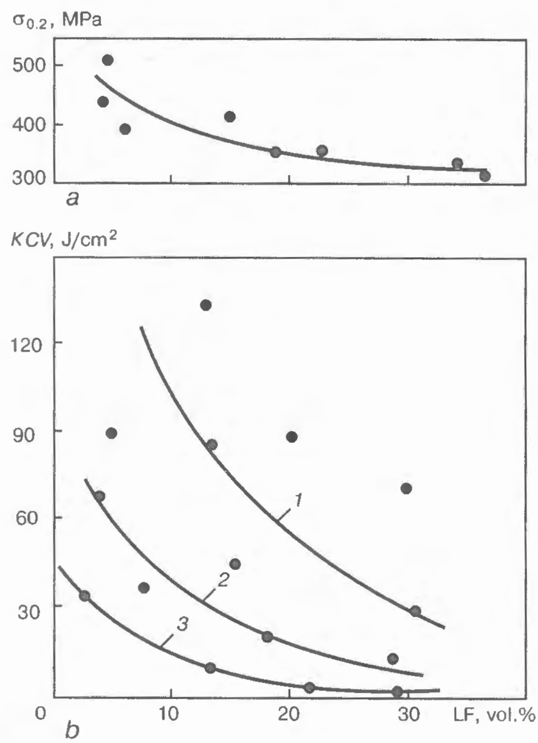

Figure 5. Effect of LF content of the weld metal on its yield stress $\sigma_{0.2}$ (*a*) and impact toughness KCV (*b*): *1–3* — see Figure 4

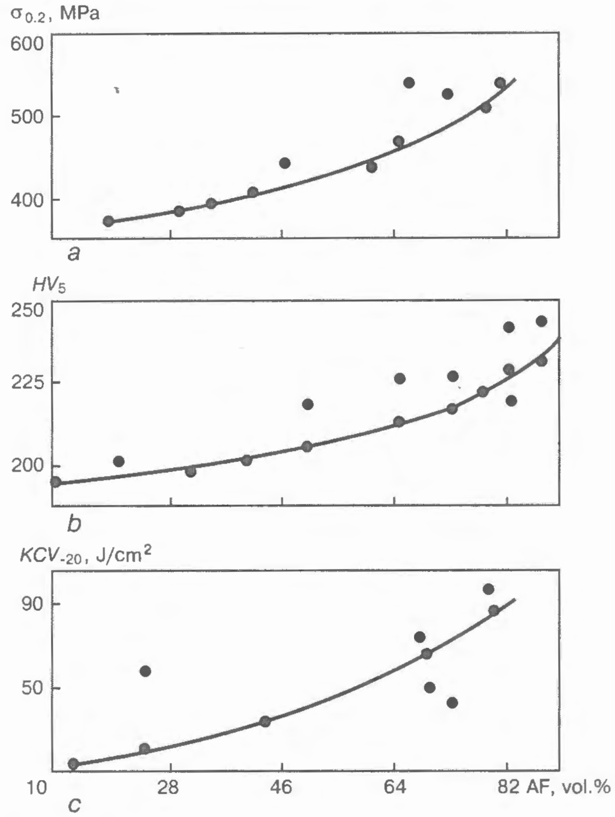

Figure 6. Effect of AF content of weld metal on its mechanical properties: *a* — yield stress $\sigma_{0.2}$; *b* — hardness HV_5; *c* — impact toughness KCV_{-20}

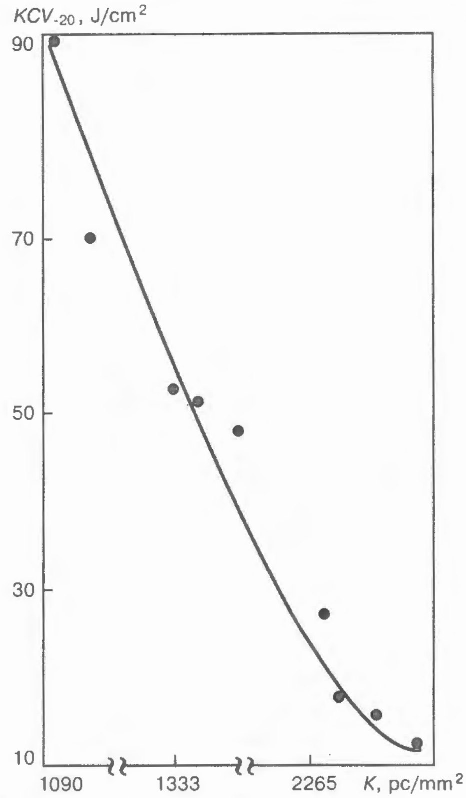

Figure 7. Effect of the content of NMI in weld metal on impact toughness KCV_{-20}

in growth of toughness of the weld metal and a simultaneous decrease it its strength.

As shown by the results of metallography (Table 2) of metal of the second series of the welds containing manganese, its alloying with minor additions of nickel and molybdenum leads to a change in the amount of structural components. Compared with metal of the first series of the welds, metal of the second series of the welds is characterised by an increased volume fraction of AF and MAC-phase, a decreased content of LF (with both ordered and unordered second phase), PF and WF. In this case the process of formation of pearlite is fully suppressed.

Mechanical properties of metal of these welds depend upon the relative volume content of structural components. The data shown in Figure 4 prove the known fact of a negative effect of structural components of PF and WF on impact toughness of the weld metal under low temperature conditions. Variation in strength properties of the weld metal also takes place in this case (Figure 5). It should be noted that increase in the LF content does not have such a marked effect on strength characteristics as the PF and WF contents do. Most probably that this is associated with a lower temperature of formation of LF.

Therefore, as shown by the investigation results, alloying of the weld metal with the Mn–Mo–Ni system allows some mitigation of the negative effect exerted by the PF and WF structures on its mechanical properties. At the same time, this provides increase in the AF content and a corresponding improvement of metal toughness. Analysis of the data given in Table 2 and Figure 6 indicates that increase in the AF content of the weld metal to more than 60 vol.% has a substantial effect on mechanical properties of the

Table 3. Oxygen content and size distribution of NMI in weld metal

Weld No.	*NMI, vol.%*	*Amount of inclusions of the following sizes, μm, in 1 mm²*							*[O], wt.%*
		≥ 1.0	*1.1–1.5*	*1.6–2.0*	*2.1–2.5*	*2.6–3.0*	*3.1–4.9*	*≥ 5.0*	
9	0.445	1478	1081	235	105	36	23	1	0.057
10	0.382	1256	931	203	76	22	21	3	0.089
11	0.473	1553	1149	244	100	36	22	2	0.051
12	0.445	1500	1124	210	106	27	31	2	0.082
13	0.419	1412	1043	234	93	25	15	2	0.075
14	0.424	1256	931	203	76	22	21	3	0.060

Note. Content of hydrogen and nitrogen in weld metal of specimens investigated was 0.00004 and 0.01500 wt.%.

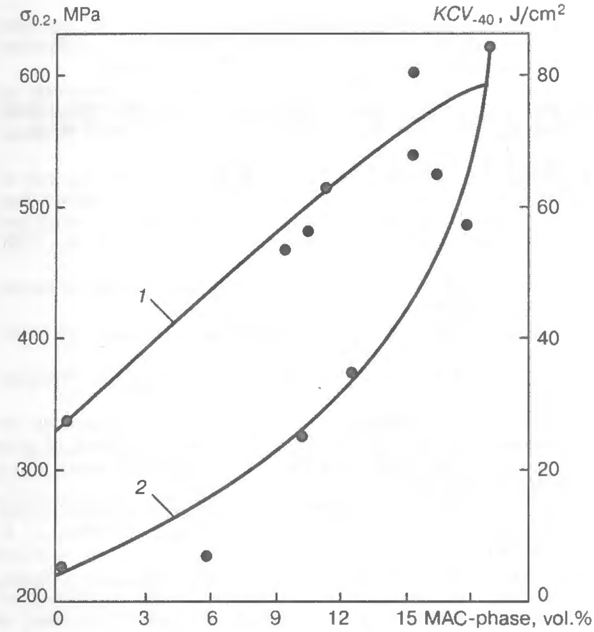

Figure 8. Effect of the MAC-phase content of weld metal on impact toughness KCV_{-40} (*1*) and yield stress $\sigma_{0.2}$ (*2*)

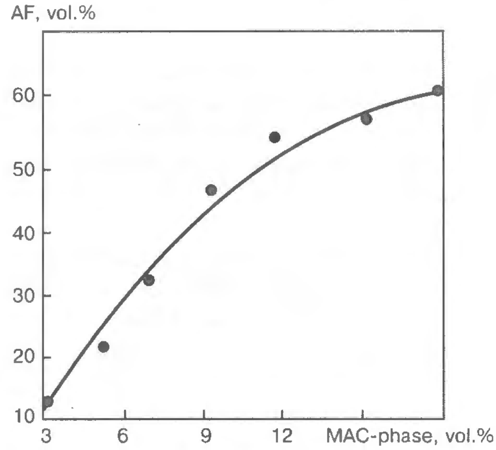

Figure 9. Relationship between the AF and MAC-phase contents of the weld metal structure

latter, whereas at a lower AF content other structural components have a competing effect.

The NMI content affects impact toughness of the weld metal (Figure 7). As shown by metallography, NMI with a size of 1.0–1.5 μm dominate in the weld metal (Table 3). Their type and composition were not considered in this study. It should be noted, however, that the extent of the effect of a structural factor can hardly be distinguished from that of NMI, although there is the evidence [9–11] that the role of the latter during the structure formation process and their effect on toughness of the weld metal may be very high.

It follows from the data obtained that AF is the most favourable structure for increase in impact toughness of the weld metal. Temperature of its formation is relatively low and close to a lower branch of the intermediate region of $\gamma \rightarrow \alpha$ transformation. This process is inevitably accompanied by dispersed precipitation of the MAC-phase.

Researchers have very contradictory opinions concerning the effect of the MAC-phase on mechanical properties of the weld metal. Some of them consider this effect to be positive [10], and others — negative [12]. As a result of the investigations, we found that increase in the AF content of the weld metal is accompanied by a simultaneous increase in volume fraction of the MAC-phase (Figure 8). Also, this causes increase in such mechanical properties of the weld metal as strength and ductility (Figure 9). Because metal contained also AF and PF, in addition to the MAC-phase, the investigation results shown in Figures 8 and 9 cover the total effect of the entire set of structural components of the weld metal.

Weld metal with such an alloying system is known to have increased susceptibility to brittle fracture. Therefore, welding in this case should be performed with pre- and concurrent heating. Susceptibility of the welds under consideration to brittle fracture was estimated using the Seferian formula [13]. This formula can be used to calculate temperature of preheating of a welded joint, at which it is possible to avoid cold cracking.

$$T = 350\sqrt{[C] - 0.25} \ [^\circ C],$$

where [C] is the total carbon equivalent,

$$[C] = [C]_c + [C]_s$$

(here $[C]_c$ and $[C]_s$ are the carbon equivalents depending upon chemical composition and thickness of the metal, respectively), and

$$[C]_s = 0.005[C]_c.$$

By substituting data given in Table 1 to the above formula, we find that temperature of preheating of the parts welded should be not lower than 80 °C. The preheating temperature grows to 110–120 °C under the effect of such an important factor as a hydrogen content of the weld metal [12]. However, it is impossible to perform welding of hull structures, drilling platform foundations, large-diameter pipes and other large-size parts at this preheating temperature, while increase in power and labour consumption in manufacture of smaller parts by the above technology may amount to about 40 %.

The investigation results obtained are indicative of the fact that further improvement of the weld metal structure can be achieved by decreasing the total carbon equivalent through using steels and welding consumables with a super low carbon content.

It should be noted in conclusion that the IIW procedure employed for the investigations, consisting in calculation of volume fraction of structural components using optical microscopes, is correct, except for the case when bainite formations are oriented across the austenite grain and look like one of the laminated forms of ferrite, i.e. with the ordered second phase. If bainite has a typical acicular (laminated) structure characteristic of upper bainite, no problems with its identification using the above procedure occur.

CONCLUSIONS

1. Alloying with manganese was found to lead to formation of a substantial amount (5–18 vol.%) of pearlite. This is not favourable for providing high values of impact toughness of the weld metal, despite the amount of up to 50 vol.% of acicular ferrite contained in it.

2. Simultaneous alloying of low-carbon steels with manganese, molybdenum and nickel, compared with alloying only with manganese, allows a higher level of mechanical properties of the weld metal to be achieved in low-alloy steels, which is attributable to decrease in the polygonal ferrite content, suppression of formation of pearlite and increase in the acicular ferrite content.

3. Increase in the acicular ferrite content of the weld metal structure to more than 60 vol.% due to alloying with manganese, molybdenum and nickel leads to cold cracking of welded joints in low-alloy steels.

4. Further improvement of composition and structure of the weld metal in low-alloy steels should be done by favouring formation of the weld metal with a decreased value of carbon equivalent.

1. Barritte, G.S., Ricks, R.A., Howell, P.R. (1982) The effect of inclusions on the structure and properties of HSLA steel weld metals. In: *Proc. of 6th Int. Conf. on Strength Metals and Alloys*, Melbourne, Aug. 16–20, 1982. Oxford.
2. Bonnet, C. (1980) Structure-resilience dans les soudures d'aciers doux et faiblement allies brutes de solidification. *Soudage et Techniques Connexes*, **7/8**, 209–230.
3. Morrison, W.B. (2000) Past and future development of HSLA steels. In: *Proc. of Int. Conf. on HSLA Steels-2000*, Beijing, Nov. 30–Dec. 5, 2000. Beijing: Technical Metallurgical Industry Press.
4. Abson, D.I., Dolby, R.E., Hart, P.M. (1979) The role of non-metallic inclusions in ferrite nucleation in carbon steel weld metals. In: *Proc. of Int. Conf. on Trends in Steel and Consumables for Welding*, London, Nov. 14–16, 1978. Abington.
5. (1988) Guide to the light microscope examination of ferritic steel weld metals. *IIW Doc. IX-1533–88*.
6. Vyaznikov, N.F. (1951) *Alloyed steel*. Moscow: Metallurgiya.
7. Gulyaev, A.P. (1977) *Metals science*. Moscow: Metallurgizdat.
8. Abson, D.I., Pargeter, R.I. (1986) Factors influencing the as-deposited strength microstructure and toughness of manual metal arc welds suitable for C–Mn steel fabrications. *IIW Doc. II-A-683–86*.
9. Liu, S., Olson, D.L. (1986) The role of inclusions in controlling HSLA steel weld microstructures. *Welding J.*, **6**, 139–149.
10. Cohrein, R.K., Morrison, W.B. (1985) Influence of manufacturing technology on characteristics of transformation and microstructure of some Nb–Mo pipe steels. In: *Proc. of Int. Conf. on Steels for Gas Pipes and Fittings*, London, Oct. 21–23, 1981. Moscow: Metallurgiya.
11. Nakasuhi, H., Matsuda, H., Tamehiro, H. (1985) Superlow-carbon bainitic steels for pipelines. *Ibid*.
12. Hrivnyak, I., Matsuda, F. (1999) Metallophysical investigations of martensite-austenite component (MAC) of the HAZ metal of high-strength low-alloy steels. *Avtomatich. Svarka*, **3**, 22–30.
13. Seferian, D. (1963) *Welding metallurgy*. Moscow: Metallurgizdat.

INTEGRATED EVALUATION OF EFFECT OF YTTRIUM ON PROPERTIES OF STEEL WELDS

N.G. EFIMENKO
Ukrainian Engineering-Pedagogical Academy, Kharkiv, Ukraine

The refining, modifying and alloying role of yttrium in the metal of low-alloyed welds, depending on its concentration, was experimentally confirmed. Yttrium influence in weld metal is most favourably manifested for its ductile properties and toughness in case of proceeding of the refining and modifying effects.

Keywords: *deposited metal, electron microscopy, dislocations, mechanical properties, modifying, non-metallic inclusions, multilayer welds, refining, low-temperature embrittlement*

Results of investigations [1] showed that, when yttrium is introduced into cast carbon steel, three interrelated effects such as refining, modifying and alloying are manifested, the degree of which depends on yttrium concentration. It can be assumed that the yttrium effect in cast weld metal produced in arc welding process can be similar to its effect in metal of steel castings. At the same time, the high-temperature metal treatment in arc gap during welding makes essential corrections in a thermodynamic pattern of processes of weld metal structure formation. This requires the conductance of additional comparative investigations on clarifying the nature of effect of rare-earth metals (REM), in particular yttrium, on the increase in cold resistance of weld metal made from carbon steels.

Metal, deposited with basic electrodes (rods were manufactured from steels containing yttrium), and also with electrodes, in which yttrium was added to the coating composition in the form of a powder metal addition, and also Y–Si master alloy, was investigated (Table). Procedure of producing test samples was given in [2]. Metal structure was examined using optical and electron microscopy. Mechanical tests were made in accordance with generally-accepted methods. In parallel with impact bend tests, the energy of crack propagation on impact samples, having a fatigue crack induced by a vibrator, was determined. Phase composition of non-metallic inclusions (NMI) was determined using a method of a diffraction microanalysis. Fine structure was examined on foils in transmission electron microscope UEM-200SKh at 200 kV accelerating voltage.

It was established by investigations that a size, shape and composition of NMI in weld metal is changed under the effect of yttrium. Adding of yttrium up to 0.6 % into electrode composition through a coating and up to 0.12 % into composition of the electrode core leads to the decrease in sizes of NMI to 0.6–2.0 μm. Inclusions acquire a globular shape. Their large clustering in any regions of structure was not observed, except separate tertiary clusters of 4–8 μm sizes, located along the boundaries of primary grains. NMI represent a mechanical mixture of sulphides, silicates, oxides, carbides, many of them containing yttrium: Y_2O_3, YSi_3, Mn_3O, $MnO{\cdot}3MnO_3{\cdot}SiO_2$, Y_2O_2S, Y_2S_3, YC_2. At subsequent increase in yttrium content in coating and core, the tendency to the increase in contamination of structure with NMI is observed.

Homogeneity and dispersity of grained structure and substructure play an important role in increase of brittle fracture resistance [3]. Figure 1 gives a probability size of grain in metal of deposits with different yttrium content. Initial deposited metal (without addition) is characterized by a high difference in grains (7–50 μm) at the most repeated size of grain of about 30 μm (35 % of volume). Yttrium adding to the coating narrows abruptly the areas of distribution of a grain size, and at content up to 0.6 % Y the grain size is decreased to 8–12 μm (largest

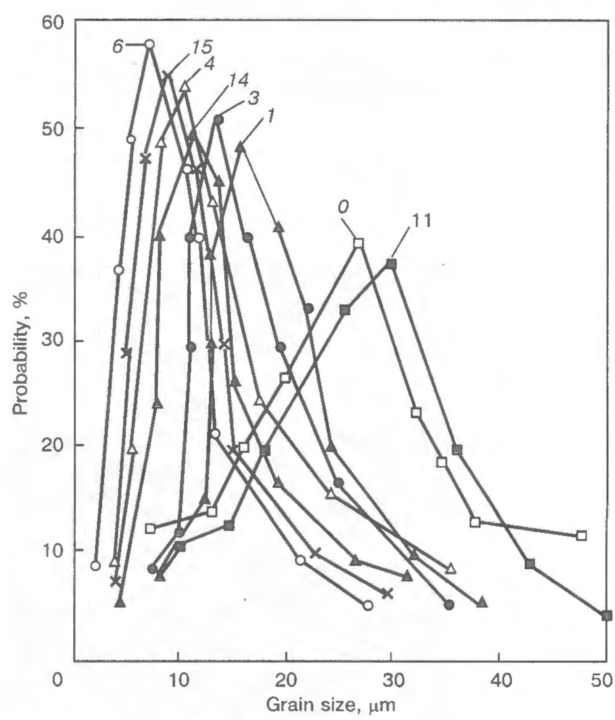

Figure 1. Size of a ferritic grain in weld metal depending on yttrium content in electrode (number of curves correspond to variants of electrodes, see the Table)

Experimental variants of compositions of experimental Fe-based welding consumables with yttrium

Series of material	Method of yttrium adding (form of adding)	No. of electrode variant	Yttrium content in electrode, wt.%	Chemical composition of deposited metal, wt.%				
				C	Mn	Si	S	P
I	Electrode coating (metallic powder with yttrium)	0	0	0.1	0.9	0.5	0.02	0.02
		1	0.1	0.09	0.94	0.5	0.018	0.021
		2	0.2	0.1	0.9	0.56	0.018	0.02
		3	0.3	0.095	0.95	0.6	0.016	0.02
		4	0.5	0.1	1.11	0.65	0.014	0.01
		5	0.6	0.1	1.2	0.65	0.012	0.019
		6	1.0	0.1	1.26	0.73	0.011	0.017
		7	2.0	0.09	1.3	0.8	0.01	0.017
II	The same (master alloy SNITMISh)	8	0.2	0.09	1.2	0.95	0.013	0.016
		9	0.35	0.09	1.24	1.1	0.009	0.015
		10	0.5	0.1	1.4	1.26	0.009	0.017
III	Metal core with yttrium [1]	11	0	0.28	0.51	0.29	0.024	0.022
		12	0.025	0.28	0.52	0.3	0.021	0.022
		13	0.084	0.3	0.54	0.3	0.02	0.021
		14	0.12	0.29	0.66	0.32	0.018	0.022
		15	0.16	0.28	0.70	0.36	0.012	0.02
		16	0.21	0.3	0.78	0.49	0.008	0.02

Note. Degree of yttrium transfer to weld metal: at adding to electrode coating in the form of powder — 1–7 wt.%; in the form of master alloy SNITMISh — 6–10 wt.%; through electrode core — 6–13 wt.%.

repetition). The same tendency was revealed also in yttrium adding to the electrode core.

Identity of structure over the entire section is characteristic of multilayer welds made by electrodes which contain up to 0.6 % Y in the coating (Table, materials of series I contain up to 0.007 % Y in weld metal). At yttrium content of 1 % and higher (yttrium content of about 0.01 % in weld metal), the significant change in structure across section is observed (Figure 2). Thermocycling in the process of layout of layers influences the structure formation. An acicular structure of a bainitic type with a small amount of a structurally-free ferrite is formed in upper layers, not subjected to a repeated heating and undergone an intensive heat dissipation (Figure 2, *a*). A growth of a ferritic constituent is observed in middle layers and, in parallel with a bainite, a structural constituent of a troostite type is appeared. The lower layers have a ferritic-pearlitic structure with a negligible content of a bainite (Figure 2, *b*). In multilayer welds made with electrodes of series III, the beginning of a layer-by-layer change in structure is observed at yttrium content in core starting from 0.16 %.

Comparative analysis of a fine structure of initial metal and variants, containing yttrium (series I), showed the different degree of homogeneity. Non-uni-

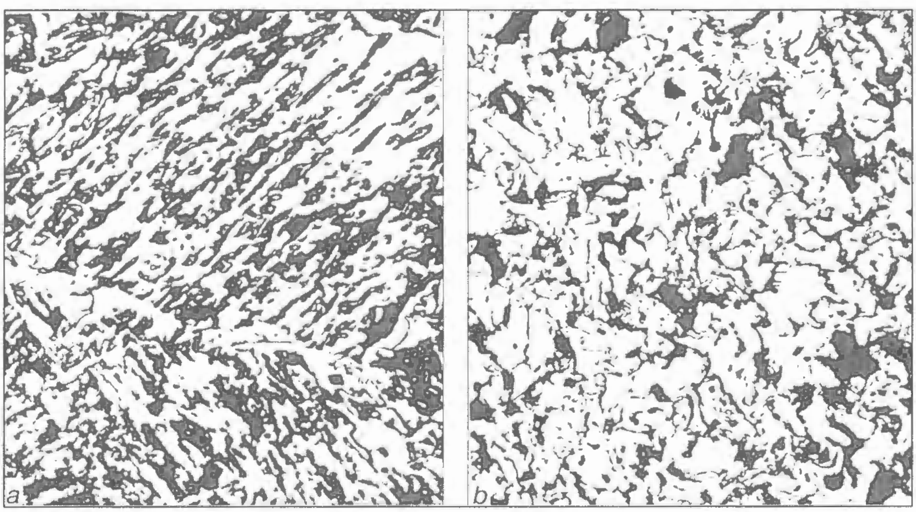

Figure 2. Microstructure of metal of multilayer weld (variant No.6, see the Table): *a* — upper layer; *b* — lower layer (×600)

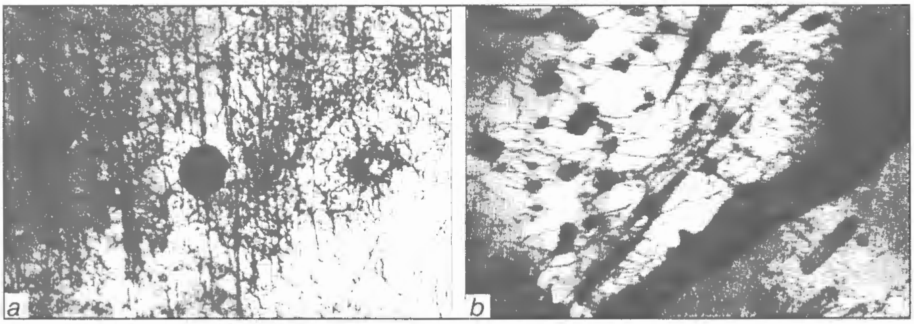

Figure 3. Dislocation structure of deposited metal: *a* — initial variant; *b* — made with electrode No.3 (see the Table) (×3000)

form distribution of dislocations of a rather high density was observed in metal of the initial variant. Maximum density is observed around large NMI (Figure 3, *a*). In metal deposited with electrodes, containing not more than 0.6 % Y, a comparatively uniform distribution of dislocations is observed (Figure 3, *b*). Their density was reduced.

The above-given changes in fine structure are correlated with results of investigation of internal friction in Y-containing steels [1], where the decrease in background of the internal friction is directly connected with the structure stabilizing (decrease in density of dislocations and their uniform distribution). Increase in yttrium concentration in the electrode leads to the decrease in homogeneity of a dislocation structure at a negligible increase in density of dislocations. This is especially seen at yttrium content in electrode of not less than 1.0 % and its content in core of not less than 0.21 %.

Structural changes under the yttrium effect lead to the change in mechanical properties of the deposited metal (Figure 4). A great growth in strength characteristic (σ_t, $\sigma_{0.2}$) at yttrium content in electrode above 0.6 % is due to the transition of elements, introduced into the metal as deoxidizers (silicon, manganese) and favourable effect of yttrium on structure formation. The adding of REM to the metal increases its impact strength, however, its value does not yet give a clear understanding about the metal resistance against the brittle fracture. Figure 5 presents such composed components, as energy of crack initiation A_i and energy of crack propagation A_p, at testing the initial deposited metal and that containing yttrium. As is followed from this Figure, the main increment in impact strength of metal with yttrium is provided by A_i within the entire interval of test temperatures, while A_p of this metal (exceeding the similar characteristic of initial metal at positive temperature) is decreased monotonically with a reduction in the latter.

The scheme of yttrium effect on increase in metal resistance to low-temperature embrittlement can be presented as follows on the basis of obtained experimental data. In welding (due to high temperature and strong convective processes in melting space) the metallurgical reactions, unlike the casting process [1], are proceeding more intensively and completely. Consequently, some initial doses of yttrium, entering the melting space from a filler, will be consumed for the formation of oxides, high-refractory sulphides in the recrystallizing period, thus neutralizing their action as liquation [4], and also removing them partially into a slag. This sufficient amount is its residual content 0.003–0.005 % (0.2 % Y in coating or 0.025 % in core). The maximum increase in solidus temperature (T_S) at the above-said yttrium content in metal confirms this [4]. The increase in concentration above 0.025 % does not change T_S and temperature interval

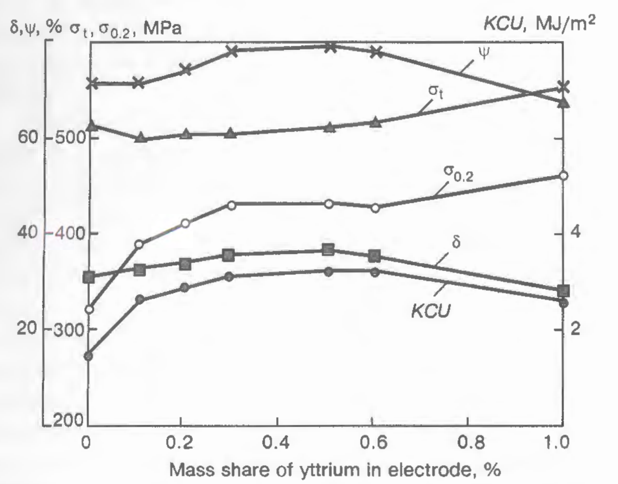

Figure 4. Dependence of mechanical properties of deposited metal on yttrium content in electrode

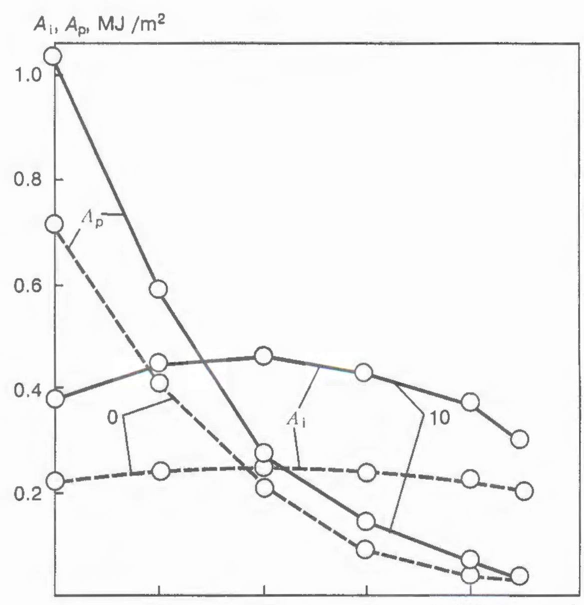

Figure 5. Effect of temperature on energy of initiation A_i and propagation A_p of crack (numbers of curves see in the Table)

of crystallization that proves a sufficient neutralizing of a fusible phase. In parallel with a refining effect of yttrium at such content, the beginning of process of the structure modifying is noted (see Figure 1).

The increase in yttrium content to 0.007 % (0.3–0.6 or 0.08–0.12 % Y content in coating or core, respectively) intensifies the process of modifying of structural constituents and NMI. The refining effect of yttrium is manifested, as was earlier established [5], in prevention of a laminar (film) distribution of sulphur that stipulates the significant increase in interatomic, intercrystalline bonds [1]. Structure becomes more equilibrium, density of dislocations is decreased at more uniform their distribution (Figure 3). The above-mentioned changes are one of the basic criteria of improving the energy of brittle fracture resistance [6]. The further increase in yttrium content in the coating of not less than 1.0 %, and similarly in core of not less than 0.16 % (residual content in weld metal ≥ 0.008 %) leads to changes in structure and phase composition of metal of multilayer welds. At such content of yttrium the stability of an overcooled austenite is increased. A comparatively high rate of cooling, typical of welds, leads to the decay of austenite at much higher overcooling that promotes the formation of structures of a bainitic type. Measurement of hardness of a middle part of multilayer welds showed its changes depending on yttrium content. In adding of 1.0 % Y through the coating the hardness is *HRB* 82–84, while at adding of 2.0 % Y *HRB* is 92–95, initial variant is *HRB* 75–77. Here, grained and subgrain structures continue to refine. Processes of recovery of elements from oxides (manganese and silicon), formation of fine-dispersed NMI of a laminar composition, containing yttrium, are intensified. The monotonous reduction in sulphur content is observed (see the Table). The above-given changes in metal structure indicate that the alloying effect is started to be manifested at such yttrium content (residual content ≥ 0.008 %). With change in its concentration the mechanical properties of weld metal are changed adequately. It was established in comparison of results of microstructure examinations with characteristics of mechanical properties that the maximum level of visco-plastic properties is observed in adding of yttrium in the amounts ensuring the refining and modifying effects.

Thus, the main factors influencing the increase in resistance to low-temperature embrittlement are the refining of structural constituents, neutralizing the harmful effect of sulphur, oxygen, increase in interatomic and intercrystalline bonds, favourable effect of yttrium on dislocation structure.

CONCLUSIONS

1. Integrated investigations allowed clarification of the nature of yttrium effect on the increase in resistance to low-temperature embrittlement of weld metal made from carbon steels.

2. When yttrium is added to the weld metal, all three closely related interactions are proceeding: refining, modifying and alloying. Degree of their manifestation depends on concentration of yttrium added to the weld.

3. Maximum level of visco-plastic properties is observed in yttrium adding to the weld metal in the amounts providing the refining and modifying effects.

1. Efimenko, N.G. (2002) Modifying, refining and alloying with yttrium in welding of steels. *The Paton Welding J.*, **6**, 8–12.
2. Efimenko, N.G. (1980) Application of REM in welding electrode coatings. *Svarochn. Proizvodstvo*, **7**, 8–9.
3. Meshkov, Yu.Ya. (1981) *Physical principles of fracture of steel structures*. Kyiv: Naukova Dumka.
4. Efimenko, N.G., Sterenbogen, Yu.A., Doroshenko, L.K. et al. (1990) Influence of yttrium on temperature range of solidification of carbon steel. *Avtomatich. Svarka*, **10**, 45–47.
5. Efimenko, N.G., Balan, L.G., Bakakin, G.N. et al. (1985) Influence of yttrium on weld metal structure in fusion welding. *Svarochn. Proizvodstvo*, **4**, 19–21.
6. Yavdoshchin, I.R., Alekseev, A.A., Pokhodnya, I.K. et al. (1987) Influence of sulfur on cold resistance of low-carbon steels. *Avtomatich. Svarka*, **9**, 19–22.

MICROSOLDERING METHODS

A.A. ROSSOSHINSKY[1], V.M. KISLITSYN[1], A.G. MUSIN[1] and S.P. PAVLYUK[2]
[1]E.O. Paton Electric Welding Institute, NASU, Kyiv, Ukraine
[2]Taras Shevchenko Kyiv National University, Kyiv, Ukraine

Several processes of welding and soldering are considered, which were developed at PWI in 1965–1985 and are used in the technologies of mass production of discrete semiconductor devices and integral microcircuits. They were not widely described in publications earlier for certain reasons.

Keywords: *welding, soldering, technology, integral microcircuits, semiconductor diodes, advanced materials*

Intensive development of electronics in 1960s led to performance of research, aimed at development of technologies of semiconductor device fabrication, advanced methods of producing metal–semiconductor joints. One of the main tasks in the technological process of fabrication of discrete semiconductor devices and integral microcircuits is joining to contact areas of the silicon or germanium chip the gold or aluminium wires of up to 60 μm diameter, which commute the electric circuits of the silicon chip with the output pins of the integral microcircuit. Several solid-phase pressure welding processes are known for solving such problems, namely thermocompression bonding, welding by ultrasonic oscillations and their combination [1–3].

Thermocompression bonding is a process, leading to formation of a joint in the solid phase. Practical application of this process may include also a variant of joining with formation of an eutectic in the zone of contact of the materials being joined. However, this involves problems, related to control of the quality of the eutectic phase, namely non-uniform depth of its penetration, as well as the possibility of formation of undesirable chemical compounds during aging, for instance «purple plague», arising under certain conditions in the zone of the gold-to-silicon joint. Use of thermocompression bonding is rather strictly limited by materials of the attached pins (gold, aluminium), their geometrical properties (for instance, just wires of a round section and diameter of 40–60 μm).

Welding with application of ultrasonic oscillations is a process, which can solve a wider range of technological problems. This process provides deformation of the metal pins being joined at a relatively small compressive force, cleaning of the contact area from oxides or other contamination, activation of the atoms, which are in the zone of contact of the materials being joined. However, the weight of piezoceramic or magnetostriction converters and concentrators of mechanical oscillations, connected to the welding electrode significantly increases the inertia of the latter, which markedly decreases the possibility of achieving a stable quality of the produced joints in the processes of welding or soldering micro-sized items.

All the current processors, incorporating in one single-crystal silicon structure the greatest part of the electronic circuit, which consists of a multitude of discrete elements and integral circuits, earlier mounted on the PC board, are currently manufactured using the above welding processes, developed more than thirty years ago. Given below is the description of microwelding and microsoldering processes, developed by us, which significantly widen the range of technological application of the existing processes, and allow moving over to a denser packing of elements in one silicon structure by reducing the dimensions of contact areas, and increasing the efficiency of assembly equipment and reliability of microjoints.

Thermal-resonance welding process, which combines the advantages of thermocompression and ultrasonic welding, consists in that heating of the working tip of a V-shaped or axially split electrode is conducted by high-frequency current pulses, which excite mechanical oscillations in the electrode as a result of electrodynamic interaction of currents, flowing through two halves of the electrode.

Increase of the amplitude of mechanical oscillations of the electrodes can be achieved at placing of the electrode in the zone of the magnetic field action (Figure 1). When the frequency of electric current coincides with that of natural oscillations of the electrode, a resonance of mechanical oscillations of the electrode component occurs, at which the amplitude of oscillations of the electrode tip is maximum. The basic parameters of this process (pressure on the electrode, frequency and current of electrode tip heating, welding time) can be quite readily controlled in wide ranges and adjusted by feedback signals by these parameters. These conditions permit achieving a higher level of reproducibility of the quality of the welded or soldered joint, despite the changes of physical characteristics of materials of the electrode component and of the materials being joined during heating. The electrode component can be designed, allowing for excitation in the electrode of not only transverse, but also torsional oscillations, where the frequency may be dozens of times higher than that of the transverse ones.

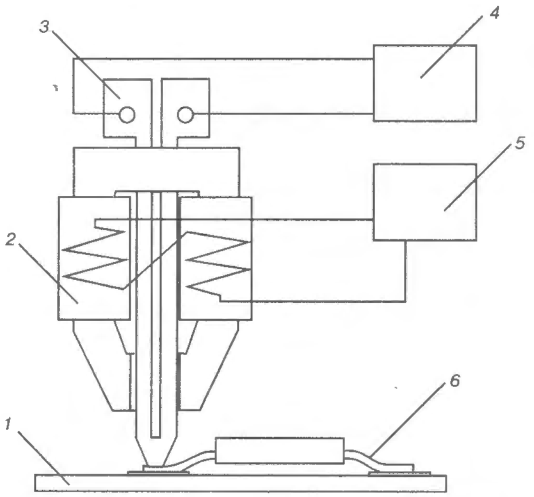

Figure 1. Diagram of the process of thermal-resonance welding: *1* — PC board; *2* — electric magnet winding; *3* — V-shaped electrode; *4*, *5* — source of high-frequency and direct current, respectively; *6* — integral microcircuit pins

One of the essential drawbacks of the devices for thermocompression or thermal-resonance bonding is lowering of the tool resistance with reduction of the geometrical dimensions of the tip (area of contact of the electrode with the workpiece). For welding more miniature items this drawback can be eliminated by using silicon crystals as a heating element [4], having hundreds of times higher electric resistance than the heating elements, made of the highest resistance metals.

In the variants of soldering copper pins to metallized diode silicon structures, developed by the E.O. Paton Electric Welding Institute [5], the process is based on heating of the Si-based semiconductor structure by electric current, passing through the metal pins, connected to the silicon chip, and the electron-hole junction (Figure 2).

The need to develop new processes of soldering the silicon diodes was related to a transition to a new,

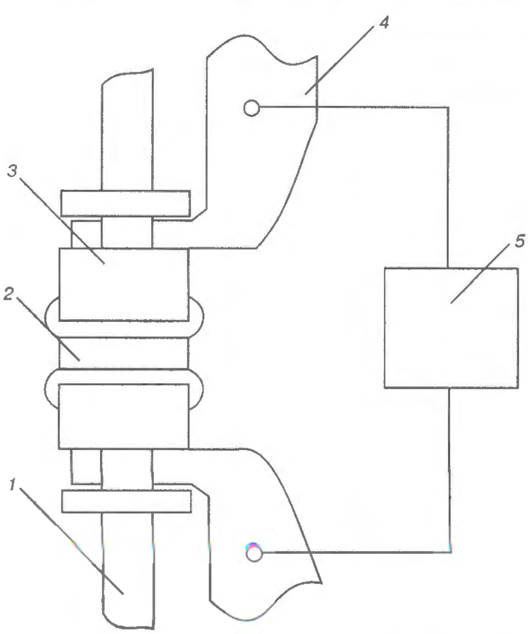

Figure 2. Diagram of the process of soldering a semiconductor diode: *1*, *3* — copper pins of the diode; *2* — diode structure; *4* — electrode; *5* — direct current source

more cost effective in fabrication design of the semiconductor device in a plastic or glass case. The existing methods of group packaging of medium-power diodes in a multiple assembly holder, heated in pusher-type furnaces, turned out to be totally unacceptable for assembly of a new structure of the semiconductor diode, consisting of a minimum of parts, namely silicon diode structure and two copper pins, where the contact areas are covered by a solder sublayer.

Soldering the elements of a diode of such a design necessitated development of the process of individual soldering of each diode separately, which in mass production requires reducing the soldering time from several tens of minutes to fractions of a second. This, in its turn, requires increasing the rate of heating and cooling of silicon structures by dozens of times, which is contradictory to the variants of heating, established in technological practices.

The most effective variant of diode element heating up to soldering temperature (200–250 °C) in a minimum time is using the silicon chip as the heating element, the electric resistance of which is almost one million times higher than that of the most effective material for heating by the resistance method, namely nichrome. However, according to the traditional approaches, it is inadmissible to perform heating of the diode structure by electric current, which is tens and hundred times higher than the rated value of current flowing in the forward direction relative to the electron-hole junction.

Practical implementation of this process of silicon structure heating led not only to revision of the existing theoretical concepts of silicon structure resistance to direct current overloads. Under the conditions of mass production of diodes revealing the diode structures with a higher level of defects in the single-crystal structure of silicon, defects of formation of the electron-hole junction, defects of applying a metallized layer on the crystal, defects of the joined metal pins is a quite complicated and economically ineffective operation. In soldering of the diode elements with heating in pusher-type furnaces these kinds of defects are not revealed during manufacture. Currently used methods of diode classification by applying short-term critical loads, conducted at the end of the technological cycle, in many cases themselves caused a lowering of the reliability of the diodes in service.

The main advantage of the developed process was the ability to reject directly during packaging the diode chips, potentially unreliable in further service. Unfortunately, this feature of the new soldering process was not fully used, as the service reliability parameter was not specified in the certificate data. It is possible, that increase of requirements to the quality of the products will result in the plants, manufacturing the semiconductor devices, focusing not only on the use of the cost-effective technologies and highly productive equipment, but also on making highly reliable products.

Further studies of this process led to development of technologies of soldering metal pins to semiconductor chips with several electron-hole junctions, for instance, with the structures of a thyristor, dinistor, stabilitron, as well as a powerful high-frequency transistor (Figure 3).

The main disadvantage of the process of soldering with heating of the silicon chip by electric current, consists in an unstable power release, which is due to the difference of electric resistance of semiconductor structures, particularly during the process of heating up to the soldering temperature. This drawback may be eliminated in heating of the soldered elements of the diode by a pulse of capacitor discharge [6]. In addition to stabilization of the amount of energy, evolved in the soldered elements and shortening of the soldering time to 350 μs, use of this process further allowed joining silicon chips to massive heat-removing plates. Heating current value in this variant of soldering exceeded the rated current several thousand times.

Cost effectiveness of soldering processes, which were developed and introduced in many large electronic engineering plants during 1970–1990 was equal to many million roubles annually.

During the same period we conducted promising developments of the processes of microwelding of aluminium pins of integral microcircuits to aluminium tracks of printed-circuit boards, as well as fluxless soldering of copper pins to copper coatings, produced by the method of spraying on ceramic substrates. During development of these joining processes several novel express-procedures were elaborated for evaluation of the quality of the initial semiconductor structures, nondestructive testing of the quality of joining silicon diodes, recording silicon chip temperature during soldering [7], which allows a significant shortening of the time taken up by technological investigations, when addressing new problems.

The found anisotropy of heat conductivity of diode silicon chips [8] allowed establishing the potential possibility of developing new structural and thermal barrier materials, where the heat conductivity can be varied under the impact of the electric field.

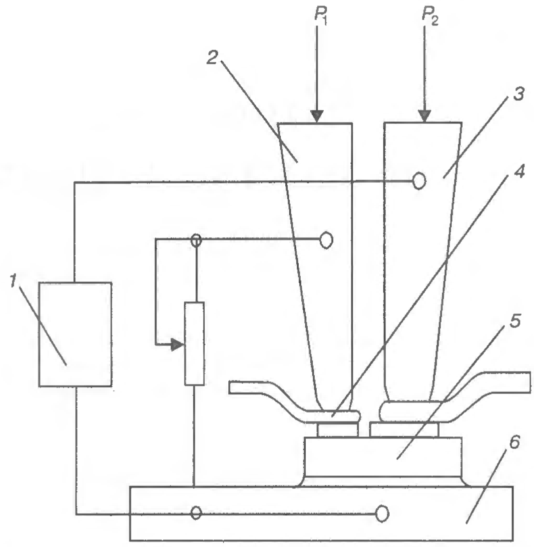

Figure 3. Schematic of heating in soldering pins to a transistor structure: *1* — power source; *2, 3* — electrodes; *4* — copper pins; 5 — semiconductor *p–n–p* structure; *6* — heat removing plate

1. Conti, R.J. (1966) Thermocompression joining techniques for electronic devices and interconnections. *J. Met. Eng.*, **2**, 29–34.
2. Rossoshinsky, A.A., Lebiga, V.A., Kislitsyn, V.M. (1968) Influence of ultrasound on metal contact resistance in microwelding. *Elektron. Tekhnika*, Series 10, Issue 1, 11–14.
3. Rossoshinsky, A.A., Lebiga, V.A., Kislitsyn, V.M. (1968) On combined methods of spot welding of microitems. *Svarochn. Proizvodstvo*, **9**, 26–27.
4. Pavlyuk, S.P., Rossoshinsky, A.A., Kislitsyn, V.M. et al. (1999) Application of silicon as the heating elements in microsoldering irons. *Avtomatich. Svarka*, **2**, 41–44.
5. Rossoshinsky, A.A., Lebiga, V.A., Kislitsyn, V.M. et al. *Method of assembly of semiconductor devices.* USSR author's cert. 355696. Int. Cl. H 01. Publ. 05.09.78.
6. Rossoshinsky, A.A., Kislitsyn, V.M., Musin, A.G. et al. *Method of soldering of semiconductor crystals of stabilitrons to metallic fixtures of devices.* USSR author's cert. 623240. Int. Cl. H 01. Publ. 05.09.78.
7. Pavlyuk, S.P., Ishchuk, L.V., Kislitsyn, V.M. (2002) Means of measurement of temperature in different areas of semiconductor crystal. *Visnyk Kyiv. Nats. Univ.*, Issue 1, 348–354.
8. Kislitsyn, V.M. (1987) *Technology of resistance soldering.* Syn. of Thesis for Cand. of Techn. Sci. Degree. Kyiv.

IMPROVING IN WEAR RESISTANCE OF PARTS OF TITANIUM ALLOYS (REVIEW)

T.V. VANZHULA, V.N. ZAMKOV and **V.P. PRILUTSKY**
E.O. Paton Electric Welding Institute, NASU, Kyiv, Ukraine

Methods for improving wear resistance of titanium alloys, including thermochemical treatment, deposition of galvanic coatings, flame and plasma spraying, laser and electric-spark surface alloying and brazing, are reviewed. Efficiency of their application is assessed. It is shown that the most promising method is argon-arc surfacing, requiring development of new filler materials.

Keywords: *titanium, tribological characteristics, wear resistance, surfacing*

Titanium alloys possess unique physical-chemical properties, such as high specific strength and heat resistance, as well as excellent corrosion resistance in atmosphere, sea water and a number of aggressive environments. Owing to these properties they are widely applied in aerospace engineering, ship and machine building, power generation and medicine. Available are alloys differing in properties and applications to ensure performance of parts under different service conditions. They include structural and heat-resistant alloys, alloys intended for operation under cryogenic conditions, corrosion-resistant ones, etc. However, independently of their type and alloying system, titanium alloys are susceptible to contact adhesion in friction. This results in substantial wear and mechanical damage of the surface of titanium alloy parts during friction. For example, the friction coefficient of commercial titanium VT1-0 in air is 0.45-0.55 (for the like friction pairs). At the same time, the friction coefficient of brass L062-1 is 0.20, and that of hardened and tempered steel 2Kh13 is no more than 0.26. Susceptibility to adhesion is an essential drawback of titanium alloys, hampering in many respects their utilisation in friction units of machines and mechanisms [1]. Susceptibility of titanium to gas-abrasive wear is also reported [2].

Technologies employed to improve tribological characteristics of titanium alloy parts are the same as those used for treatment of rubbing surfaces of other metals (allowing for physical-chemical peculiarities of titanium). They include thermochemical treatment (TCT), deposition of galvanic coatings, thermal spraying, plasma-powder cladding, laser and electric-spark surface alloying etc. It should be noted that literature data on commercial application of such a widespread method of improving wear resistance of titanium parts as surfacing are scarce.

The most common methods of TCT of titanium alloy parts used to regulate properties of surface layers of metal are oxidising and nitriding [3, 4]. Oxygen and nitrogen are elements which stabilise α-phase in titanium. Oxygen dissolves in α-Ti to a substantial amount (up to 33 at.%) to form interstitial solid solution. Strength and hardness of titanium increase in this case, although its ductility dramatically falls [5]. Independently of chemical composition of a titanium alloy, its surface layer after oxidising consists mostly of α-solid solution. Oxidising leads to decrease in the friction coefficient of titanium to 0.06, while the load that causes scoring increases from 100 to 2000 N. Hardness of the surface layer in this case amounts to *HV* 600–800, and thickness of the layer is 80–100 μm. Oxidising of titanium alloys, e.g. VT14, is performed in air atmosphere at a temperature of 750 °C for 16 h or at 800 °C for 4 h [4]. Oxidising is a very complicated and labour-consuming process. Cracks are formed on the metal surface, and cleavages result from operation even with an insignificant deviation of the process parameters from the optimal ones [3].

Ultimate solubility of nitrogen in α-Ti is no more than 0.75 wt.%. At a higher mass fraction of nitrogen the layer containing titanium nitrides is formed on the surface, and α-solid solution is transformed into a separate nitride phase. So, nitrogen hardens titanium to a higher extent than oxygen. However, the rate of interaction of titanium with nitrogen is by an order of magnitude lower than that with oxygen. Thereby, thermal-diffusion nitriding (TDN) of conventional-purity titanium alloys [6, 7] should be carried out for 8–10 h at a temperature of 850–950 °C, as at lower temperatures the process of formation of titanium oxides is dominating, thus hindering diffusion of nitrogen into titanium. The use of ammonia for nitriding leads to a simultaneous saturation of titanium with hydrogen, which may cause brittleness of nitrided parts.

Ion nitriding (IN) [8] is performed by the vacuum-arc method in an argon and nitrogen mixture at a temperature of up to 600 °C for 15–60 min at a substantially lower (about 1 keV) energy of ions than in ion implantation (about 40–50 keV) [9, 10]. The temperature at which the IN process takes place causes no deterioration of technological properties of the base material.

The most important difference between IN and TDN is that the solid solution zone during IN increases to 60 μm in size during 45 min at a temperature of

600 °C, whereas in TDN this zone does not propagate deeper than 10 μm even after holding for 8 h at a temperature of 950 °C [8].

The method was suggested in [11] for saturation of the surface layer of titanium alloys with gas, consisting in affecting the surface of a part by the non-transferred arc with air (used as a reactive gas) added to the discharge zone. The controlled access of atmospheric gases to the surface of a titanium part is provided through a regulated decrease of the rate of a shielding gas flowing out from the torch (argon in this case).

Hardness of the surface layer after nitriding is *HV* 800–1200 MPa. As reported in [12], the combined effect of nitriding and thermal cycling provides an increase of 2–2.5 times in wear resistance of titanium alloy VT1-0. However, subsequent treatment leads to spalling of sharp edges, which does not allow an expedient utilisation of nitriding for hardening of the surface of parts with a complex configuration and fails to ensure the required quality of finishing operations.

The less labour-consuming and more practicable methods for improvement of tribological characteristics of titanium parts are galvanic deposition and flame spraying (plasma spraying is used more rarely) [13]. These processes have a number of advantages over TCT. For example, in thermal spraying there is no need to subject an entire part to heating to high temperatures. Moreover, these processes allow using a wide range of coating materials and make it possible to deposit layers by «building up» of linear sizes of parts, thus enabling restoration of their initial geometry after wear.

The method of galvanic deposition of chromium, i.e. chromium plating, is used to advantage to improve wear resistance and adhesion strength of titanium parts. Hardness of chromium coatings deposited from electrolytic solution on a titanium surface is *HRC* 55–60, while strength of their adhesion to the substrate is more than 100 MPa [14]. Maximum service temperature of a chromium plated surface amounts to 400 °C. However, its hardness starts to decrease at a temperature as low as 200 °C. Surface with a chromium coating has a low friction coefficient and good wear resistance. At the same time, it is characterised by low fatigue properties. A «network» of cracks is formed in the deposited layer, which is associated with the effect of internal tensile stresses. Therefore, care should be taken when using the above coatings in friction units. Moreover, the risk exists that titanium might be hydrogenated during the electrolytic process, which may lead to deterioration of performance of an entire part.

It is recommended that a long-time diffusion annealing, i.e. heat treatment, of an entire part should be performed after deposition of a galvanic coating [15] in order to decrease the hydrogen content of the base metal and ensure an increased strength of adhesion of titanium to the galvanic coating. When doing this, one should bear in mind that if a heating temperature is higher than 500 °C, annealing of titanium and titanium alloys should be performed in inert gases or in vacuum [5].

The method of high-velocity oxy-fuel (HVOF) spraying of alloys on the base of cobalt (Co–Mo–Cr–Si) and carbides WC–Co and WC–CrCo, as well as boride-containing materials [16], is employed to form wear-resistant coatings on the surface of titanium alloys. The velocity of flame with this method is 2100 m/s, and the velocity of particles equals 750 m/s (for metals) [14]. Despite a very high rate of the process (the deposition efficiency amounts to 0.25–0.54 mm/h per square millimetre of the surface for the WC–CrCo coatings), the deposited layers have very high service characteristics: hardness is higher than *HRC* 60, adhesion strength is 100 MPa and working temperature is 550 °C [14]. The coatings are characterised by an excellent wear and corrosion resistance, and their fatigue resistance is superior to that of galvanic coatings. The HVOF process has some advantages over chromium plating, such as lower toxicity of wastes, reduced costs of disposal of these wastes, decreased labour consumption owing to elimination of some types of treatment before and after the process, possibility of treating local surface regions etc. This process is successfully applied instead of chromium plating in aircraft engineering.

However, one should bear in mind that because titanium has a low linear thermal expansion coefficient [5], this inevitably leads to formation of tensile stresses in surface layers of coatings on titanium [17], which also adds to deterioration of performance of a coating. To alter sign of stresses and change their values, it is necessary to properly regulate the thermal cycle of spraying. Deposited coatings have a laminated structure, structural and chemical heterogeneity and substantial anisotropy of physical and mechanical properties, which in a number of cases exerts a positive effect on their performance.

Wear resistance of titanium can be increased by using laser surface alloying. Materials for this process include chromium, manganese, iron and nickel [18]. Surface of a titanium part is melted by the laser beam in a jet of commercial nitrogen with an addition of a required alloying element. As a result, microhardness of the surface layer amounts to *HV* 7.5–9.5 GPa, and depth of the molten zone is 30–37 μm for chromium and 50–120 μm for iron. The effect of increase in hardness on the surface of titanium alloy parts can be achieved also as a result of their laser glazing in air or nitrogen atmosphere [19]. Also, it is possible to perform alloying with carbides and borides of tungsten, chromium and titanium. Laser surface modification with silicon carbide is considered to be most promising in this respect [20, 21]. However, high power density of the laser beam leads to formation of a high temperature gradient in the sub-surface layers, which is caused by rapid heating and cooling. High stresses induced in this case may lead to cracking.

This applies also to the process of alloying of the surface of titanium alloy parts using the electron beam with a high energy of electrons [22, 23].

Increase in wear resistance of titanium by surface alloying is achieved by using electric-spark treatment, where materials with self-fluxing additions (WC–Co–Ni–Cr–B–Si) are applied as the electrode ones [24]. In a number of cases, wear resistance is increased by treatment with heterogeneous plasma beams [25] or high-temperature pulsed plasma [26].

Brazing-on is a method favourable for increasing wear resistance and restoration of geometric sizes of worn out surfaces of parts of titanium alloys in terms of preventing grain growth during deposition of a wear-resistant layer on the titanium surface and maintaining properties of titanium at an initial level. This method can be employed to deposit wear-resistant layers on the surface of titanium by avoiding incipient melting of the base metal. In this case the filler metal consists of hard reinforcing particles (e.g. carbides of refractory metals) and a low-melting point matrix in the form of a brazing alloy based on titanium of the Ti–Cu–Ni–Zr system [27]. However, most components of a brazing alloy have a limited solubility in α-phase of titanium, and intermetallic compounds characterised by an increased brittleness are formed during cooling as a result of eutectoid decomposition of β-solid solution. This determines low ductility of the brazed joints [28].

Formation of intermetallic compounds can be restricted by reducing time of the brazing process [29]. However, brazing of titanium using composite brazing alloys is performed as a rule in vacuum furnaces. Therefore, high heating and cooling rates, as well as a substantial reduction of the time of metal dwelling at a brazing temperature can hardly be achieved in this case. The fact that the temperature range of melting of the Ti-base brazing alloy is close to the point of beginning of an intensive grain growth [30] also adds to complexity of the process. Some regulation of temperature conditions can be achieved in the case of arc brazing in vacuum [31].

Therefore, the above technological processes allow surface hardness and wear resistance of titanium and its alloys to be increased to some extent. However, they fail to solve the entire problem of performance of titanium alloys in friction units. Issues associated with quality of deposited wear-resistant layers, strength of their adhesion to the surface of titanium, maintaining its properties, ductility of the transition zone and, therefore, service life of titanium parts under friction conditions remain unsolved so far. These issues can be partially solved by using double surface treatment [32], which includes electron beam and laser treatment by vacuum-arc or plasma spraying, TCT etc. [33].

The extensive use is made of arc and plasma-arc surfacing processes, which are the most productive methods for a desired modification of tribological characteristics of surface layers of parts. It has been reported lately that wear resistance of titanium can be increased by using plasma-arc and argon-arc surfacing. Thus, study [34] gives description of the method for surfacing valves of automobile engines made from titanium alloy Ti–6Al–4V. This surfacing method comprises deposition of a sub-layer of alloy Co–Ni–Cr–Al–Y on the working surface of a valve, and then deposition on it of the Stellite-12 layer. In this case no deterioration of properties is seen in the zone of fusion of the sub-layer with titanium or Ti-base alloy. This is attributable to the fact that fusion of titanium to chromium results in formation of a structure based on the β-phase. Nickel and cobalt dissolve in it in considerable amounts to form no intermetallic phases. However, no brittle phases are formed when Stellite is deposited on the sub-layer. It is reported that surfacing can be carried out not only by the TIG method in argon, but also by the electron and laser beams. Total thickness of the layer deposited, for example, by the TIG method in argon is 1.2 mm, and its hardness is *HV* 5000 MPa. Drawbacks of this method include considerable costs of the materials used, sophistication of the surfacing technology and small thickness of the deposited layer. It should be noted that increase in the arc current leads to the probability of cracking and separation of the deposited layer from the base metal. Sometimes it is recommended to use cobalt for deposition of the sub-layer [35]. Study [36] shows the possibility of using the nickel and titanium mixture as a filler material. Hastelloy-C (Ni–16Mo–15Cr–5Fe–4W) and Inconel-625 (Ni–21Cr–9Mo–4Nb) are also used for these purposes. An attempt to perform surfacing in a mixture of argon and active gases (CO_2, O_2, N_2), meaning that the presence of oxygen and nitrogen leads to hardening of titanium [36], failed to give positive results.

It should be noted that in the case of deposition of Hastelloy hardness of the deposited layer gradually decreases in a direction from its surface to the zone of fusion with the base metal. At the same time, in the case of deposition of alloys containing cobalt, an increased hardness in the deposited layer persists from its surface through thickness to a certain depth. Then, after a sudden increase, it decreases to a level of hardness of the base metal. The cause of this abrupt local change is formation of an interlayer of intermetallics TiCo and Ti_2Co in the fusion zone, which may lead to cracking and separation during operation of a treated part.

Study [37] suggests a method for arc hard-facing of a titanium substrate using a filler metal in the form of titanium wire with a cobalt powder or Co-base alloy covering, and titanium wire inserted into a cobalt tube. In the former case the process of manufacture of a filler has something in common with the process of manufacture of stick electrodes meant for manual arc welding, whereas in the latter case the rods of 3.2 mm wire (Ti–6Al–4V) are inserted into a cobalt tube with an inner diameter of 3.25 mm and wall thickness of 0.3 mm and drawn through a hole with a diameter of 3.5 mm. The resulting hard-facing rod is a titanium core covered with cobalt (covering is 0.15 mm thick). The process of manufacture of filler materials is very complicated and labour-consuming. Moreover, because of design peculiarities of these materials, the fillers made from them have the form of rods, which makes automation of the hard-facing process impossible. In turn, this causes heterogeneity of composition and properties of deposited layers.

The authors of [38] conducted investigations of wear resistance of titanium alloys. Materials for the investigations were made by precipitation hardening of titanium alloy Ti–6Al–4V using different types of carbides. Two methods were employed for this purpose – plasma-powder cladding and argon-arc remelting. The resulting materials were used to investigate the effect of a mixture of different carbides in an alloy on wear resistance and find mechanisms for improving it. The material produced by the vacuum-arc remelting method was employed to evaluate service characteristics of the developed composite titanium alloy to be used as a structural material.

Deposition of a mixture of carbides on titanium resulted in a substantial scatter of the values of hardness depending upon the type of carbide (*HV* 4000–4600 MPa), and wear resistance depending upon the mixture composition detected in the cast zone. When using a filler material containing W_2C and Cr_3C_2, wear resistance of the deposited layer was at a level of that of Stellite. In deposition of a mixture of other carbides (NbC, TiC) on alloy Ti–6Al–4V, wear resistance of the cast zone was almost equal to that of the base metal. This is attributable to the fact that in the case of using a filler material containing W_2C and Cr_3C_2 the matrix structure of the cast zone consisted of the β-phase. If no β-phase was formed (using a filler material containing NbC and TiC), no effect of increase in wear resistance was seen. The presence of insignificant amounts of W_2C and Cr_3C_2 leads to formation of the α-phase, which also hampers increase in wear resistance. Relationship between hardness and wear resistance depends to a considerable degree upon the content of the α- and β-phases in the matrix. Supposedly, the relationship between phase composition of the matrix and wear resistance of the deposited metal is caused by a high ductility of the β-phase, compared with the α-phase.

The authors of that study indicate to the possibility of production of titanium alloys precipitation-hardened with carbides by a traditional method, i.e. vacuum-arc remelting. But despite the fact that such alloys have high wear resistance, their deformability is so low that it is almost impossible to use them to make a filler material in the form of wire. In turn, this makes development of the technology for reconditioning and hardening of surfaces of titanium parts by the argon-arc surfacing method much more difficult.

Therefore, development of a material and technology for wear-resistant surfacing of titanium alloys is a very topical problem. It can be reduced to providing the required tribological characteristics of the treated surface, possibility of automation of the surfacing process, production of deposited layers of desired sizes, minimum penetration depth and optimal technological properties of the base metal.

It can be concluded from the above-said that titanium and alloys on its base have unsatisfactory tribological characteristics, which limits their application in machine building, and in friction units in particular. Wear resistance of parts of titanium alloys can be increased by TCT, deposition of galvanic and plasma coatings, laser surface alloying etc.

Arc surfacing as a method of improving wear resistance of titanium parts has found no commercial application until now, despite the development of compositions of alloys that provide high wear resistance and long service life, and can be successfully deposited on titanium. To expand utilisation of titanium alloys in friction units, it is necessary to develop new filler materials and technology for surfacing using these materials.

1. Moroz, L.S., Polin, I.V., Butalov, L.V. et al. (1960) *Titanium and its alloys*. Leningrad: Sudpromgiz.
2. Natakov, E.B., Rajtses, V.B., Usachyova, V.V. et al. (1988) Gas-abrasive wear of titanium alloys. In: *Diffusion saturation and coatings on metals*. Kyiv: IPM.
3. Borisyonok, G.V., Vasiliev, L.A., Voroshnin, L.G. et al. (1981) *Thermochemical treatment of metals and alloys*. Moscow: Metallurgiya.
4. Klabukov, A.G., Zuev, A.M., Davydov, K.N. (1974) Improvement of wear resistance of titanium alloy by oxidising. *Izv. Vuzov, Mashinostroenie*, **3**, 120–124.
5. Tsvikker, U. (1979) *Titanium and its alloys*. Moscow: Metallurgiya.
6. Fedirko, V.N., Pogrelyuk, I.N., Yaskiv, O.I. et al. (1999) Corrosion behavior of titanium alloys with nitride films in hydrochloric acid solutions. *Zashchita Metallov*, **3**, 293–295.
7. Pogrelyuk, I.N. (2001) *Physical-chemical principles of intensification of titanium alloy nitriding process and design of hardened layers with increased wear and corrosion resistance*. Syn. of Thesis for Dr. of Techn. Sci. Degree. Lviv.
8. Iliin, A.A., Betsofen, S.Ya., Skvortsova, S.V. et al. (2002) Structural aspects of ion nitriding of titanium alloys. *Metally*, **3**, 6–10.
9. Itoh, J., Itoh, A., Azuma, H. et al. (1999) Improving the tribological properties of Ti–6Al–4V alloy by nitrogen ion implantation. *Surface Coat. Technology*, **111**, 172–176.
10. Guseva, M.I., Martynenko, Yu.V., Smyslov, A.M. (2000) Deep modification of titanium alloy by ion implantation. *Metally*, **3**, 108–112.
11. Peremitko, V.V. (2001) Improvement of wear resistance of titanium alloy parts. *Svarshchik*, **2**, 13.
12. Novikov, I.I., Levin, V.P., Minina, N.A. (2002) Study of influence of thermochemical and thermocyclic treatments on mechanical properties of parts from VT1-0 titanium alloy. *Metally*, **2**, 18–21.
13. Lugscheider, E., Fisher, A., Zhao, L. (2000) Reactive plasma spraying of titanium. *Adv. Eng. Mat.*, **5**, 281–284.
14. Nestler, M.C., Prenzel, G., Seits, T. (1998) HVOF-spraying vs. hard chrome plating-coatings characteristics and aircraft applications. In: *Proc. of 15th Int. Thermal Spray Conf.*, Nice, France, May 25–29, 1998.
15. Xia Yixiang, Li Di (2001) Influence of heat treatment after electrolytic coating on adhesion for TS4 titanium alloys. *Rare Metal Mater. and Eng.*, **5**, 388–391.
16. Epik, A.P., Bovkun, G.A., Golubchik, I.V. et al. (1965) *Some properties of diffusion carbide and boride coatings on refractory metals*. Kyiv: Naukova Dumka.
17. Eftifeev, S.L., Onishchenko, G.G., Sinkovsky, S.A. (1988) Residual stresses in sprayed coatings. In: *Diffusion saturation and coatings on metals*. Kyiv: IPM.

18. Bekrenev, A.N., Morozova, E.A. (1991) Modification of structure and properties of titanium surface layers in laser alloying. *Fizika i Khimiya Obrab. Materialov*, **6**, 117–123.
19. Liu, S. (2000) Treatment of titanium alloy surface by gas laser alloying. In: *Proc. of Int. Welding and Joining'2000 Conf. on New Materials and New Prospects*, Israel, July 18–20, 2000. Moscow.
20. Pleshakov, E., Senyavsky, Ya., Filip, R. (2002) Laser surface modification of Ti–6Al–4V alloy with silicon carbide. *Fizyko-Khimichna Mekhanika Materialiv*, **5**, 37–42.
21. Pey, Y.T., Ocelik, V., Hosson, J.T. (2002) SiC/Ti–6Al–4V functionally graded materials produced by laser melt injection. *Acta Materialia*, **8**, 2035–2051.
22. Euh, K.J., Lee, J.M., Lee, S.H. (2001) Microstructural modification and hardness improvement in boride/Ti–6Al–4V surface-alloyed materials fabricated by high-energy electron beam irradiation. *Metallurgical and Materials Transact. A*, **10**, 2499–2508.
23. Oh, J.S., Lee, S.H., Golkovsky, M.G. (2001) Improvements of the hardness and wear resistance of (TiC, TiN)/Ti–6Al–4V surface-alloyed materials fabricated by high-energy electron beam irradiation. *Ibid.*, **12**, 2995–3005.
24. Nikolenko, S.V., Verkhoturov, A.D., Kovalenko, S.V. (2002) Surface treatment of VT-20 titanium alloy by electric spark alloying. *Perspekt. Materialy*, **3**, 13–19.
25. Simakov, V.P., Budovskikh, E.A., Nosarev, P.S. et al. (1991) Treatment of titanium alloy with pulsed heterogeneous plasma by melting and alloying of surface layer with aluminium and nickel. *Fizika i Khimiya Obrab. Materialov*, **5**, 60–66.
26. Nadezhin, A.M., Iliin, A.A., Nikolaenko, V.V. et al. (2002) Influence of parameters of high-temperature pulsed plasma treatment on structure and properties of surface layer of VT3-1 titanium alloy samples. *Tekhnologiya Lyog. Splavov*, **3**, 12–16.
27. Onsawa, T., Suzumura, A. (1990) Brazing of titanium using low-melting point Ti-based filler metals. *Welding J.*, **11**, 462–467.
28. Lashko, S.F., Lashko, N.F. (1988) *Brazing of metals*. Moscow: Mashinostroenie.
29. Ilievsky, I.I., Kochukov, N.S. (1963) Brazing of titanium in high-rate heating. *Svarochn. Proizvodstvo*, **5**, 21–24.
30. Muraviov, R.S., Shalunov, S.A., Shirokikh, D.P. et al. (1989) Influence of VPr16 brazing alloy on resistance of titanium alloys. In: *Transact. on Progressive Methods of Brazing*. Kyiv: PWI.
31. Nerovny, V.M., Peremitko, V.V. (1995) Hardening and repair of working surfaces of titanium parts by arc vacuum brazing. *Svarochn. Proizvodstvo*, **3**, 3–5.
32. Teplova, L.A., Fetisov, G.P. (2002) Efficiency of double surface treatment of titanium and its alloys. *Tekhnologiya Metallov*, **8**, 10–16.
33. Gordienko, A.I., Pobol, I.L. (2000) Combined technologies of electron beam and laser welding for treatment of steel and titanium alloy surfaces. In: *Proc. of Int. Welding and Joining'2000 Conf. on New Materials and New Prospects*, Israel, July 18–20, 2000. Moscow.
34. Kitaguchi, S., Motoma, H. *Method of surfacing of engine valves*. Pat. 64–8306 Japan. Int. Cl. B 23 K 9/04. Publ. 12.01.89.
35. Kitaguchi, S., Nakada, Ya., Saito, T. *Method of surfacing of engine valves*. Pat. 64–48673 Japan. Int. Cl. B 23 K 9/04. Publ. 23.02.89.
36. Takeuchi, Yu., Nakata, M., Suzuki, F. et al. *Method of surface hardening of titanium or its alloys*. Pat. 2–277762 Japan. Int. Cl. C 23 C 4/12, C 21 D 1/06, C 23 C 4/18. Publ. 14.11.90.
37. Kitaguchi, S., Takayama, X., Tsukahara, T. et al. *Material for hardfacing of titanium substrate*. Pat. 4–94870 Japan. Int. Cl. B 23 K 9/04, B 21 K 35/30. Publ. 26.03.92.
38. Takahashi, W., Okada, M., Shida, Y. et al. Wear-resistant titanium alloys. *J. Jap. Soc. Heat Treat.*, **5**, 283–288.

HARDFACING THE WORKING COMPONENTS OF TILLAGE AND HARVESTING AGRICULTURAL MACHINERY (REVIEW)

Ch.V. PULKA
I. Pulyuj Ternopil State Technical University, Ternopil, Ukraine

The paper presents a review of the existing methods of hardfacing the tools of agricultural machinery and considers their advantages and drawbacks.

Keywords: *hardfacing processes (arc, gas, resistance, plasma, explosion, rolling, laser, induction), flat parts, agricultural machinery*

Tools of tillage and harvesting machinery (plough shares, hoeing plough discs, cultivator blades, toper cutters, etc.), operating under the conditions of intensive abrasive wear and considerable static and dynamic loads, should have a high wear resistance and strength [1–5]. In addition, in order to provide the cutting properties in operation, they should be self-sharpening. Experience shows that these requirements are best satisfied by bimetal tools. Steel of the main layer provides the strength, and the cladding layer, applied by some method on the base metal, provides the wear resistance. Self-sharpening effect depends on the ratio of thicknesses and wear resistance of the base and cladding layers [6]:

$$\omega = \varepsilon_2 h_2 / \varepsilon_1 h_1,$$

where $\varepsilon_2 h_2$, $\varepsilon_1 h_1$ are the wear resistance and thickness of the base and cladding layers, respectively.

The best self-sharpening is provided at $\omega = 1.5$.

Gas, resistance, plasma and induction hardfacing, cladding by explosion, rolling and other processes can be used for strengthening the tools of tillage and harvesting machinery [7–14].

It is proposed to use gas hardfacing to improve the wear resistance of disc cutters of beet harvesters, discs of seeders and hoeing ploughs [7]. The heat source in this process is the acetylene-oxygen flame, and rods or powders of wear-resistant alloys are used as filler material. Several multiflame tips for standard torches were developed [7]. Hardfacing with torches with such tips may be performed not only by a manual, but also by a mechanized process.

The advantages of gas hardfacing are as follows: shallow penetration of base metal and minimum dilution (8–10 %) of the deposited metal, simplicity and availability of the equipment and technology, ability to produce deposited metal of practically any alloying system. The main disadvantages of the process are low efficiency, and inconsistent quality of the deposited metal, which depends on the worker qualification.

Known is a method of hardfacing the tools of agricultural machinery, using resistance heating [11, 15–17]. The filler material in resistance hardfacing may be powders, wires and strips. Diagram of a unit for resistance hardfacing of disc cutters with a filler of wear-resistant alloy powders is shown in Figure 1. The advantages of this process are absence of base metal penetration, minimum deformations of the hardfaced parts, ability to deposit thin layers. The disadvantages are a low efficiency of the process, lack of batch-production of the equipment and unstable quality of the deposited layer.

To produce bimetal tools, in particular, hoeing plough discs, it is recommended to apply the process of resistance cladding with a wear-resistant strip [18]. The disc cutters are subjected to bulk quenching and tempering before cladding to provide the required strength and elasticity. Scale formed during rolling and heat-treatment is removed by etching in a 20 % solution of sulphuric acid with addition of 1 % OP-1 inhibitor, heated up to the temperature of 70 °C. The main drawbacks of this method are the great labour consumption of preparatory operations, difficulties of making strips of highly wear-resistant alloys.

The E.O. Paton Electric Welding Institute developed a process of constricted-arc hardfacing, namely plasma hardfacing [19]. Works [20–24] describe the technology of plasma hardfacing various parts and tools, including those of tillage machinery. Powders of Fe-base alloys and self-fluxing Ni-base alloys can be used as materials for hardfacing such parts. The method features shallow penetration of the base metal, high quality of the deposited metal, ability of deposition of thin layers with application of a wide range of filler materials. Relatively low efficiency and need for a complex and expensive equipment should be regarded as its disadvantages. High requirements to particle-size distribution and particle shape of powders for plasma hardfacing with powdered materials make them much more expensive. All this limits the application of this hardfacing process, also in agricultural machinery construction.

It was proposed to apply the methods of cladding by explosion and rolling for strengthening the working surfaces of various flat parts. The advantages of

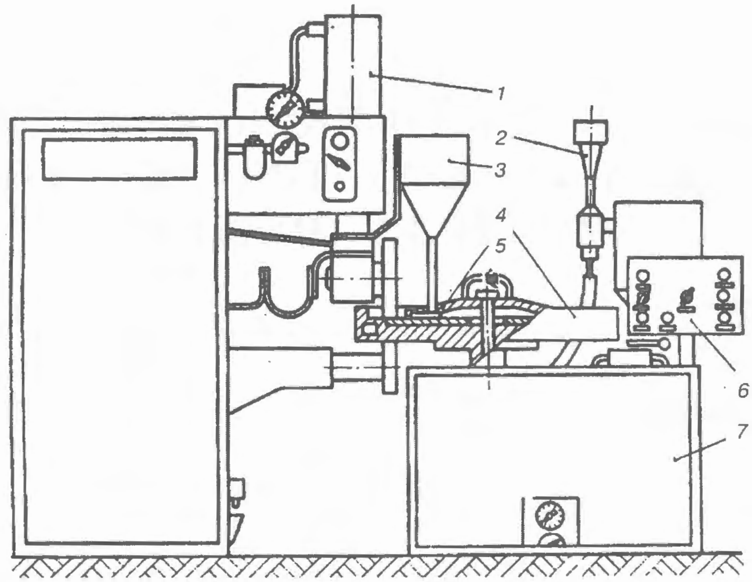

Figure 1. Diagram of a unit for resistance hardfacing of disc cutters [17]: *1* — resistance seam welding machine MSh-3201; *2* — hopper-type feeder; *3* — pneumatic clamp; *4* — water-cooled face-plate; *5* — ejector; *6* — control panel; *7* — base

explosion cladding include primarily the high speed of the process; ability to produce metal joints, which are impossible or difficult to produce by other methods; relative simplicity of the technology (no need to apply complex equipment) [12]. In Czechia the technology of explosion cladding was suggested for application in manufacture of bimetal cutters and other thin flat parts [25]. Evaluation of the effectiveness of the technology, compared to the traditional metallurgical process of cladding by casting, showed that its application is well-grounded in engineering and technical terms.

The E.O. Paton Electric Welding Institute developed and tried out a method to produce a wear-resistant bimetal at rolling of packs with PG-S1 powder [26], which is based on the principle of autovacuum pressure welding. The authors of [27] have successfully applied this process to produce a tool bimetal with the cladding layer of PR-10R6M5 powder. The main disadvantage of the process are technological difficulties in assembly of a large-sized pack, which are related to the need to compact the power to achieve a minimum volume of the air in the pack cavity.

This drawback can be eliminated by pre-compacting the powder. Work [28] shows that in production of bimetal shapes for tools of tillage machinery the cladding layer powder PG-S1 was first compacted by the method of hot isostatic pressing. However, application of this technology in production is prevented by the complexity and high labour consumption. More promising are the methods of producing bimetals, where the energy of explosion is used to apply and compact the powder layer.

Work [29] describes the results of experiments on explosion cladding with wear-resistant powders of the tools of agricultural machinery. Satisfactory properties of the bimetal joint and the high wear-resistance of the cladding powder layer are noted. The method of explosion powder cladding is simple in its implementation (does not require application of expensive equipment). However, its practical use is hindered by the long time, required for preparatory operations, considerable deformations of the items and billets, which have small thickness and developed cladding surface. In addition, the ability to produce sound coatings of great thickness appears to be problematic.

The authors of [13, 14] suggest a technology of producing a wear-resistant share strip with local cladding by rolling an asymmetrical pack. The pack design envisages making a slot in the corner of a blank of a square cross-section of steel 45, placing an insert of steel U20Kh6T2D of appropriate dimensions in it, welding of angle sections and plugs to it [30]. The technology was tried in manufacture of a two-layer share section for shares of general-purpose ploughs and shares of land-clearers [13, 30]. Its introduction into industry is restrained by a lack of rolled stock of steel U20Kh6T2D, and of the required shaped sections of steel 45, and the associated need for milling out the slot, which significantly increases the labour and material consumption of the process. A significant drawback of the method of pack rolling to produce wear-resistant and tool bimetals, which limits its wide application, is the low deformability of low-ductility materials of the cladding layer, which have, as a rule, a narrow temperature interval of rolling modes.

Arc hardfacing is also used for strengthening the tools of agricultural and road construction machinery [31]. However, application of this process for hardfacing thin flat parts 2–5 mm thick is restrained by deep penetration of the base metal, particularly in hardfacing with wires, and by considerable deformation of the hardfaced parts.

Other methods of strengthening the tools of tillage machines were also developed. They include hardfacing with an electron accelerator [32], laser surfacing [33], etc. However, these processes have not yet been accepted by industry, because of the complex technology and lack of equipment, its imperfection and high cost.

Induction process of hardfacing is widely applied for strengthening thin flat parts, including the working components of agricultural machinery. Its advantages include the possibility of deposition of thin layers; high efficiency; possibility of process mechanization and automation (which is important in batch production). The disadvantages include the high power consumption, overheating of base metal, and the need for filler material to be more low-melting than the base metal. Despite that, this process is the most widely accepted in the plants, producing agricultural machinery, ploughs, hoeing ploughs, cultivators, etc. [5, 34–36]. Induction melting is performed using a special charge, consisting of a mixture of powder of a wear-resistant alloy and flux. The charge is applied on the part surface in the form of a layer of a certain thickness. Then the section of the part, which is to be processed, is placed into the inductor of the high-frequency unit (Figure 2), where the power source is a lamp generator.

When high-frequency currents pass through the inductor, eddy currents are induced in the surface layers of the metal, which preheat the part. The charge is heated and melted by the heat, coming from the part. After its melting the part is taken out of the inductor and cooled. Figure 3 shows the tools of agricultural machinery, strengthened by induction hardfacing.

Automated lines and units were developed to improve the labour condition and process efficiency in induction hardfacing of thin flat parts [37–39]. A semi-automatic unit and an automatic line were developed for hardfacing cultivator wedges and blades, and carousel-type units are used for hardfacing the

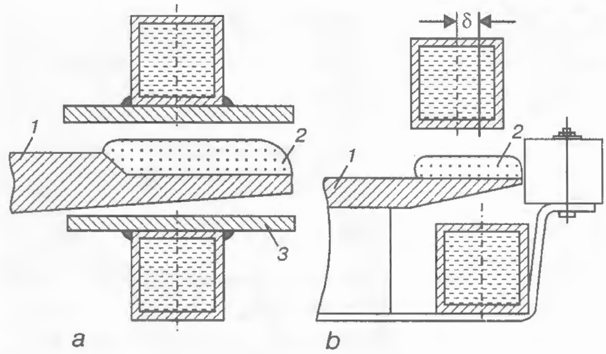

Figure 2. Set up for hardfacing of a shear (*a*) and blade (*b*) of a cultivator: *1* — part; *2* — charge layer; *3* — inductor

cultivator blades, having a curvilinear cutting surface [39]. Carousel-type unit also permit hardfacing wedge-shaped shares. The main disadvantages of these lines and units are low efficiency of the hardfacing process proper, as well as the low level of mechanization in the stations of billet feed, charge pouring and unloading.

The most difficult is hardfacing of thin discs with a continuous or intermittent working surface (cutting part), where a continuous-successive method of induction hardfacing is used (Figures 4 and 5). In this case, a segment inductor is fixedly attached to the high-frequency generator, and the part with the hardfacing charge is rotating relative to it (Figure 4). The advantages of the continuous-successive hardfacing process are as follows: technological flexibility, ability to surface parts of various diameters at a relatively low power of the high-frequency generators. The disadvantages include a relatively low efficiency; high power consumption; part distortion (which affects the uniformity of the deposited layer thickness); need for straightening to eliminate disc deformations.

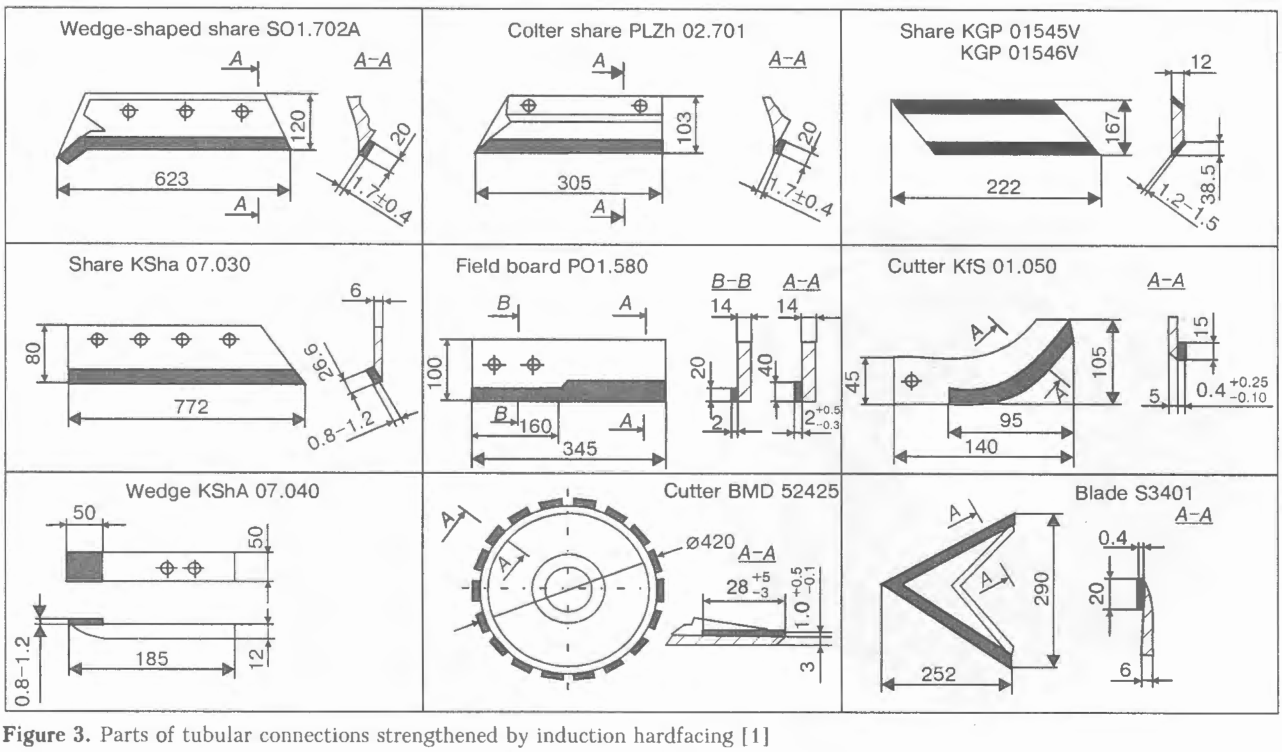

Figure 3. Parts of tubular connections strengthened by induction hardfacing [1]

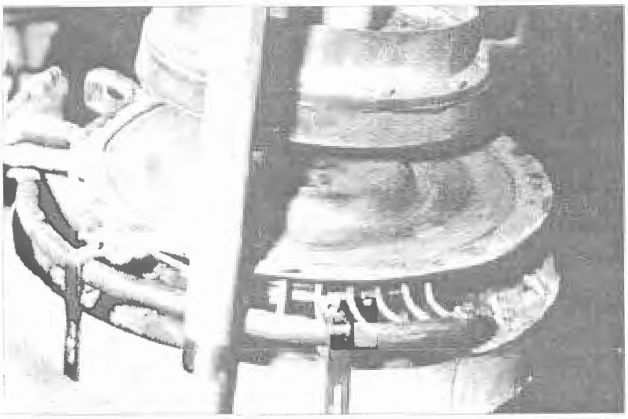

Figure 4. Device for hardfacing a solid-drawn cutter using a segment inductor

In order to automate the process of induction hardfacing of thin shaped discs — topper-cutters of haulm gatherers BM-6B by the continuous-successive method Company «Ternopil Combine Plant» developed and introduced an automatic transfer line [40], allowing complete automation of the process, including loading-unloading of the blanks, their displacement in the rotor device through the stations of part mounting, charge pouring, hardfacing and part removal after hardfacing (Figure 6).

The automatic line consists of the following main components: horizontal-mobile platform *11*, to which three-position rotary carousel *10*, pick-and-place robot *6* with two electromagnetic grips, two lifters *8* and *3*, container with blank pack *7* and container for hardfaced products *5*, charge pouring assembly *9*, cabinet with the switching and regulation pneumatic equipment *4*, high-frequency generator with inductor *1* and control cabinet *2* are fixedly attached.

The line operates in the automatic mode as follows. Pick-and-place robot *6* simultaneously loads a blank into the station of carousel loading-unloading *10* and unloads the hardfaced parts (if available) into container *5*, and then returns to the initial position. Then at rotation of the carousel by 120° the stations are shifted, and the blank moves into the station of charge pouring. After that the blank is fed to the hardfacing

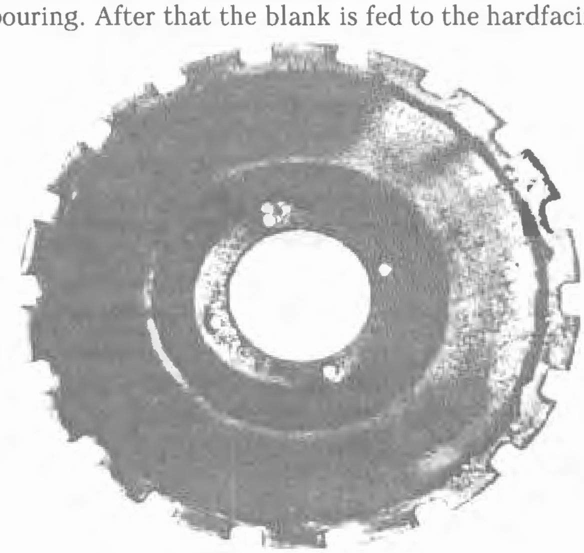

Figure 5. Topper-cutter BMD 52425 after hardfacing

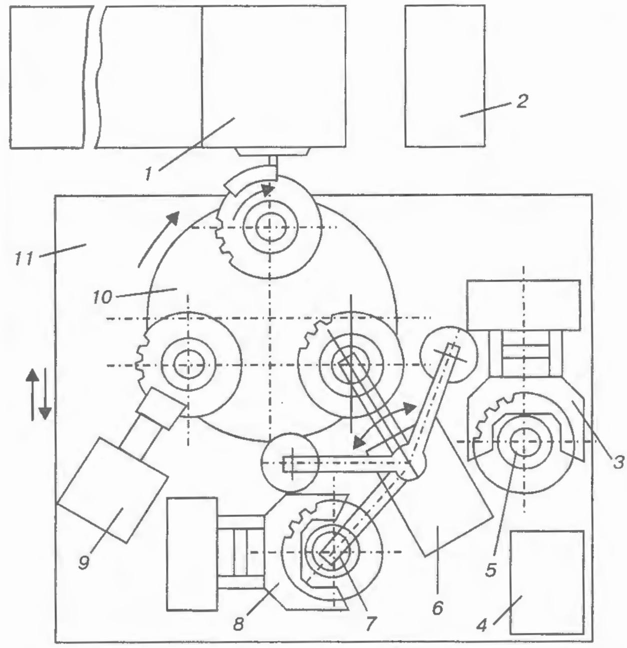

Figure 6. Block diagram of an automatic flow line for hardfacing thin shaped discs by the continuous-successive method (for designations see the text)

station by rotation of the carousel. After completion of hardfacing, the hardfaced item is fed to the loading-unloading zone by rotation of the carousel. Rotation of carousel *10* proceeds with platform *11* withdrawn from the inductor. This transfer line has the disadvantages of a comparatively low efficiency of the hardfacing process proper (time of hardfacing one topper-cutter is more than 3 min); high power consumption of the process; distortion of the processed part, which requires additional straitening operation to eliminate it.

The efficiency can be increased by simultaneous hardfacing of the disc over the entire working surface, using more powerful high-frequency generators, produced by the local industry, and applying more powerful inductors. The power can be saved by optimizing the modes of power supply to the inductor, including development of equipment for automation of the hardfacing process as a whole.

Application of the known multi-stage modes of induction hardfacing to save power within the specified time does not yield a positive effect. This is related to great difficulties of control and practical implementation of such a technology under industrial conditions. In addition, multiple switching of the generator during hardfacing of one part (3–4 times) adversely affects its performance and efficiency.

More promising in terms of power saving is development of other control circuits of power supply to the inductor, which is performed continuously, without switching of the generator. This allows a rather simple implementation of the hardfacing process on the shop floor, and thus improvement of the fatigue life and performance of high-frequency generators and efficiency of the process as a whole.

Inductor design makes a great influence on power consumption, efficiency and quality of the hardfacing process. A large number of various designs of the inductor are currently available, which are applied for part heating for quenching or hardfacing. However, the continuously changing and expanding range of hardfaced parts, continuous improvement of the process, require careful selection or development of special inductors. Their dimensions, shape and mode parameters are selected by the experimental method for each specific part. For instance, single-turn ring inductors are used for hardfacing solid discs of a small diameter, and segment and two-loop inductors, where the hardfacing efficiency depends on the power of high-frequency generators, are used for large-sized toothed discs. Application of single-turn ring inductors for hardfacing toothed discs in order to increase the efficiency, often runs into difficulties in provision of a uniform distribution of the electromagnetic field in the hardfacing region, which affects the quality of the deposited layer. The disadvantages of the two-loop inductor are the same as those of the segment one: comparatively low efficiency, high power consumption, part distortion due to local heating, as well as the impossibility of using it for simultaneous hardfacing of the entire working surface of thin toothed discs with the deposit width greater than the tooth height.

The process of improvement of induction hardfacing of thin flat parts develops in the following directions: improvement of the efficiency of the hardfacing process; optimization of heating modes in order to save power; optimization of the design parameters of inductors for hardfacing discs of various diameters and dimensions of the hardfacing zone without allowing for electromagnetic field shielding, with allowing for just the electromagnetic shielding, as well as combined shielding of the electromagnetic and thermal fields simultaneously; mathematical simulation of the hardfacing process to determine residual stresses, displacements and deformation of parts; mechanization and automation of the hardfacing processes with development of new inductor designs, taking into account the process ecology, protection of man from the impact of electromagnetic and thermal fields and improvement of the inductor efficiency.

Improvement of the efficiency of the hardfacing process and reduction of deformation may be achieved by replacement of the continuous-successive process by simultaneous hardfacing of the entire working surface. For instance, a two-turn ring inductor was developed for hardfacing thin toothed discs with the deposit height greater than the tooth height. This inductor is used for simultaneous hardfacing of the entire working surface. Up to 15–25 % of power can be saved due to exponential increase of power during hardfacing. Shielding of the thermal and electromagnetic fields in disc hardfacing allows control of power in the hardfacing zone, in order to achieve a uniform thickness of the deposited layer over the entire working surface.

In order to implement the technology of induction hardfacing of disc-shaped tools of agricultural machinery by the method of simultaneous hardfacing of the entire working surface, mechanized and automated lines were developed, which were introduced in Company «Ternopil Combine Factory». The line design is novel in that the inductors with high-frequency heating are not rigidly coupled to generators for the first time in the world practice. The number of inductors is selected, depending on the number of positions in the automatic line. The rotary table of the latter is fitted with two-turn ring inductors by the number of rotary face-plates with the device for connection of the high-frequency generator taps to the inductors, mounted on the base between the rotary table and the generator.

The results of improvement of the process of induction hardfacing of disc-shaped tools in agricultural machinery in the above directions were published in [40–51].

1. Bol, A.A., Leskov, S.P. (1985) Induction hardfacing of parts in agricultural engineering. In: *Hardfacing. Experience and efficiency of application*. Kyiv: PWI.
2. Vishnevsky, A.A., Kostylyov, Yu.M., Ostrov, D.D. (1978) *Technology of manufacturing of hardfaced disc cutters. Hardfacing of parts of metallurgical and mining equipment*. Abstracts. Moscow: NIIInformtyazhmash.
3. Strelbitsky, V.F. (1978) *Disk tillage machines*. Moscow: Mashinostroenie.
4. Lozovsky, V.P., Ostapenko, A.T., Prokopenko, V.A. (1983) Investigation of working capacity and criteria of marginal state of hoeing plough discs. *Trakrory i Selkhozmashiny*, **6**, 15–16.
5. Tkachyov, V.N. (1971) *Wear and improvement of life of agricultural machinery parts*. Moscow: Mashinostroenie.
6. Rabinovich, A.Sh. (1962) *Self-sharpening plough shares and other soil-cutting machine parts*. Moscow: GOSNITI.
7. Sidorov, A.M. (1987) *Repair of machine parts by spraying and hardfacing. Moscow*: Mashinostroenie.
8. Bol, A.A., Leskov, S.P., Sviridenko, E.P. et al. (1986) Hardfacing of hoeing plough discs. In: *Hardfacing in manufacturing of machine parts and equipment*. Kyiv: PWI.
9. Lehman, H., Herrmann, J. (1979) Auftragsschweissen von Packerscheiben. *ZIS Mitt.*, **8**, 826–840.
10. Blume, F., Kretschmann, G., Rosert, R. (1982) Dünnschichtauftragschweissen Moeglichkeiten und Anwendung. *Schweisstechnik*, **11**, 501–503.
11. Nikolaenko, M.R., Rymorov, E.V. (1976) *New technological processes of electric arc and electric resistance hardfacing of high-wear parts of structural and road machines*. Moscow: TsNIITEstrojmash.
12. Gelman, A.S., Tsemakhovich, B.D., Chudnovsky, A.D. et al. (1978) *Explosion cladding of steel*. Moscow: Mashinostroenie.
13. Ryabtsev, I.A. (1982) *Wear-resistant clad rolled metal*. Kyiv: Znanie.
14. Ryabtsev, I.A., Rozenfeld, Kh.Kh., Chin, A.I. (1984) Technology of manufacturing of clad plough shares of land clearers. In: *Design and technology of manufacturing of agriculture machinery*. Issue 14.
15. Klimenko, Yu.V. (1982) Electric resistance hardfacing. Applications and prospects of development. In: *Current methods of hardfacing and their application*. Kyiv: PWI.
16. Klimenko, Yu.V. (1978) *Electric resistance hardfacing*. Moscow: Metallurgiya.
17. Turkin, V.P., Putilin, V.G., Nikolaenko, M.R. et al. (1978) Electric resistance hardfacing of cutter discs. *Avtomatich. Svarka*, **2**, 74–76.
18. Mamuliya, G.E., Murov, G.F., Tyulenev, V.P. et al. (1984) Resistance cladding of tillage machine tools. *Svarochn. Proizvodstvo*, **2**, 37–39.
19. Kalensky, V.K., Gladky, V.P., Frumin, I.N. (1963) Investigation and development of automatic method for hardfacing of car exhaust valves. *Avtomatich. Svarka*, **1**, 17–18.

20. Kosilov, A.I. (1983) Plasma hardfacing of parts with powder compositions. *Tekhnika v Sel. Khoz.*, **1**, 30–32.
21. Danilov, A.I., Komarcheva, E.S. (1982) Plasma surfacing of corrosion- and wear-resistant materials. *Elektrotekhnika*, **5**, 58–60.
22. Podlekarev, N.N., Belozersky, L.N., Olekseenko, I.D. (1980) Optimum technological conditions of plasma hardfacing of agriculture machinery parts. In: *Mechanisation and electrification of agriculture industry of Non-Black Earth Zone of the USSR*. Issue 23.
23. Salkova, S.S., Komarcheva, E.S., Mishchenko, L.G. (1987) Strengthening of tillage machine tools by plasma hardfacing method. In: *Advanced methods of hardfacing by corrosion- and wear-resistant materials*. Leningrad: Energiya.
24. Podlekarev, N.N., Belozersky, L.N. (1980) Semi-automatic machine for plasma hardfacing of plough share blades. In: *Mechanisation and electrification of agricultural industry of Non-Black Earth Zone of the USSR*. Issue 23.
25. Tsukr, V., Vild, I. (1976) Experience in cladding of tool steels and their heat treatment. In: *Proc. of 3rd Int. Symp. on Application of Explosion Energy in Welding, Cladding, Compacting and Pressing with Metallic Powder for Manufacturing of Metallic Materials*.
26. Ryabtsev, I.A. (1981) Bimetallic rolled metal with clad layer of granulated powder PG-S1. In: *Abstr. of pap. of 3rd Republ. Sci.-Techn. Conf. on Current Methods of Hardfacing and Consumables*. Kharkiv.
27. Kalner, V.D., Goryushina, M.N., Sichuzhnikova, A.A. (1984) Processes of interaction on boundary of bimetallic billet manufactured by rolling of non-sintered powder. *Metalloved. i Term. Obrab. Metallov*, **3**, 28–29.
28. Fyodorov, B.N., Osadchy, V.A., Tits, M.Yu. et al. (1975) Prospects of application of compacted materials in parts of agricultural machinery tools. *Traktory i Selkhozmashiny*, **9**, 39–41.
29. Kretzchmar, H., Sporl, D., Schwable, H. (1983) Aufplattiren Verschleissfaster Schichten. *ZIS Mitt.*, **2**, 108–115.
30. Ryabtsev, I.A. (1981) Application of wear-resistant clad rolled metal in manufacturing of tillage machine tools. In: *Theoretical and technological principles of hardfacing. Hardfacing in mechanical engineering and repair*. Kyiv: PWI.
31. Ryabtsev, I.A. (1998) Classification and characteristics of methods of hardfacing. *Svarshchik*, **3**, 23–25.
32. Fominsky, L.P., Levchuk, M.V., Bajsman, A.F. et al. (1987) Hardfacing of agricultural machinery tools with electron accelerator. *Svarochn. Proizvodstvo*, **11**, 4–6.
33. Kovalenko, V.S., Golovko, L.F., Merkulov, G.V. et al. (1981) *Laser beam strengthening of parts*. Ed. by V.S. Kovalenko. Kyiv: Tekhnika.
34. Bol, A.A., Leskov, S.P. (1986) State and prospects of strengthening of agricultural machinery tools by induction hardfacing. In: *Abstr. of pap. of All-Union Seminar on State and Prospects of Strengthening of Tractor and Agricultural Machinery Tools*. Moscow.
35. Ryabtsev, I.A. (2000) Induction hardfacing. *Svarshchik*, **5**, 13–16.
36. Tkachyov, V.N., Fishtejn, B.M., Kasintsev, N.V. et al. (1970) *Induction hardfacing of hard alloys*. Moscow: Mashinostroenie.
37. Tkachyov, V.N., Lakosin, N.I., Vlasov, E.I. et al. *Machine for induction hardfacing of hoes*. USSR author's cert. 214696. Publ. 1968.
38. Smirnov, I.A., Vinokur, I.Sh., Moshlevsky, E.L. et al. *Machine for induction hardfacing*. USSR author's cert. 284213. Publ. 1970.
39. Bol, A.A. (1984) Development of induction hardfacing in agricultural machinery. In: *Technology*. Issue 3.
40. Shably, O.N., Pulka, Ch.V., Budzan, B.P. (1988) Ways of energy saving in induction hardfacing of thin-wall discs. *Avtomatich. Svarka*, **12**, 56–58.
41. Pulka, Ch.V., Shably, O.N., Budzan, B.P. et al. *Method of hardfacing of thin shaped discs*. USSR author's cert. 1619571. Int. Cl. B 23 K 13/00.
42. Pulka, Ch.V., Shably, O.N., Grabin, V.F. et al. (1991) Improvement of technology of induction hardfacing of shaped discs. *Avtomatich. Svarka*, **1**, 57–61.
43. Pulka, Ch.V. (1991) *Study and optimisation of technology of induction hardfacing of thin shaped discs*. Thesis for Cand. of Techn. Sci. Degree. Kyiv.
44. Shably, O.N., Pulka, Ch.V. (1994) Technology and equipment for induction hardfacing of thin shaped discs. *Avtomatich. Svarka*, **5/6**, 48–50.
45. Shably, O.N., Pulka, Ch.V., Pismenny, A.S. (1997) Optimisation of design values of inductor for induction hardfacing of thin steel discs. *Ibid.*, **6**, 17–20.
46. Pulka, Ch.V. (1997) Influence of induction hardfacing conditions on thickness of deposited layer and deformation value of thin steel discs. *Ibid.*, **10**, 57–58.
47. Pulka, Ch.V. (1998) Programming of heating condition in induction hardfacing of thin steel discs. *Ibid.*, **1**, 48–50.
48. Shably, O.N., Pulka, Ch.V., Mikhajlishin, V.M. et al. (1999) Residual displacements of thin steel discs in induction hardfacing with wear-resistant powder-like hard alloys. *Ibid.*, **9**, 57–59.
49. Shably, O.N., Pulka, Ch.V., Pismenny, A.S. (2002) Optimisation of inductor parameters for uniform heating of discs across the width of the hardfacing zone, allowing for screening. *The Paton Welding J.*, **11**, 24–26.
50. Pulka, Ch. (2002) Mechanised line for continuous-successive induction hardfacing of thin shaped discs. *Visnyk TDTU*, **2**, 83–90.
51. Pulka, Ch. (2002) Energy-saving automated line for simultaneous induction hardfacing of thin shaped discs. *Ibid.*, **3**, 41–48.

SANITARY-HYGIENIC EVALUATION OF FLUX-CORED WIRES FOR ELECTRIC ARC SURFACING

O.G. LEVCHENKO, V.A. METLITSKY, I.A. RYABTSEV and **S.A. GRISHCHENKO**
E.O. Paton Electric Welding Institute, NASU, Kyiv, Ukraine

Results of investigation of chemical composition and level of evolution of welding aerosols entering the air of working zone in flux-cored wire submerged arc and open arc surfacing are presented. Recommendations are suggested for protection of workers-welders and environment from welding aerosols.

Keywords: *flux-cored wires, surfacing, welding aerosols, harmful elements, levels of evolutions, sanitary-hygienic recommendations, means of protection*

In fulfillment of welding and surfacing jobs, the harmful elements in the composition of welding aerosols (WA), representing a hazard for the human organism, enter the working zone air and environment. Chemical composition and levels of WA evolutions, as well as the selection of necessary means of protection from a harmful effect are determined by a composition of welding (surfacing) materials and condition of welding (surfacing) [1, 2]. At present the problems of protection of workers-welders in Ukraine are regulated by a system of standards of labour safety and technical specifications for welding and surfacing materials.

However, one of the main standardized documents is GOST 26101–84 «Flux-Cored Wire for Surfacing. Technical Specifications», on the basis of which the manufacturers of surfacing flux-cored wires were coming recently to a market, became already obsolete. This document contains information about more than 20 grades of surfacing flux-cored wires, most of which were developed at the E.O. Paton Electric Welding Institute in different periods of time. However, there are no data concerning sanitary-hygienic evaluation of these flux-cored wires in accordance with present rates in the standard, that is a serious disadvantage.

A great attention is paid at PWI to the safety of labour in flux-cored wire surfacing. The sanitary-hygienic evaluation of some flux-cored wires, earlier developed (PP-Np-25Kh5MSGF, PP-Np-35V9Kh3GSF, PP-Np-30Kh2M2SGF), which are manufactured at present by TSU 05416923.024–97, was made.

The aim of this work is to make the sanitary-hygienic evaluation of flux-cored wires, developed at PWI for submerged arc and open arc surfacing, and to take it into account in chapter «Requirements for Safety and Protection of Environment» of technical specifications of Ukraine, being developed for flux-cored wires and also in recommendations for protection of workers-welders and environment from harmful elements in surfacing using these wires.

The flux-cored wires investigated are designed for surfacing of parts operating under different conditions of wear almost in all the branches of industry (PP-AN198 and PP-AN199 – under the conditions of metal friction on metal; PP-AN105, PP-AN192, PP-AN197, PP-AN201 – under the conditions of abrasive wear at impacts of different intensity; PP-AN202 and PP-AN203 – surfacing of tram rails and other parts under similar conditions; PP-AN130, PP-AN132, PP-AN193, PP-AN195, PP-AN196, PP-AN199 – submerged arc and open arc surfacing of different parts of metallurgical equipment).

Chemical composition and characteristics of levels of WA evolutions were determined experimentally according to the methodological recommendations [3, 4] and processing of obtained data and selection of appropriate means of protection from WA were made using a computerized information-retrieval system «ECO-WELD», developed at PWI for hygienic evaluation of welding consumables [5]. Selection of samples of a hard component of WA (HCWA) was made in the process of surfacing beads on plates from steel VSt3sp (killed) at optimum conditions (Table 1) using the flux-cored wires investigated. Open arc surfacing was made by the welding semi-automatic machine of the PDG-516 type, and submerged arc surfacing was made in surfacing installation of the U-653 type. Direct current of reverse polarity was used. WA were trapped using a special shelter, isolating the surfacing zone. Here, HCWA were deposited on filters of FPP-15-1.5 cloth for determination of levels of their evolution and on filters AFA-KhA-18 for chemical analysis of HCWA samples. Amount of evolving HCWA and its components was determined by a gravimetric method using two parameters [3], such as intensity of formation (g/min) and specific evolution (g/kg) of wire.

In addition, the data obtained were processed using system «ECO-WELD» [5] and entered its bank in the form of additional characteristics necessary for the objective hygienic evaluation of wires, such as coefficients of intensity (g/kW·h) and specific evolutions (g/kW·kg), and also the required volume of ventilation air for dilution of harmful elements up to

Table 1. Conditions of flux-cored wire surfacing

Wire grade	*Wire diameter, mm*	*Shielding medium*	*Current, A*	*Voltage, V*	*Surfacing speed, m/h*
PP-AN105	2.2	Self-shielding	200–240	25–27	15
PP-AN130	1.6	Same	120–160	24–25	15
PP-AN192	2.6	»	260–300	26–28	15
PP-AN193	1.6	»	130–170	24–28	15
PP-AN196	2.0	»	150–180	25–26	15
PP-AN197	2.5	»	200–250	26–28	15
PP-AN198	2.8	»	220–250	28–32	15
PP-AN199	1.6	»	100–120	28–32	15
PP-AN203	2.6	»	200–250	26–30	20
PP-AN132	3.6	Flux AN-26	300–350	30–32	10
PP-AN194	2.0	Same	200–230	28–32	15
PP-AN195	2.0	»	180–220	28–32	15
PP-AN201	2.6	Flux AN-348	340–360	30–32	15
PP-AN202	2.6	Flux AN-26	300–360	30–32	15

limiting admissible concentrations (LAC), expressed in m^3/kg [3] and m^3/h [6].

In accordance with the methodological recommendations [4] the content of harmful elements, for example, manganese, nickel, molybdenum, copper, aluminium, vanadium in the composition of HCWA is presented in the form of chemical elements, chromium compounds in recalculation for CrO_3 and Cr_2O_3, silicon — for SiO_2, iron — for Fe_2O_3, and fluorides, soluble F_{sol} and insoluble F_{insol} in recalculation for fluorine. HCWA components can be not only in the form of oxides, but also in the form of complex compounds, such as spinel, silicates, etc. [7, 8]. Therefore, the terminology «compound of elements» is used in this work.

The results of determination of HCWA chemical composition in flux-cored submerged arc and open-arc surfacing are given in Tables 2 and 3, results of intensity and specific evolutions of HCWA are presented in Tables 4 and 5, and results of evolution of harmful elements of HCWA are shown in Table 6.

Results of examination of chemical composition of HCWA, formed in flux-cored wire submerged arc and open arc surfacing, showed that they contain compounds of iron, manganese, tri- and sexivalent chromium, soluble and insoluble fluorides, silicon, nickel and others (Table 2). The larger share in HCWA belongs to iron compounds, and also to volatile compounds of manganese and insoluble fluorides.

In open arc flux-cored wire surfacing the HCWA has, except trivalent chromium, a soluble carcinogenic sexivalent chromium, whose concentration is increased with increase in chromium content in the composition of wires. Maximum concentrations of tri- (13.8 %) and sexivalent (0.37 %) chromium were revealed in application of wire PP-AN197 containing its maximum amount (25 %).

In submerged arc flux-cored wire surfacing the sexivalent chromium was not revealed in HCWA composition in all cases, except the use of flux-cored wire PP-AN201 containing 15 % Cr (Table 3). This is explained by that the protective layer of flux exerts also effect on transition of components in HCWA evaporating from the weld pool, which can precipitate on flux grains. And only at a large content of chromium in the wire it can transfer to HCWA in the form of

Table 2. Chemical composition of HCWA in open arc flux-cored wire surfacing

Wire grade	*Mass share of HCWA components, %*									
	CrO_3	Cr_2O_3	*Mn*	SiO_2	Fe_2O_3	F_{sol}	F_{insol}	*Ni*	*Mo*	*Others*
PP-AN105	–	–	13.1	–	70.9	0.6	1.8	2.3	–	–
PP-AN130	0.05	2.9	–	2.6	70.7	1.1	11.7	–	1.5	0.3V
PP-AN192	0.15	3.4	–	–	48.2	0.1	0.6	–	0.5	–
PP-AN193	0.03	3.0	–	–	33.4	4.0	8.3	1.8	1.2	2.3Cu
PP-AN196	0.35	4.1	4.5	–	45.2	6.2	14.6	–	0.7	0.8V, 1.9Cu
PP-AN197	0.37	13.8	2.8	3.2	62.5	0.7	3.1	–	–	–
PP-AN198	–	–	1.2	4.2	33.3	6.5	4.4	–	–	4.7Al
PP-AN199	0.28	4.5	2.0	3.0	48.7	0.3	9.5	–	–	–
PP-AN203	–	–	3.5	–	38.2	4.2	13.5	–	–	–

Table 3. Chemical composition of HCWA in submerged arc flux-cored surfacing

Wire grade	Mass share of HCWA components, %								
	CrO_3	Cr_2O_3	Mn	SiO_2	Fe_2O_3	F_{sol}	F_{insol}	Ni	Mo
PP-AN132	–	2.8	2.0	3.4	70.2	0.5	7.5	–	–
PP-AN194	–	2.9	2.2	28.6	35.5	1.7	12.4	–	–
PP-AN195	–	9.3	3.7	24.3	23.8	2.1	10.7	–	–
PP-AN201	0.05	17.4	18.6	14.7	27.8	0.5	4.4	–	1.7
PP-AN202	–	2.7	4.6	2.7	74.9	0.5	5.8	0.8	–

instable sexivalent chromium. In addition, the flux introduces it share to the aerosol composition. Thus, in application of high-manganese flux AN-348 (Table 3) the largest amount of manganese was revealed in HCWA composition. Thus, flux can exert both useful effect on the HCWA composition (screens the enter of sexivalent chromium into HCWA) and also negative effect (promotes the transition of compounds of manganese, silicon, fluorides and other components contained in flux into HCWA composition).

It was established as a result of investigation of intensity of formation and evolution of HCWA in use of mentioned wires (Table 4) that their characteristics depend on the wire diameter and surfacing conditions. When the large-diameter self-shielding flux-cored wires are used the HCWA evolution is increased at appropriate conditions, and their specific evolutions, as a rule, are decreased. This is explained by the fact that, when the large-diameter wires are used, the welding arc power is increased, leading to increase in intensity of HCWA formation. Reduction of specific HCWA evolutions here can be explained by an appropriate decrease in specific arc power due to increase in volume of the metal being melted.

In submerged arc surfacing (Table 5) this regularity was not revealed, as in this case the process of HCWA evolution is mostly affected not only by arc power, but the presence of layer of a protective flux, depositing a significant part of evolving HCWA flow on flux grains. Therefore, the intensity of HCWA formation also in submerged arc welding is approximately 20 times, and specific evolution is 30 times lower than in open arc welding with self-shielding flux-cored wires.

Table 4. Intensity and specific evolutions of HCWA in open arc flux-cored wire surfacing

Wire grade	Wire diameter, mm	Intensity of HCWA formation, g/min	Specific evolution of HCWA, g/kg
PP-AN105	2.2	1.06	20.6
PP-AN130	1.6	0.63	21.8
PP-AN192	2.6	1.78	23.4
PP-AN193	1.6	0.88	27.2
PP-AN196	2.0	1.15	26.6
PP-AN197	2.5	0.92	24.6
PP-AN198	2.8	1.19	16.0
PP-AN199	1.6	0.98	33.6
PP-AN203	2.6	1.47	20.0

Results of determination of specific evolutions of HCWA components (Table 6) were used in calculation using system «ECO-WELD» of the required volume of ventilation air for dilution of harmful elements up to LAC (Table 7). These data can be used in calculation of efficiency of ventilation of industrial rooms for determination of air changes per hour [6] or as a level of WA toxicity in the process of using flux-cored wires.

The carried out investigations of sanitary-hygienic properties of surfacing flux-cored wires became the bases of chapter «Requirements for Safety and Protection of Environment» TSU 28.7.05416923.066–2002, according to which the fourteen grades of flux-cored wires, developed at PWI, are manufactured now.

It follows from Table 7 that the required volume of the ventilation air, proving also the HCWA toxicity at the above-mentioned surfacing process, is increased in the presence of elements in the aerosols of the 1st (sexivalent chromium, nickel) and 2nd (manganese, soluble fluorides) classes of risk (GOST 12.1.005–88). As this hygienic characteristic depends on content of harmful elements in HCWA, so it is maximum (13490 m^3/kg) in surfacing with a wire having the highest concentration of manganese (PP-AN105). In submerged arc surfacing the required amount of ventilation air is maximum (400 m^3/kg) in case of using the high-manganese flux AN-348 in spite of the fact that the wire PP-AN194, used in this case, contains the minimum amount of chromium and manganese. This is confirmed by that the protective layer of flux screens the transfer of wire components into HCWA,

Table 5. Intensity and specific evolutions of HCWA in submerged arc flux-cored wire surfacing

Wire grade	Wire diameter, mm	Flux grade	Intensity of HCWA formation, g/min	Specific evolution of HCWA, g/kg
PP-AN132	3.6	AN-26	0.072	0.88
PP-AN194	2.0	AN-26	0.040	0.51
PP-AN195	2.0	AN-26	0.037	0.64
PP-AN201	2.6	AN-348	0.028	0.43
PP-AN202	2.6	AN-26	0.122	1.49

Table 6. Specific evolutions of HCWA harmful elements in flux-cored wire surfacing

Wire grade	*Specific evolutions of HCWA, g/kg*						
	CrO_3	Cr_2O_3	*Mn*	SiO_2	Fe_2O_3	F_{sol}	F_{insol}
			Open arc surfacing				
PP-AN105	–	–	2.690	–	14.63	0.130	0.370
PP-AN130	0.010	0.630	–	0.580	15.45	0.240	2.560
PP-AN192	0.035	0.790	–	–	11.26	0.033	0.149
PP-AN193	0.008	0.829	–	–	9.095	1.093	2.240
PP-AN196	0.093	1.080	1.197	–	12.03	1.650	3.880
PP-AN197	0.091	3.401	0.690	0.798	15.41	0.182	0.759
PP-AN198	–	–	1.790	0.670	5.32	1.040	0.710
PP-AN199	0.094	1.526	0.675	1.109	16.38	1.780	3.195
PP-AN203	–	–	0.710	–	7.64	0.840	2.700
			Submerged arc surfacing				
PP-AN194	–	0.015	0.011	0.146	0.181	0.009	0.064
PP-AN195	–	0.059	0.024	0.156	0.152	0.013	0.068
PP-AN202	–	0.040	0.070	0.040	1.12	0.008	0.086
PP-AN201	0.0002	0.075	0.081	0.064	0.12	0.002	0.019
PP-AN132	–	0.025	0.018	0.029	0.62	0.004	0.066

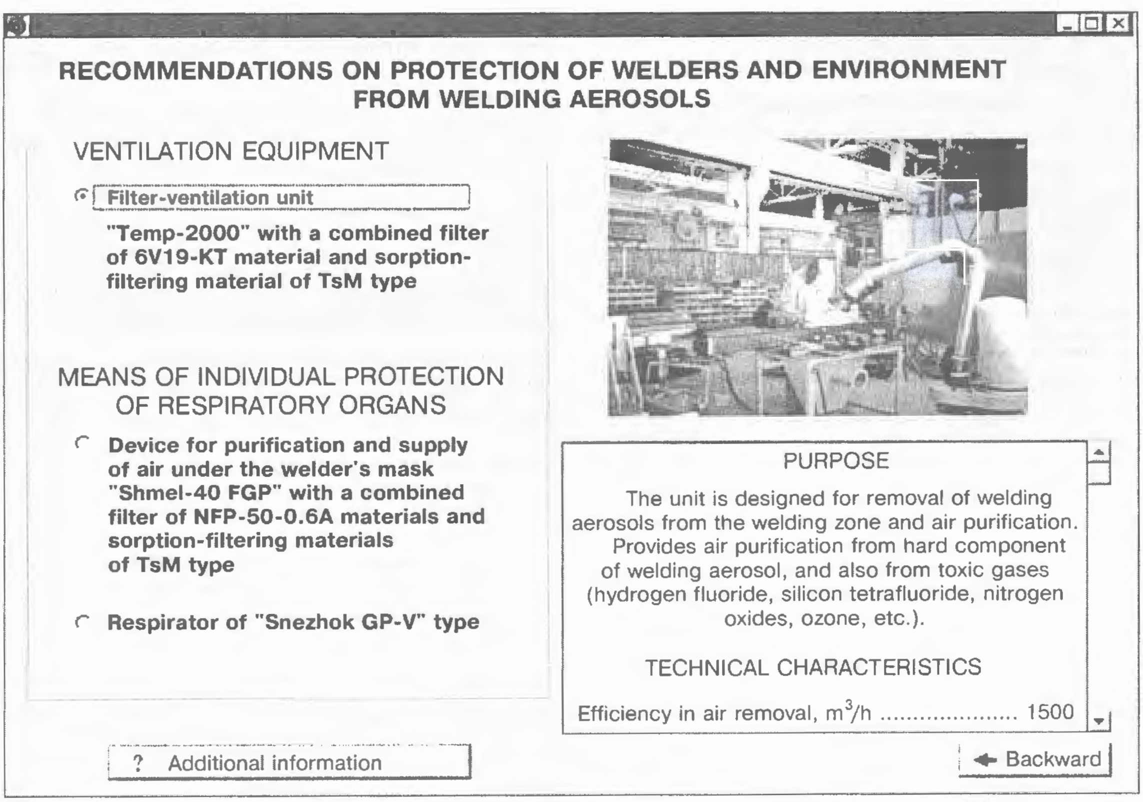

Selection of means of protection from WA using system «ECO-WELD» but increases the content of own harmful elements in it. Thus, to decrease the concentration of toxic elements in HCWA composition it is desirable to use flux with their low content.

Selection of means of protection of industrial and surrounding environment in use of a definite grade of the flux-cored wire is realized using the system «ECO-WELD». For this, the wire grade, its diameter and surfacing conditions are entered by the operator. Then, the system issues recommendations (Figure) about the necessary means of protection in surfacing with flux-cored wires. The illustrated example recommends to use filter-ventilation units (FVU), for example of «Temp-2000» type [9] of efficiency of not less than 1000 m^3/h providing the use of an air intake cup at the minimum distance from welding arc (up to 30 cm). In use of the submerged arc surfacing it is enough to use FVU of efficiency of not less than 100 m^3/h and to remove WA from the distance of not more than 10 cm from arc. In automatic surfacing the air intake cup can be mounted directly on the surfacing automatic machine nozzle.

At the absence of a local or generally-exchanged ventilation of air up to LAC levels (arc welding inside the products) it is necessary to provide a forced supply of pure air under a mask in the volume of 6–8 m^3/h, heated in the cold period of year to the temperature of not lower than +18 °C [10]. This can be realized using the protective masks of welders with a system of purification and supplying the air [9] using special filters designed for air purification from HCWA and fluoric gas.

CONCLUSIONS

1. Investigations of sanitary-hygienic properties of flux-cored surfacing wires have been made, the results of which became the bases of chapter «Requirements for Safety and Protection of Environment» TSU 28.7.05416923.066–2002. Using these standards the 14 grades of flux-cored wires, developed at PWI and designed for surfacing parts operating under different conditions of wear in various branches of industry, are manufactured now.

2. Recommendations are issued on systems of ventilation in open arc and submerged arc flux-cored wire surfacing. Maximum volumes of ventilation air are required in that case when the surfacing is performed with self-shielding wires, whose aerosols contain elements of the 1st (sexivalent chromium, nickel) and 2nd (manganese, soluble flourides) classes of risk (GOST 12.12.005–88). In submerged arc surfacing the evolutions of harmful elements are much lower and the required volumes of the ventilation air in this case are tens of times smaller.

Table 7. Required volume of ventilation air, V

Wire grade	*Shielding medium*	*m^3/kg of wire*	*V, m^3/h*
PP-AN105	Self-shielding	13490	40480
PP-AN130	Same	5100	9180
PP-AN192	»	3510	16850
PP-AN193	»	9250	16650
PP-AN196	»	9310	22340
PP-AN197	»	9100	21840
PP-AN198	»	5200	21840
PP-AN199	»	9410	16930
PP-AN203	»	5400	22680
PP-AN132	AN-26	130	630
PP-AN194	AN-348	400	1680
PP-AN195	AN-26P	340	1640
PP-AN201	AN-26	150	700
PP-AN202	AN-26	160	560

1. Levchenko, O.G. (1996) Processes of welding aerosol formation (Review). *Avtomatich. Svarka*, **4**, 17–22.
2. Levchenko, O.G. (1999) Classification of welding aerosols and selection of methods of their neutralising. *Ibid.*, **6**, 38–41.
3. (1980) *Methodological recommendations 1924–78*. Hygienic evaluation of welding consumables and methods of welding, surfacing and cutting of metals. Moscow: Minzdrav SSSR.
4. (1990) *Methodological recommendations 4945–88*. Determination of harmful substances in welding aerosol (solid phase and gases).-Moscow: Minzdrav SSSR.
5. Demchenko, V.F., Levchenko, O.G., Metlitsky, V.A. et al. (2001) Retrieval system of hygienic characteristics of welding aerosols. *Svarochn. Proizvodstvo*, **8**, 15–20.
6. Kupchyk, M.P., Gandzyuk, M.P., Stepanets, I.F. et al. (2000) *Principles of protection of labor*. Kyiv: Osnova.
7. Veblaya, T.S., Levchenko, O.G., Kharchenko, N.P. et al. (1983) Examination of chemical compounds in solid component of welding aerosols by methods of IR-spectroscopy and X-ray phase analysis. In: *Labour Hygiene*. Issue 19.
8. Golovatyuk, A.P., Levchenko, O.G., Veblaya, T.S. et al. (1984) Application of physical methods for examination of solid component composition in welding aerosols. *Svarochn. Proizvodstvo*, **3**, 37–38.
9. Levchenko, O.G., Metlitsky, V.A. (2001) *Current means of protection of welders*. Kyiv: Ekotekhnologiya.
10. *DSTU 2456–94*. Arc and electroslag welding. Safety requirements. Kyiv: Derzhstandart Ukrainy.

EXPERIENCE IN WELDING OF COPPER-STEEL MOULDS AT NKMZ COMPANY

V.A. NEVIDOMSKY, S.G. KRASILNIKOV, A.D. PANIN, V.Ya. GERASHCHENKO and **K.P. SHAPOVALOV**
NKMZ Company, Novo-Kramatorsk, Ukraine

Specialized fixture, equipment and technological procedures are presented which make it possible to manufacture large-sized copper metal structures, such as moulds for electroslag cladding of composite mill rolls.

Keywords: *copper metal structures, water-cooled movable mould, pulsed-arc welding, shielding gases, furnace-manipulator, welding torch, inverter power source, collapse pulse*

NKMZ Company (Novo-Kramatorsk Machine-Building Works) is known as the largest supplier of rolls in the world, including composite rolls, whose working layer is deposited by a method of electroslag cladding using a filler in the form of a liquid metal (ESC LM).

A key element of the installation for ESC LM is a movable copper water-cooled mould consisting of separate circular sections. Casings of most sections are welded from two semi-rings. Channels of cooling are closed by steel cover plates. Section of welds, joining semi-rings, is given in Figure 1, and the most typical sections of mould are given in Figure 2.

Difficulties in welding of metal structures of copper are well-known and defined by its physical-chemical properties, and, in general, they are reduced to the following:

• significant effect of impurities on properties and weldability of copper, requiring the use of metal for welded structures with a strictly regulated content of oxygen, bismuth, lead, sulphur and antimony;

• high heat conductivity of copper, leading to high rates of cooling and requiring the use of either welding heat sources with a high energy input or high temperatures of preliminary and additional heating, and, often, both of them;

• low time of a weld pool existence in a molten state, limiting the feasibility of its metallurgical treatment and requiring active deoxidizers;

• high coefficient of thermal expansion, making the fastening and preserving the position of parts being welded more difficult;

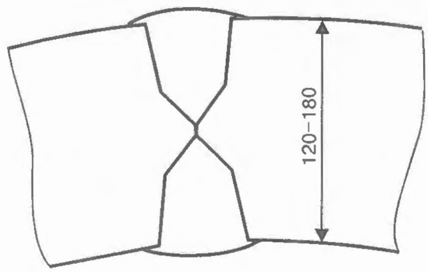

Figure 1. Section of welds forming the casing sections

• high copper fluidity limiting the used space positions of parts being welded;

• high copper sensitivity to hydrogen, requiring to take measures for its content reduction in the zone of welding, and others.

The task of welding mould sections for ESC LM was complicated also by a large mass of billets (mass of large-diameter section reaches 1000 kg), the presence in the structure of dissimilar joints of copper with steel (coefficient of thermal expansion is 1.5 times differed), specifics of welds layout on the workpiece and special requirements to their density and water-tightness.

All the above-listed peculiarities were taken into account when developing the welding technology according to which the moulds were manufactured and are used at present for composite rolls of 650, 700, 740, 780, 852, 965 and 1370 mm diameters.

Copper of M1r grade (GOST 859–78) was taken as a parent material for manufacture of casings of sections. This selection was made with allowance for requirements to weldability and real proposals at the market of non-ferrous metals.

The selected method of welding, the mechanized and automatic consumable electrode pulsed-arc

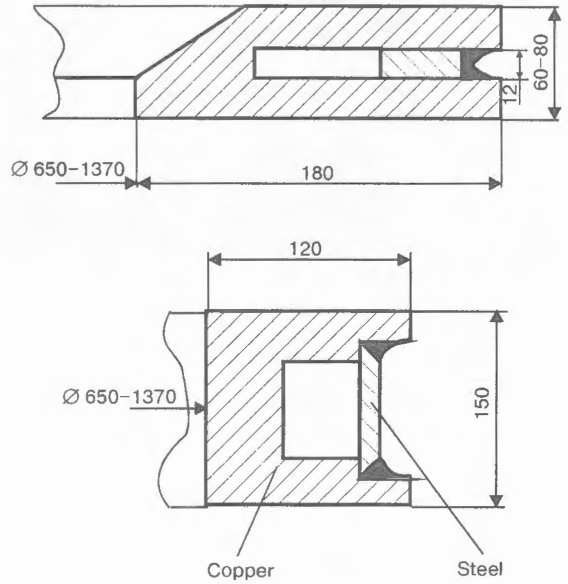

Figure 2. Sections of welds forming the cooling channels

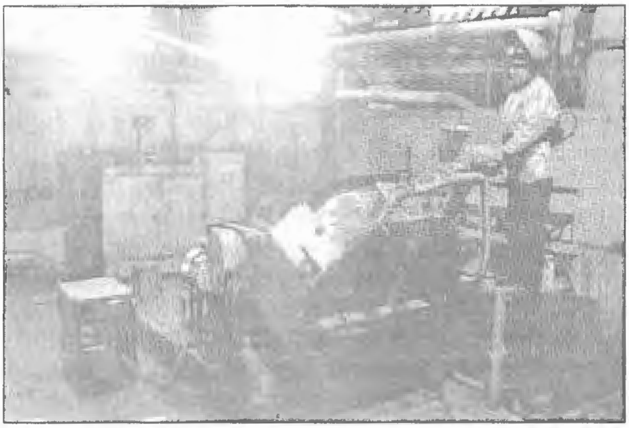

Figure 3. Furnace-manipulator for welding sections for rolls of 650–852 mm diameter

shielded-gas welding, is characterized by a high versatility, simplicity in solution of problem of weld pool protection from the effect of surrounding atmosphere and gives an opportunity of a visual observation of the process and its in-process correction.

To realize the technological process, special installations (furnaces-manipulators) have been designed and manufactured, providing control and keeping the temperature of about 700 °C in the process of welding, rotation of workpiece inside the furnace at welding and travel speeds, inclination of workpiece together with the furnace in positions convenient for welding. One of these installations is given in Figure 3. Using these installations, it is possible to weld mould sections for producing composite rolls from 650 to 1670 mm diameter. Heating of part inside the furnace is realized by electric heaters of own design, supplied from welding sources VDU-1201 and TDFZh-1001. The feasibility of adjustment of heating rate and control of temperature by using thermocouple, built-in into furnace, is provided.

Elements of section for welding are assembled and fastened (without tacks) at a removable element of a rotating hearth of the furnace-manipulator. After appropriate control the as-assembled section is mounted into the furnace and fixed by a cover. Usually, the heating up to 720 °C temperature is continued for 3–3.5 h.

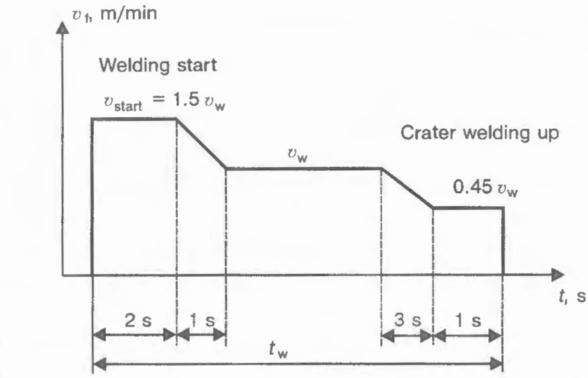

Figure 5. Cyclogram of changing in wire feed speed during welding

Hatches are provided in a casing and cover of the furnace-manipulator through which a successive access to welds of section is provided.

For automatic consumable electrode welding, a torch with a liquid cooling has been designed and manufactured at the plant (Figure 4), which can operate for a long time at currents of about 500 °C at surrounding temperature up to 800 °C. It is fastened to a special bracket, which is an element of a metal structure of furnace casing and inclined together with it. The accurate positioning of torch is provided by a three-coordinate mechanism of displacement.

Mixture of 70 % He + 30 % Ar was used as a shielding gas, which increases the heat capacity of the arc and, thus, provides the required depth of penetration. The mixture was prepared by a single-station mixer BM-2M of German company WITT.

Welding was performed by machines INTEGRAL INVERTER MIG-500 or PHOENIX-500 of company EWM (Germany). Using a special program for the pulsed-arc welding it is possible to control automatically all the stages of the welding process, including the metal transfer, metal motion in the weld pool, weld crystallization and its degassing, imparting of necessary shape and quality of the weld surface. Digital system of control of these machines constructs of a mathematical model of arc and calculates welding process parameters. With 50000 times periodicity per second the system compares the real arc parameters

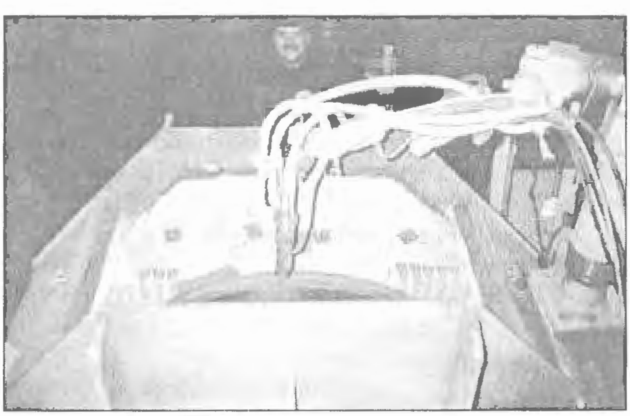

Figure 4. Welding torch with a liquid cooling

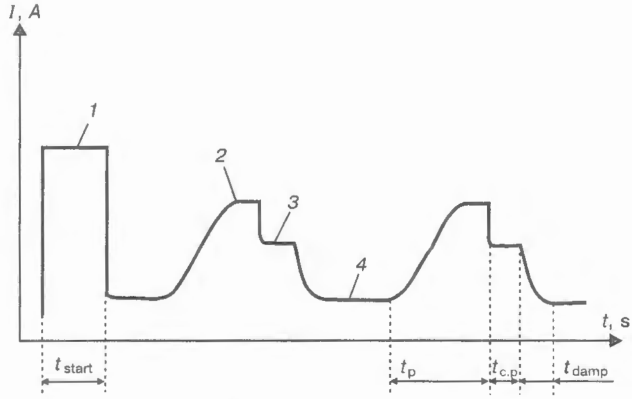

Figure 6. Shape of current pulses: *1* — start current; *2* — maximum value of a pulsed current; *3* — collapse pulse; *4* — minimum value of basic current; t_{start} — duration of of start current; t_p — duration of a pulse; $t_{c.p}$ — duration of collapse pulse; t_{damp} — duration of damping of collapse pulse

with estimated values obtained from the mathematical model and, at the presence of deviations, energizes the inverter. Highly-dynamic power part of the inverter, operating with a clock frequency up to 150 kHz, eliminates deviations for several seconds and, thus, optimizes instantaneously the arc parameters.

The cycle of welding is programmed so that the process is started at wire feed speed v_{start}, amounting to 150 % of main operating feed (Figure 5). This procedure allowed us to avoid lack of penetration at the initial areas of welds.

The nature of changing in pulsed current is shown in Figure 6. The collapse pulse at the end of a pulsed phase provides a softer metal transfer to the weld pool and there is no almost spattering at a correct setting of this parameter.

Welding wire MNZhKT 5-1-0.2-0.2 of 1.6 mm diameter was used as electrode material.

Welding was performed at the following condition: I = 330–350 A (v_f = 6.2 m/min); U_a = 32–33 V; $v_w \approx$ 20 m/h.

Thus, the comprehensive technological studies, application of a mechanized fixture and advanced welding equipment made it possible to solve successfully such complex technological problem, as the manufacture of large-sized copper-steel sections of moulds for ESC LM of composite rolls.

EFFECTIVENESS OF FATIGUE CRACK RETARDATION BY THE FIELD OF COMPRESSIVE RESIDUAL STRESSES

V.A. BRODOVOJ, P.P. MIKHEEV, V.V. KNYSH, O.I. GUSHCHA, A.Z. KUZMENKO and T.M. LABUR
E.O. Paton Electric Welding Institute, NASU, Kyiv, Ukraine

Methods of fatigue crack retardation are studied, which are based on inducing compressive residual stresses in front of crack tips. Experiments were performed on specimens of aluminium alloy D16AT and steel St3sp (killed) with inducing residual stresses by a spot argon-arc surfacing and local heating. It is shown that inducing residual stresses in front of a crack at the level of just 0.3–0.5σ_y of those of the base metal increases the life of a sample by an order of magnitude or more.

Keywords: *welded structures, residual stresses, fatigue cracks, crack retardation, cyclic fatigue life*

In structures, used under normal climatic conditions without the impact of shock loads, the stage of crack propagation can be equal up to 90 % of the total fatigue life of a welded element. Therefore, development of measures, aimed at retardation of fatigue cracks in elements of metal structures, is highly urgent.

Among several methods, applied for retardation of fatigue crack propagation, a significant role is played by those based on the principle of inducing a field of residual compressive stresses ahead of the crack front. Cyclic loading of welded joints results in partial relaxation and redistribution of the residual stresses [1, 2]. Artificially induced residual stresses also interact with the residual welding stresses and stresses, induced under cyclic loading in the zones of stress raisers or near the fatigue crack tips [3]. This results in formation of a new field of residual stresses, which is exactly what determines the rate of fatigue crack propagation.

Given below are the results of experimental investigations of the influence of compressive residual stresses, artificially induced ahead of the crack tip, on the rate of fatigue crack propagation.

Investigations were conducted on specimens of 135×250×650 mm size of steel St3sp (killed) (σ_y = = 296 MPa, σ_t = 476 MPa) and those of aluminium alloy D16AT (σ_y = 256 MPa, σ_t = 471 MPa) of 3×170×500 mm size. By their parameters the specimens corresponded to the existing procedural recommendations [4].

Specimens were tested with a pre-grown fatigue crack, which was initiated, using an artificial concentrator. For this purpose a 4 mm diameter hole was drilled out in the specimen center. Notches 1 mm deep with rounding-off radius of 0.05 mm were made in its walls.

Two sets of specimens were tested to determine the effectiveness of retardation of a fatigue crack with residual compressive stresses, artificially induced ahead of its tip. The first group of specimens of steel St3sp and D16AT were tested to complete fracture without crack retardation.

In the second group residual compressive stresses were induced by point heating for specimens of steel St3sp or spot weld deposition for specimens of aluminuim alloy D16AT. Point heating was performed by a flame of a mixture of oxygen and natural gas for 30 s. Thus, a temperature of about 350 °C was ensured in the heating point. Deposition was performed in argon with filler wire AMg6 of 1.6 mm diameter at current I = 100 A. Heating duration was 0.5 s.

Specimens were tested in hydraulic testing machines TsDM-200Pu and UPS-20 at zero-to-tension tensile loading cycle. The level of the acting nominal stresses was controlled with strain gauges and by the load, in keeping with the accepted procedure [5]. The level of residual stresses, induced after local treatment in the fatigue crack zone was controlled by an acoustic non-destructive method [6]. The length of fatigue crack was measured on the surface of a specimen with optical microscope MPB-2M with 0.1 mm scale graduation value.

The Figure, *I*, *a* gives the schematic of a specimen of steel St3sp and graphs of distribution of the components of the resultant residual stresses in the zone of the fatigue crack after inducing a field of residual compressive stresses ahead of its front. The level of the longitudinal component σ_θ of the measured residual stresses in the zone of the fatigue crack was equal to –60 MPa. Initial half-length of the crack l_0 = 18 mm. Then the specimen was tested for crack resistance under cyclic loading at maximum stress of 170 MPa. The Figure, *II*, *b* gives for this specimen the dependence of fatigue crack length on the number of external loading cycles up to the moment of crack retardation and after specimen processing by point heating. As is seen from the graph, crack growth was significantly slowed down after residual compressive stresses were induced ahead of its front, which resulted in a considerable extension of the specimen fatigue life.

Similar graphs of distribution of residual stresses in the zone of fatigue cracks and crack growth under cyclic loading in a specimen of aluminium alloy D16AT are shown in Figure, *II*. Specimens of the first group with a fatigue crack of initial length $2l_0$ = = 20 mm were first tested for crack resistance at initial

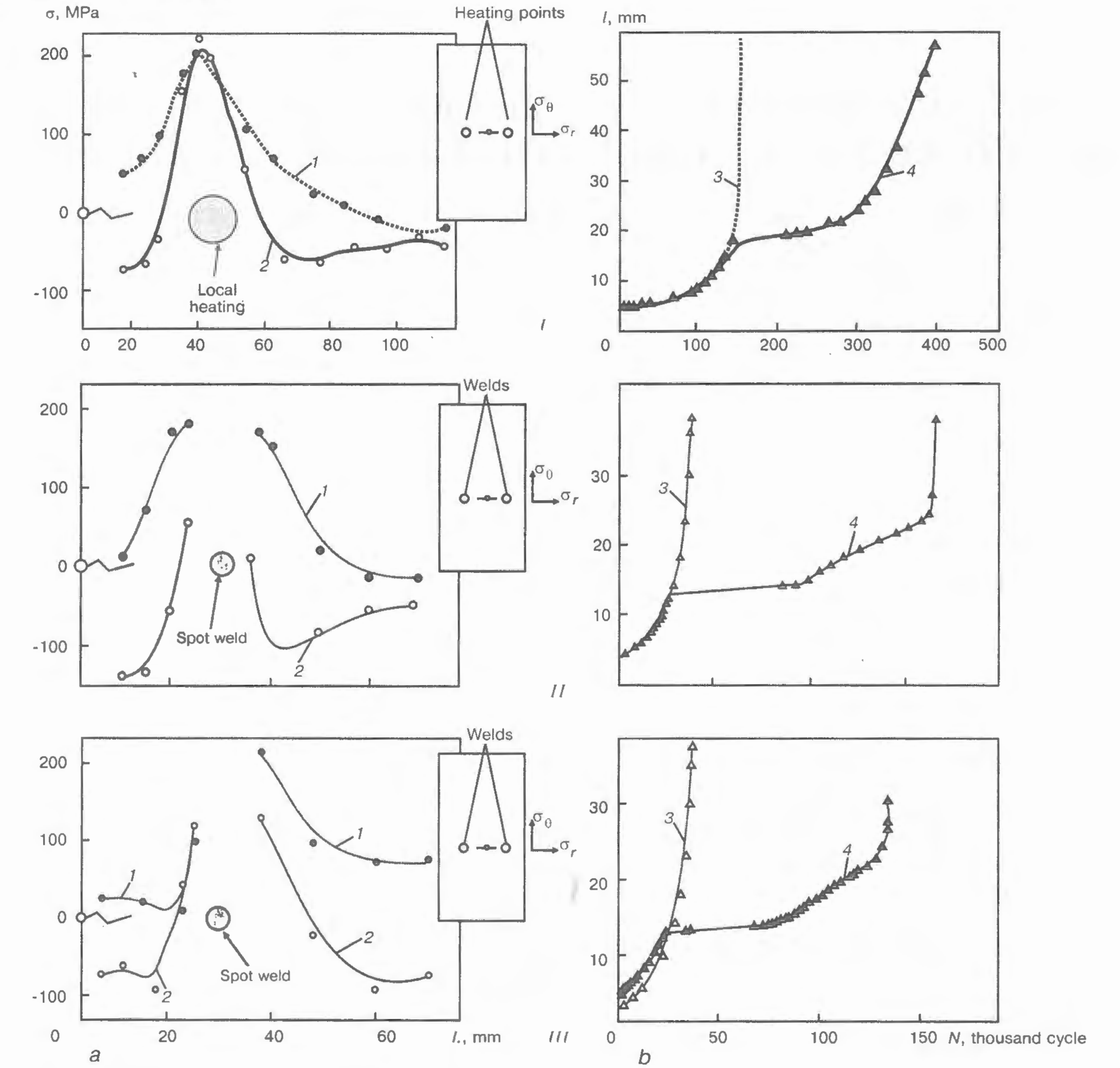

Distribution of residual stresses (a — σ_r (*1*) and σ_θ (*2*)) from one of the sides of a specimen of steel St3sp (*I*), aluminium alloy D16AT with a deposit (*II*), D16AT with a deposit after removal of the reinforcement (*III*) and variation of the specimen fatigue life (b — without (*3*) and after (*4*) inducing residual stresses)

cycle stress of 90 MPa. Then an identical specimen was tested under the same conditions after inducing in the crack tip zone residual compressive stresses on the level of −120 MPa. The Figure, *II*, *b* shows that inducing compression in the fatigue crack zone extended the period of the fatigue crack growing from the initial half-length l_0 = 13 mm to half-length l = = 27 mm by 15 times, compared to the same growing of the crack without its retardation.

The Figure, *III* gives the graphs of aluminium alloy D16AT for a specimen, where the convexity was removed after deposition to reduce stress concentration. The measured longitudinal component of residual stresses σ_θ in the crack zone was −90 MPa. In this case the period of crack growth decreased by 20 %, compared to the previous specimen.

Therefore, inducing compressive residual stresses ahead of the front of the developing fatigue crack on the level of just 0.3–$0.5\sigma_y$ of the base metal may increase the fatigue life of a specimen by an order of magnitude or more.

1. Trufiakov, V.I., Gushcha, O.I., Kudriavtzev, Yu.F. (1981) Alternation of residual stresses in welded joints at cyclic loading. *IIW Doc. XIII-1031–81*.
2. Makhnenko, V.I. (1976) *Computational methods of study of kinetics of residual stresses and strains*. Kyiv: Naukova Dumka.
3. Brodovoj, V.A., Gushcha, O.I., Kuzmenko, A.Z. et al. (2001) Interaction of residual stresses in the zones of stress concentrators and fatigue cracks. *The Paton Welding J.*, **9**, 42–43.
4. *RD50-345–82*. Calculations and strength tests. Methods of mechanical tests of metals. Determination of characteristics of crack resistance (fracture toughness) under cyclic loading. Moscow.
5. Lebedev, V.K., Fedko, B.A., Marchuk, I.V. (1977) Automation of measurements of effective stresses in fatigue tests of welded joints. *Avtomatich. Svarka*, **9**, 4–6.
6. Gushcha, O.I., Makhort, F.G. (1995) Application of an acoustic method for determination of residual stresses in welded structures. *Tekhn. Diagnostika i Nerazrush. Kontrol*, **4**, 8–15.

DETERMINATION OF OPTIMUM LENGTH OF AN ILLUMINATOR IN TECHNICAL VISION SYSTEMS FOR ARC WELDING

F.N. KISILEVSKY and **E.V. SHAPOVALOV**
E.O. Paton Electric Welding Institute, NASU, Kyiv, Ukraine

The paper gives the main technical characteristics of the existing optical sensors in systems of technical vision for arc welding. Spectral characteristics of welding arc are studied to determine the local minimums of luminosity in the wave length range from 500 to 1100 nm. Ranges of wave lengths of illuminator operation are recommended to increase the signal-to-noise ratio of arc welding.

Keywords: *arc welding, optical sensor, welding arc spectrum, technical vision system, signal-to-noise ratio, light section, illuminator*

Attempts to develop a sensor of the torch position on the welded joint line (WJL) relative to the butt were made as far back as fifty years ago. A multitude of various sensors have currently been developed for following the geometrical parameters of a welded joint, which differ by the principle of operation, accuracy, cost, reliability, etc., namely contact (tactile), eddy current, ultrasonic, butt following by measurement of welding current and voltage at oscillating electrode.

Main technical characteristics of some of existing optical sensors for arc welding

Model, manufacturer company, country	*Illuminator type*	*Power, mW*	*Wave-length, nm*
SU 274-UKhL-4 sensor, PWI, Kyiv, Ukraine	Light-emitting diode rule AL107V	100	980
JST model, Jetline Engineering, Inc., California, USA	Laser diode of 3A class	40	670
OS-3 model, VNIIESO, St.-Petersburg, Russia	ILPN-108 laser	40	830–840
NINI-i model, Servo-Robot Inc., Quebec, Canada	Laser diode of 3B class	50	685
Laser Probe model, Meta Vision Systems, Ltd., England	Same	30	650–699
CSS model, Oxford Sensor Technologies, Ltd., England	Same, classes 3A and 3B	3.5 and 10	633–670

Introduction of relatively inexpensive video cameras, based on charge-coupled devices (CCD), namely CCD-matrices, gave a new impetus to development of optical sensors. Proceeding from their versatility, information content, reliability and field of application, it may be assumed that in the near future optical sensors, used for automation of the welding process, will have a priority role [1]. Scientists continue working to improve their quality.

Optical sensors are usually constructed, using the triangulation principle. The most widely spread method, applied in technical vision systems in arc welding is the light section method. A laser or light-emitting diode matrix (rule) are most often used as an illuminator, where cylindrical optics is used for illumination structuring. An image of a light strip is recorded by CCD camera (Figure 1). A welding head is rigidly coupled to a video camera and illuminators. As the base distance between the camera and the illuminator, as well as the triangulation angle are known, then proceeding from the parameters of the

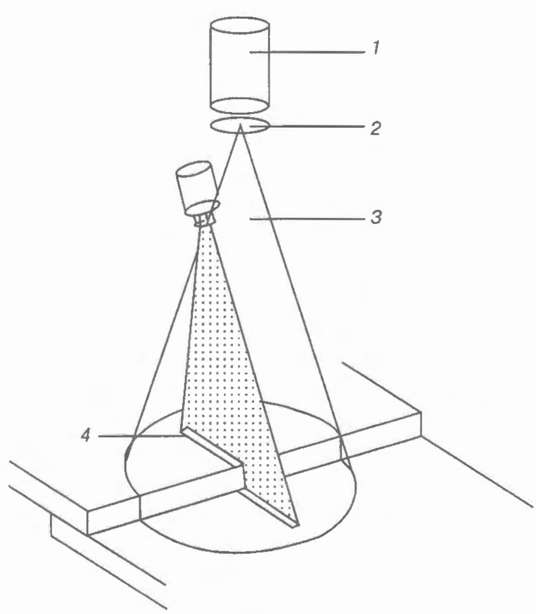

Figure 1. Schematic of operation of a sensor by the light section method: *1* — video camera; *2* — interference filter; *3* — illuminator; *4* — light strip

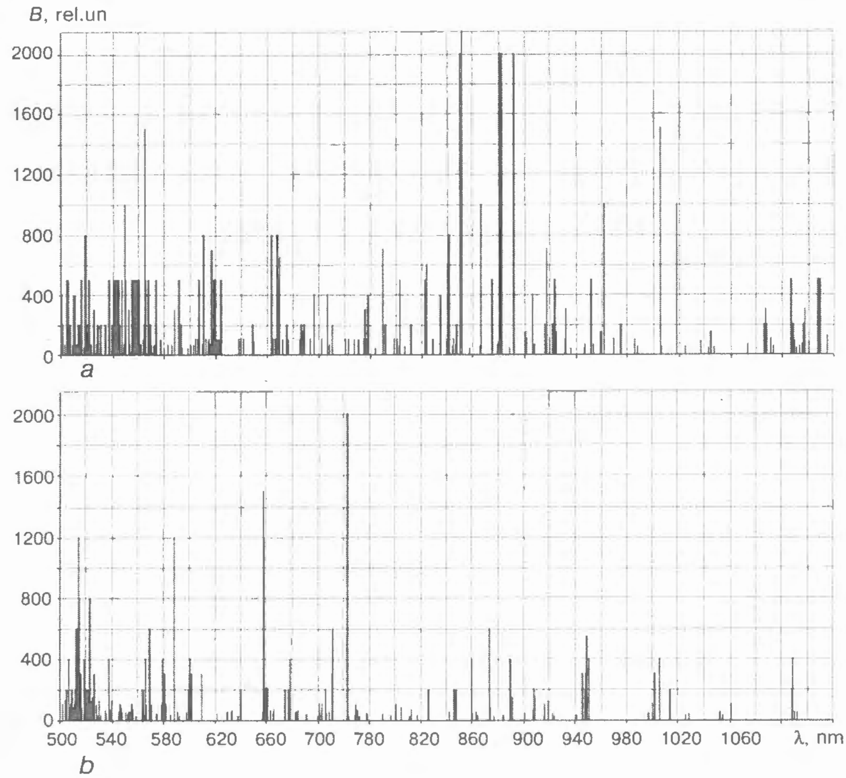

Figure 2. Line spectra of argon, aluminium, tungsten (*a*) and iron, carbon, oxygen (*b*) in an arc discharge: *B* — radiation brightness; λ — radiation wavelength

image obtained, using the camera, it is possible to evaluate the distance from the welding head to the surface being welded and the butt profile.

One of the sensors of this type was developed at PWI by Yu.I. Streletsky. The illuminator incorporated into it is designed as a rule of the light-emitting diodes AL107V, its power is equal to 100 mW. Radiation wavelength is 980 nm.

At All-Russia Research Institute of Electric Welding Equipment (VNIIESO) in St.-Petersburg, N.G. Ustinov and A.V. Karpilenko developed a sensor, where the illuminator is a 40 mW ILPN-108 laser with the working wavelength of radiation of 830–840 nm [2].

A sensor of a similar design (JST model), using two laser diodes to generate the light band, was developed by Jetline Engineering, Inc., California, USA [3]. Laser diodes of class 3A of such a sensor have the power of 40 mW and radiation wavelength of 670 nm.

A following sensor (3D model) was developed at Oxford. It uses a laser as an illuminator, the laser beam being projected in the form of a circumference onto the surfaces being welded. Laser diode of class 3A or 3B of 3.5 and 10 mW power has the working wavelength of radiation of 633–670 nm.

Meta Vision Systems, Ltd. (Great Britain) developed a laser sensor with an illuminator, consisting of two 3B class laser diodes of 30 mW power with radiation wavelength of 650–699 nm.

Servo-Robot, Inc. Company (Canada) [4] developed a range of sensors for following the geometrical parameters of a welded joint, torch guiding along the WJL, as well as for diagnostics of welding quality.

One of the main problems in designing this type of sensors is selection of the working wavelength of the illuminator. Proceeding from general physical concepts, preference, as a rule, is given to the infrared region of the spectrum, in which the influence of arc light is manifested much less than in the short-wave region.

Spectral characteristics of the welding arc are affected by all the chemical elements, present in welding consumables (even in small amounts), and such an influence is quite difficult to investigate. This accounts for selection of different radiation wavelengths for investigations in fabrication of optical sensors (Table).

There currently is a scientific problem of selection of an optimal wavelength of the illuminator. Its solution required studying the welding arc spectrum. According to [5], linear spectra were plotted for the basic chemical elements, used in argon-arc welding of aluminium (Figure 2, *a*) and CO_2 welding of steel (Figure 2, *b*) in the range of radiation wavelength λ = 500–1100 nm.

As is seen from Figure 2, *a*, in radiation ranges of 625–660, 710–730, 940–960, 990–1040 nm the linear spectrum corresponding to argon and aluminium has local brightness minimums, which are the most favourable for illuminator operation. In CO_2 welding of steel they are in the range of wavelengths of 620–650, 740–800, 860–900, 920–950, 980–1060 nm (Figure 2, *b*).

It should be noted that use of silicon CCD cameras with the radiation wavelength close to 1000 nm, is undesirable, in view of an abrupt lowering of their sensitivity, and use of germanium video cameras greatly increases the sensor cost. In the visible part of the spectrum, as a rule, a rather strong influence of extaneous light sources is observed (daylight and electric light, heated metal). This should be taken into account in designing the laser power. Increase of the laser power leads to its higher cost, and the influence of outside illumination creates extra difficulties in signal processing.

Illuminator operation in the recommended range of wavelengths allows increasing the signal-to-noise ratio in the systems of technical vision of arc welding. The recommended ranges of radiation wavelengths became a prerequisite for development of technical vision systems with higher characteristics, such as reliability and accuracy, and it further became possible to reduce the sensor cost due to simplification of development of adaptive image processing algorithm.

1. Ushio, M., Oshima, S., Asai, S. et al. (1999) The state of the art of arc welding in vessel and pipe. *IIW Doc. XII-1585–99*.
2. Ustinov, N.G., Karpilenko, A.V. (1992) Optical sensor for automatic welding. *Avtomatich. Svarka*, **7/8**, 37–40.
3. Kolbl, W. (1995) Affordable optical seam tracking. *Industrial Robot*, **6**, 19–21.
4. Boillot, J., Noruk, J. (2002) The benefits of laser vision in robotic arc welding. *Welding J.*, August, 32–34.
5. Zajdel, A.N., Prokofiev, V.K., Rajsky, S.M. et al. (1977) *Tables of spectral lines*. Moscow: Nauka.